Flow Pulsation Measurement in Hydraulic Systems

Von der Fakultät für Maschinenbau, Verfahrens- und Energietechnik

der Technischen Universität Bergakademie Freiberg

genehmigte

DISSERTATION

zur Erlangung des akademischen Grades

Doktor-Ingenieur

(Dr.-Ing.)

vorgelegt

von Dipl.-Ing. Róbert Nagy

geboren am 31.01.1976 in Miskolc (Ungarn)

Gutachter.: Prof. Dr. rer. nat. habil. Frank Obermeier, Freiberg

Prof. Dr.-Ing. habil. Volkmar Weise, Zittau/Görlitz

Dr.-Ing. László Baranyi, Miskolc

Tag der Verleihung: 06. Dezember 2004

Abstract

In the hydraulic industry there is a demand for a simple method that can measure flow pulsation. This work contains the development of a new technique for this purpose. It is based on the differential pressure measurement between two points in an unsteady flow field. In order to obtain the dynamic response of the sensor the governing equation between the flow pulsation and the differential pressure was evaluated. Previous versions of the sensor had a low natural frequency that was increased with an optical pressure transducer. An optical method was adapted for this special purpose, including the analysis of the reflective membrane that transforms the differential pressure into mechanical motion. A compact positioning of the optics was achieved, which was used to detect the deflection of the membrane. After the construction of the optical pulsation sensor, it was built into a hydraulic circuit. The sensor was capable of detecting the signal of interest, however the dynamic response of the total circuit deviates from the expected result. Its reason was investigated with a transmission line model, including viscous losses, but an understanding of the system behaviour is far from complete. Air contamination of the working fluid and resonance frequencies of the system disturbed the measurements. Nevertheless, this method proved its applicability by the detection of a broken tooth of a gear pump.

Keywords: flow rate, hydraulic, pulsation, speed of sound, viscous damping.

Kurzfassung

In der Hydraulikindustrie gibt es einen großen Bedarf, mit einer einfachen Methode Volumenstrompulsationen messen zu können. Diese Arbeit beinhaltet die Entwicklung einer neuen Technik, die auf Differenzdruckmessung zwischen zwei Punkten der instationären Strömung basiert. Um die dynamische Antwort des Sensors zu bestimmen wurde der Zusammenhang zwischen Volumenstrompulsation und Druckdifferenz bestimmt. Die niedrige Eigenfrequenz der vorherigen Sensorversionen wurde mit Hilfe eines optischen Druckwandlers erhöht. Dieser Wandler wurde zu diesem besonderen Zweck adaptiert, einschließlich die Analyse der reflektierenden Membran, die die Druckdifferenz in mechanische Bewegung umwandelt. Es wurde eine kompakte Positionierung der Optik entwickelt, die es ermöglicht, die Verformung der Membran zu messen. Nach der Konstruktion des optischen Sensors wurde er in einem hydraulischen Versuchstand eingebaut. Der Sensor kann die Frequenz des Erregersignals gut messen jedoch ist die dynamische Antwort des ganzen Systems anders als erwartet. Die Ursache dafür wurde mit einem Rohrleitungsmodell untersucht, das viskose Verluste beinhaltet aber auch dieses Modell konnte keine hundertprozentige Systemantwort liefern. Die Messungen wurden durch Lufteinschlüsse der Messflüssigkeit und Resonanzfrequenzen des Versuchstandes gestört. Dennoch konnte die Funktion des Sensors bei der Erkennung eines gebrochenen Zahnes einer Zahnradpumpe nachgewiesen werden.

Schlagworte: Volumenstrom, Hydraulik, Pulsation, Schallgeschwindigkeit, viskose Dämpfung.

Acknowledgements

I would like to express my deepest appreciation to Prof. Obermeier, my academic supervisor, for being patient with me during all the problems, which I have faced during this work.

This work would have never been possible without the initiation of Dr. Hein who has given me valuable inputs and constructive support. Special thanks must also go to Dr. Chaves for his interest and helpful comments in the discussion of this thesis.

Much appreciation goes to the technical members of the institute for their friendship and practical support throughout my research activity.

I am also grateful to the Government of Saxony for the financial support of my work.

Last, but not least, I would also like to thank to Ana and my family for their support during the last years. I hope they will forgive me for all the overtime I spent at the university instead of being with them.

Table of contents

Table of figures

Nomenclature

A	cross-section area	$[m^2]$
A_{Id}	intensity at the detector	$[W/m^2]$
A_{Imax}	maximal detectable intensity	$[W/m^2]$
b	tooth width	$[m]$
c	speed of sound	$[m/s]$
c_m	measured speed of sound	$[m/s]$
c_t	theoretical speed of sound	$[m/s]$
C_{cor}	correlation coefficitent	[-]
d	diameter	$[m]$
d_b	beam diameter	$[m]$
d_f	fibre diameter	$[m]$
dh	elevation difference	$[m]$
dp	differential pressure	$[Pa]$
dp_m	differential pressure acting on the membrane	$[Pa]$
E	bulk modulus	$[N/m^2]$
E_f	fluid bulk modulus	$[N/m^2]$
E_{fa}	fluid-air bulk modulus	$[N/m^2]$
f	frequency	$[Hz]$
f_b	basic frequency	$[Hz]$
f_m	measured natural frequency	$[Hz]$
f_{mo}	natural frequency of the membrane-oil system	$[Hz]$
f_n	natural frequency	$[Hz]$
f_r	resonance frequency	$[Hz]$
F_g	gravity force	$[N]$
F_m	membrane force	$[N]$
F_0	tensile force	$[N]$
g	acceleration due to gravity	$[m/s^2]$
h	height	$[m]$
i	imaginary unit	[-]
I	intensity	$[W/m^2]$
I_b	normalised intensity distribution	[-]
J	Bessel function	[-]
k	wave number	$[1/m]$
k_g	modified trapped oil correction factor	[-]
k_m	membrane spring constant	$[N/m]$
k_t	tension parameter	[-]
l	distance	$[m]$
l_f	focal distance	$[m]$
l_{fl}	fluid length	$[m]$
l_i	image distance	$[m]$
l_{lm}	distance between lens and membrane	$[m]$
l_o	object distance	$[m]$
m	mass	$[kg]$
m_o	oil mass	$[kg]$
n	revolution speed	$[Hz]$
N	friction loss factor	[-]
N_0	initial tension	$[N/m]$
p	pressure	$[Pa]$
p_0	atmospheric pressure	$[Pa]$

Q	flow rate	$[m^3/s]$
Q_c	calculated flow rate	$[m^3/s]$
Q_g	geometrical flow rate	$[m^3/s]$
Q_{ga}	average geometrical flow rate	$[m^3/s]$
Q_{gmax}	maximal geometrical flow rate	$[m^3/s]$
Q_{gmin}	minimal geometrical flow rate	$[m^3/s]$
Q_{OPS}	flow rate of the optical pulsation sensor	$[m^3/s]$
Q_{sha}	flow rate of the shaker	$[m^3/s]$
r	radius	$[m]$
r_b	beam radius	$[m]$
r_c	radius of curvature	$[m]$
r_d	detector radius	$[m]$
r_h	head radius	$[m]$
r_i	image radius	$[m]$
r_o	object radius	$[m]$
r_s	source centre radius	$[m]$
R	radius	$[m]$
Re	Reynolds number	[-]
s	Laplace operation parameter	$[rad/s]$
t	time	$[s]$
T	inviscid propagation time	$[s]$
u	flow velocity	$[m/s]$
u_a	average flow velocity	$[m/s]$
u_{ax}	axial flow velocity	$[m/s]$
u_0	steady flow velocity	$[m/s]$
U	electrical voltage	$[V]$
U_{mag}	output voltage of the magnetic transducer	$[V]$
V	volume	$[m^3]$
V_a	air volume	$[m^3]$
V_f	fluid volume	$[m^3]$
w	deflection	$[m]$
w_a	average membrane deflection	$[m]$
x	distance	$[m]$
z	number of teeth	[-]
Z	acoustic impedance	$[Ns/m^3]$
Z_c	characteristic acoustic impedance	$[Ns/m^5]$
a	coefficient of absorption	$[1/mm]$
a_d	angle of deflection	$[rad]$
a_k	centre distance	$[m]$
a_P	Poiseuille coefficient	$[1/s]$
d	pulsation factor	[-]
e_e	strain	[-]
e_o	overlap ratio	[-]
e_t	peripheral deformation	[-]
l	wavelength	$[m]$
m	dynamic viscosity	$[Ns/m^2]$
n	kinematic viscosity	$[m^2/s]$
n_P	Poisson's ratio	[-]
r	density	$[kg/m^3]$

s	stress	$[N/m^2]$
s_{dp}	stress caused by differential pressure	$[N/m^2]$
s_e	elastic stress	$[N/m^2]$
s_r	radial stress	$[N/m^2]$
s_t	tangential stress	$[N/m^2]$
s_0	tensile stress	$[N/m^2]$
w	angular frequency	$[1/s]$
W	non-dimensional frequency	[-]
z	loss factor	[-]

1 Introduction

Before starting with technical topics regarding flow engineering, I would like to draw a parallel between the human body and machines. Our body is a perfect mechanism that allows us to live and work. Understanding how our body operates can help us to produce better machines.

The human body is a special “transformer” that converts food into motion in several steps. The whole process is a chain that contains transform and transport stages. All the different kinds of food we eat are broken down by our digestive system and transported to the muscular organs that produce mechanical motion. With machines the process is a similar one, containing transformation and transportation stages. These stages are necessary as every kind of energy has its advantages and disadvantages: one is easy to produce, but difficult to transport and the other has difficulties with the generation, but is easier to lead from one place to another.

In our body the energy transportation happens via the flow engineering part of the body, known as the circulatory system. The heart acts as a pump, developing a pulsated flow, hence carrying the energy from one organ to the other around the body. In case of any problem with the heart, the veins or other organs can change the flow. Monitoring the flow parameters (pressure or flow rate) problems can be detected at an early stage and prevention treatment can begin. The sooner this process begins the less difficulties are likely to arise. This is valid also for machines, besides a significant impairment system break down can be also avoided.

To be able to monitor the system, special measuring devices are necessary. The aim of this work is to develop a unit to measure volume fluctuations that can be applied for this purpose in hydraulic systems.

Hydraulic is also an energy transformation and transportation method, where, for example electricity is transformed into different kinds of motions. The most important advantage of hydraulic drives is that they have a large force and energy density. These devices are used in a wide application field, especially, where heavy loads have to be moved. In the last years the main purpose of the pressure and flow measurement techniques applied in the hydraulic industry was the measurement of the steady pressure and flow rate. As the design and manufacturing are always more supported by computers, the quality of the hydraulic components are continuously increased. It allows faster operating of hydraulic elements, thus the dynamic behaviour of the system has always an increasing importance. For this reason, there is a demand in the hydraulic

industry for a simple technique to measure flow pulsation. There are several methods to measure the unsteady flow parameters (e.g. anemomety, ultrasonic technique and particle image velocimetry) however, they are too complex and expensive for industrial application.

1.1 Milestones of the development

The German engineer Julius L. Weisbach (*1806-1871*) was a pioneer in the field of hydraulic; he investigated experimentally steady pipe flow parameters. Our aim is to study this field as well, however, in unsteady flows.

Pulsation sensors have been investigated at the Institute of Mechanics and Fluid Dynamics of the Freiberg University of Mining and Technology since the early nineties. Two versions were developed and tested [*1*], [*2*]. A common feature of the sensors was their operating principle that was based on differential pressure measurement. It is a well-known technique, however up till now it has not been used in an unsteady case. Its reasons are the low sensitivity and dynamic response of the previous pressure transducers and difficulties with the dynamic calibration.

The first problem is solved with an optical transducer that transforms the differential pressure into an electrical signal. This new kind of transducer has a high natural frequency and appropriates in order to detect a differential pressure of some *mbar*. A solution for the dynamic calibration presented here, however, there are some open questions still remaining.

If one would detect differential pressure with means of two individual pressure transmitters, the range of the individual instruments would limit the system pressure. Applying only one unit has the advantage that the system pressure can be arbitrarily high. Another drawback of the application of two transmitters is that they must have exactly the same response to record the true value of the pressure difference.

The advantages of the differential pressure sensors are their simple working principle, low flow disturbance and a wide pressure range. There are several differential pressure sensors that have been developed mainly to measure steady flow rate. Nevertheless, to the author's knowledge, no differential pressure device has been implemented for flow pulsation measurement up to *1000 Hz* in hydraulic systems.

1.2 Pressure and flow measurement techniques

In process measurement there is no universal sensor, the criteria by selecting an instrument depends on many parameters: range, accuracy, costs, temperature and size etc. The main purpose of the flow measurement techniques applied in industrial applications is the measurement of steady process parameters. As the speed of the operation is continuously increasing, the dynamic parameters have always more importance, consequently, there is a great demand on a simple technique to detect flow pulsation. To make a clear distinction between steady and unsteady flow there are no international standards. A suggestive comment regarding this topic can be found in [*3*]: "If you cannot measure it, damp it!". This train of thought can be found in other works dealing with flow measurement, respectively.

In industrial flow measurement the most widely used methods are based on the differential pressure measurement [*4*], [*5*], [*6*], [*7*], [*8*], [*9*], [*10*]. These kinds of meters consist of two parts; the primary one contains a pipe restriction and pressure taps, which are located at different positions. The secondary element has connecting lines, in which the pressure from the taps is transmitted to the transducer. To reduce the high-pressure loss caused by the restriction, the Pitot-tube was developed where the difference between the total pressure on the impact port and the static pressure is measured. To overcome the limitation of the Pitot-tube, it detects only a point velocity, special sensors were developed (Annubar), where the velocities are measured at several points and are averaged.

The above-mentioned techniques have a restriction at the metering position, hence, the flow field is modified and unsteady disturbance appears. As the purpose of these instruments is the detection of the steady flow rate so the disturbance has minor effect on the measurements. If one would like to detect the flow pulsation with these sensors, the effect of the unsteady disturbance becomes significant. Locating the pressure taps at the wall of the pipe and eliminating the restriction, the measuring unit does not disturb the flow. To be able to measure the flow pulsation the pressure-sensing element must have a high resolution and must be fast. The Optical Pulsation Sensor (OPS) presented in this work fulfils these criterions.

A standardized pressure measurement package, so called "pressure transmitter", consisting of three basis components [*7*]: pressure transducer, its power supply and signal conditioner that converts the transducer signal into standardized output. A transducer is a device that converts energy from one form to another. The most common pressure transducer types are piezoelectric,

capacitive, magnetic, strain gauges and optical. The new technique presented in this work is an optical type with high sensitivity and dynamic response.

The tubing significantly influences the dynamic response of a pressure probe. In many cases the pressure ports are connected to external transducers using long tubing, which result in a slow probe response and therefore low measurement frequency range. In the case of long tubing significant pressure attenuation and phase lag can occur between the measurement point and the transducer. The tubing of the OPS is made as short as possible to provide a proper dynamic response of the instrument.

The tubing system must be carefully designed and analysed to be able to fully reconstruct the measured pressure at the measuring point. Pathak and Rediniotis [*11*] presented a simple method to correct pressure measurement errors resulting from long tubing (*450 mm*) with an inner diameter of *6 mm*. The working medium was air and the frequency of the unsteady pressure pulsation was lower than *1 Hz*. In the pressure measuring unit the pressure at the transducer was different from the pressure at the source. From these two signals a lag constant was determined which was then used as a characteristic of the tubing. In our case the geometrical dimensions are much smaller ($l = 40$ *mm* and $d = 3$ *mm*) and the frequency is higher (up to *1000 Hz*) that makes the problem more complex. Johansen et al. [*12*] presented a similar work for air and water, however the oscillation frequency was also low (*6 Hz*). Air bubbles in the tubing result in measuring failures, depending on the system pressure [*13*]. During the design of the OPS, extra attention was taken to avoid air contamination in the tubing.

An indirect method to measure flow pulsation was presented by Weddfelt [*14*], where the flow pulsation was determined from the measured pressure pulsation with the knowledge of the impedance of the measurement system at the transducers. The point impedance at the location of either of the transducers was determined from the transfer function that was based on the mathematical model of the pipe. The main drawback of this technique is that it can be applied only in case of simple piping. This limitation does not exist with the application of the OPS.

Unsteady flow parameters can be measured by hot film anemometry, ultrasonic techniques (Laser Doppler Anemometry, Ultrasonic Velocity Profile) or Particle Image Velocimetry. These methods provide accurate results, however they require the use of expensive components and painstaking alignment of the components. For this reason they are rather applied in a laboratory environment than in industrial applications.

1.3 Velocity profile in pulsating flow

In case of steady laminar flow in a pipe the velocity distribution is parabolic [*15*], illustrated in *Figure 1.1*.

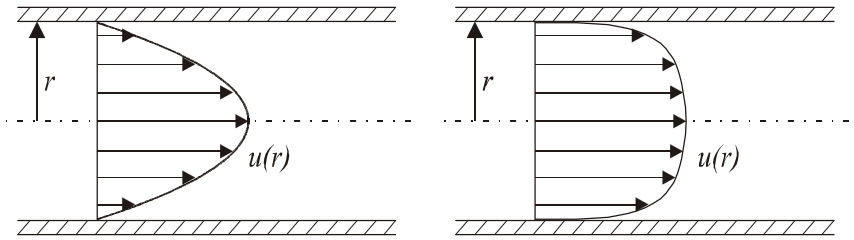

Figure 1.1: Velocity profile in steady laminar and turbulent flow.

The maximum of the flow velocity is in the centre-line of the pipe. The Reynolds number is a flow parameter that is often used to determine if the flow is laminar or turbulent:

$$\mathrm{Re} = \frac{u_a d}{n}, \qquad (1.1)$$

where u_a is the average flow velocity, d is the pipe diameter and n is the kinematic viscosity. A commonly used limit for the laminar flow is $Re = 2300$ above this value the flow is called turbulent. Comparing the laminar velocity profile to the turbulent one, near the centre line the second is much flatter and near the wall the turbulent profile has a large gradient. If there is a fluctuation, the velocity distribution is modified.

A mathematical description of a pure pulsating flow exists since the middle of the last century [*16*], but due to technical difficulties really detailed measurements were only later possible. Nowadays with modern instrumentation and computers not only the theory, but also the experiments can be better investigated [*17*], [*18*], [*19*], [*20*], [*21*], [*22*], [*23*], [*24*]. A special characteristic of this kind of flow is that the amplitude of the pulsation has a maximum near the pipe wall at discrete phases during the cycle. The effect is found also experimentally and it is called the “annular effect”. If the flow velocity in the middle of the pipe is decreased rapidly it causes a reversed flow in the wall region. Near the pipe wall the flow velocity gradient has a large slope and if the pressure gradient is negative the direction of the flow velocity is opposed. *Figure 1.2* shows the variation of axial velocity u_{ax} during a half period of a sine function ($w = p/6, p/3, p/2, 2p/3, 5p/6, p$).

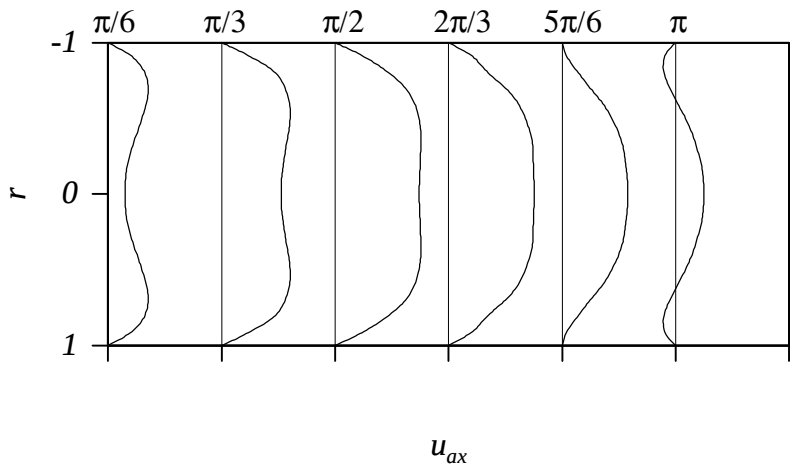

Figure 1.2: Velocity profile in pulsating flow [*25*].

Summing up, as the velocity profile is not steady it is difficult to define a radial position in the pipe where the pressure tap should be positioned in order to measure the flow pulsation of the total cross-section. To average a sector of the cross-section a small slot would be appropriate, however, it results in a complex flow field. Since the diameter of hydraulic pipes is relatively small, the pressure tap would influence the flow and result in a pressure loss. For this reason the pressure taps of the sensors of [*1*] and [*2*], just like the Pitot-tube and Annubar, cause significant problems with the theoretical discussion of these methods. The OPS has no cross-section reduction and the pressure taps are mounted flush on the pipe wall. Consequently, there is a simple correlation between the flow pulsation and the output of the OPS.

1.4 Vibration in hydraulic systems

From the dynamical point of view hydraulic systems are fairly complex [*26*], [*27*], [*28*], [*29*], [*30*], [*31*], [*32*], [*33*], [*34*], [*35*], [*36*], [*37*], [*38*], [*39*]. The vibration can be associated to noise and it can be classified into three groups: fluid born noise, structure born noise and air born noise. The fluid born noise is caused by the unsteady component of the pressure and flow rate. It generates fluctuating forces not only on the piping, but also on the attached components and supporting structures. The vibration of these elements leads to air noise. Based on the operating principle of the hydraulic components (pumps, valves and motors etc.), they produce structural excitation of their body and as a consequence, the supporting structure and the attached piping. They also emit air noise, illustrated in *Figure 1.3*.

With pulsations, the fluid and the pipe are tightly coupled; therefore, their interaction is a complex problem. Leslie and Vardy [*40*] published a review of fluid-structure interaction. They found out that there is a lack of information referring to this topic. This work contains a list of

standards that state the necessity of fluid structure interaction analysis, but do not give any guidance about how to do it.

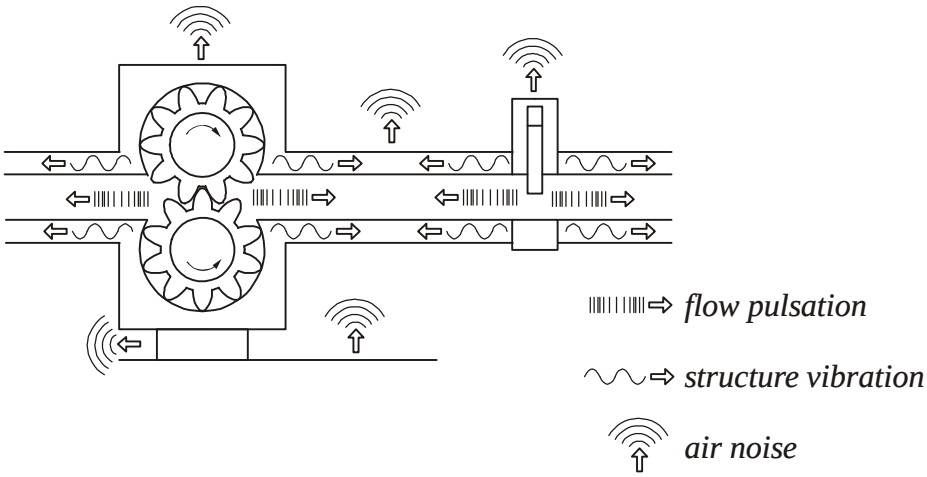

Figure 1.3: Vibration in hydraulic systems.

To perform vibration-free or low-vibration operation an attenuator can reduce the pulsations. Detailed description of pulsation damping methods can be found in the following works [*41*], [*42*], [*43*], [*44*], [*45*].

Also, guidelines concerning vibration in hydraulic engineering applications can be found in [*46*], [*47*], [*48*], [*49*], [*50*].

The reduction of pulsation is an important aim already at the design stage of single hydraulic elements or complete systems. Its reason is not only the noise, which is unwelcome for the machine operator and the surrounding environment, but pulsation is also responsible for many machinery and pipe failures. The advantage of pulsation is that it contains important information about the condition of the system. Hence, pulsation and condition monitoring belong close together.

1.5 Condition monitoring

The scope of condition monitoring is to supply information on the gradual deterioration of a component or system in order to avoid unwanted breakdown and/or system stop. Thus, monitoring the operating condition is, without doubt, important [*51*], [*52*].

The earliest and still applied condition monitoring is the human ear. The most common indication of failure in a system is unusual noise. With appropriate practical experience some special failure sources can be determined based on the type of noise [*53*]:

- air contamination in the system results in a popping and sputtering noise,
- with high speed operation or when a heavy load is applied, a pounding or a rattling noise occurs as the effect of a partial vacuum,
- foreign material in the oil, worn or scored parts or over tightness of some adjustment generates a grinding noise,
- vibrating spring actuated valves, erroneous clamped long pipes or air contamination can cause so called “hydraulic chatter”,
- high frequency vibration in a relief valve or too tight packing around moving parts result in squeals or squeaks.

As the human hearing is limited, needs experience and training and is still subjective, the trouble detection based on this sense organ does not work perfectly.

Mechanical vibrations can be measured with an accelerometer, however, the direct measurement of flow parameters gives more accurate information concerning the condition of the hydraulic systems.

2 Construction and theoretical background of the optical pulsation sensor

The purpose of this chapter is to present the construction and the theoretical background of the optical pulsation sensor [*54*]. One of the most important features is the application of an optical transducer that resulted in a high sensitivity and high natural frequency of the sensor. This method is based on a patent of Chaves et al. [*55*] and it was implemented for our special case. Since, the previous versions of the pulsation sensor had significant effects on the design of the OPS, these versions are presented within this section. The second part of this chapter deals with the theoretical basis of the optical pulsation sensor. First, the pressure difference between two points of an unsteady flow field in a duct is obtained. The model of the bypass of the OPS is evaluated on the basis of the unsteady energy equation, as well.

2.1 Construction of the optical pulsation sensor

The construction of the sensor body is presented in *Figure 2.1*. During the operation of the sensor, the pulsating fluid flows through the device. The sensor has two pressure taps (*1*) and (*2*), mounted flush on the pipe wall to record the pressures. Pulsations are transmitted to the measuring duct via two channels. In the middle of the duct there is a stretched thin foil (*3*), which function is to follow the oscillation of the fluid column. With the assistance of this membrane the differential pressure is transformed into mechanical motion. The surface of the foil is coated thus it works like a mirror, whose deflection is measured by a light beam.

During the design of this sensor extra attention was taken to avoid air contamination in the bypass. Gas bubbles in the measuring tubing have two effects:

- as gas is compressible it works like a pulsation absorber, hence, the dynamic response is deteriorated and
- the bubbles in hydraulic oil behaves like lenses, therefore, they disturb the light beam.

To reduce these disturbances gas contamination must be avoided. For this purpose there are two small diameter tubes (*4*) in the sensor housing where the gas can be removed.

To avoid inconvenient optical effects (on both sides of the lens there should be air), the measuring duct with the oil is separated from the lens by a glass window (*5*).

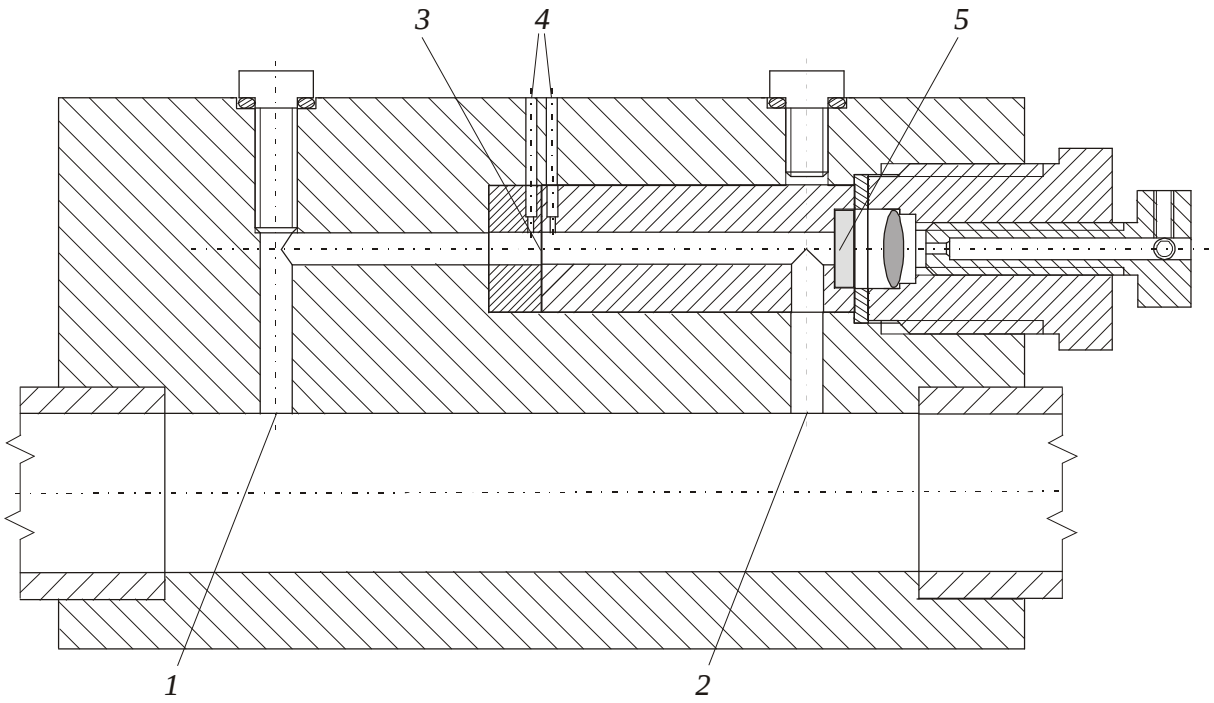

Figure 2.1: Construction of the optical pulsation sensor.

A light beam is pointed onto the circular diaphragm, whose surface has a reflecting coating. Hence, it behaves like a mirror. The reflected light is detected by a photo detector that transforms the optical signal into an electrical one. Without differential pressure the diaphragm is a simple planar mirror. If a differential pressure acts on its surface it is deflected (deformable concave-convex mirror), therefore, the reflected image is modified.

The material of the membrane is elastic, thus even a small pressure difference can cause a relatively large displacement. Although a large displacement is desirable for a given pressure difference this means that the stiffness should be low. This results in a low resonance frequency and corresponding limited frequency response. The resonance frequency depends on the stiffness of the diaphragm and on the moving mass of the fluid. To increase the resonance frequency the foil is pre-tensed. Hence, the deflection is only some tens of a *micrometer*. Nevertheless, the optical system is sensitive enough to detect this small deformation.

The membrane has two functions in the sensor, first it converts the differential pressure into deformation and secondly, it is part of the optical system presented in the *Figure 2.2*. The light beam (*1*) is produced outside the sensor housing and coupled through a condensing lens (*2*) into an optical fibre (*3*). This fibre transmits the light into the sensor housing. Its tip functions as a light source, from where it passes the convex lens (*4*) and reaches the diaphragm (*5*). From here it is reflected, passes the lens again and is coupled into the second optical fibre (*6*). Through this fibre the ray reaches a photo detector (*7*) where the light is transformed into an electrical signal.

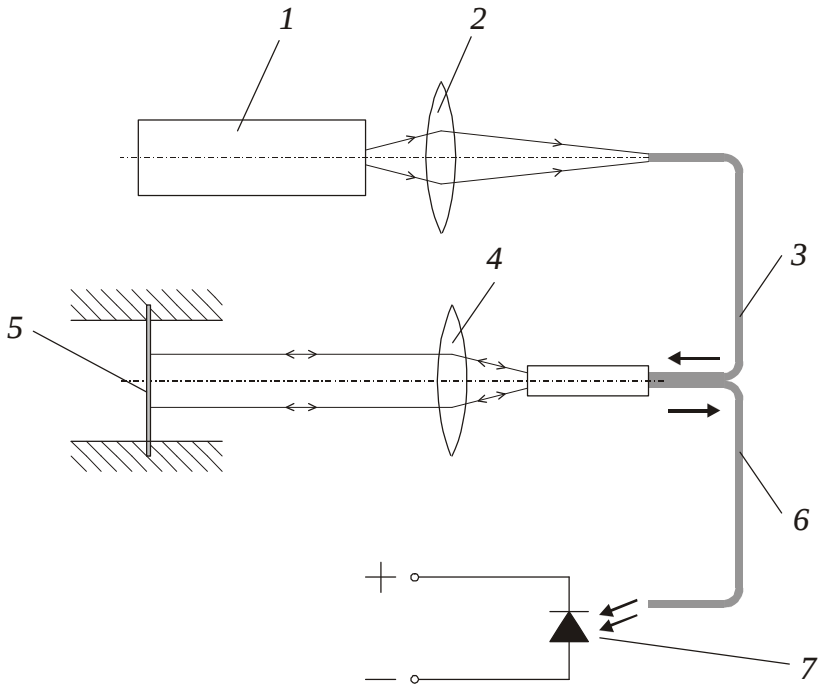

Figure 2.2: Construction of the optics.

2.1.1 Previous versions of the sensor

The first version of the pulsation sensor [*1*], [*56*] had a magnetic transducer with a relatively low natural frequency. The operating principle of this version of the pulsation sensor was based on that of the Pitot-tube. The total pressure was measured at the central hole where the velocity was brought to zero and the static pressure was detected on the wall of the instrument, represented in *Figure 2.3*.

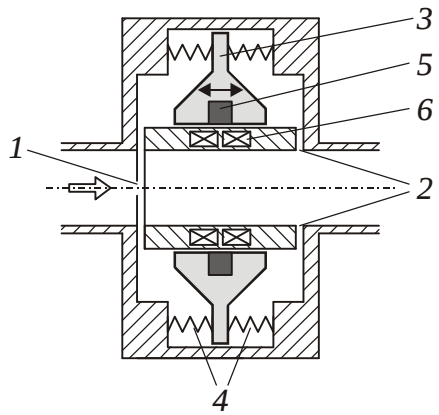

Figure 2.3: Construction of the first version of the pulsation sensor.

A small diameter tube with an opening *(1)* was positioned perpendicular to the main flow to measure the total pressure. The static pressure was measured at different locations *(2)* on the wall and the pressure reading points were connected to the measuring duct. The pressure transducer

was a magnet-coil unit that transformed the flow pulsation into an electrical signal. The two parts of the measuring duct were separated by a disc *(3)*, which was supported from both sides by springs *(4)*. Without a differential pressure the disc was in the middle of the duct, if differential pressure was acting it moved in an axial direction. A ring magnet *(5)* surrounded by a stationary coil *(6)*, was mounted in the disc. Due to the relative motion between the magnet and the coil, voltage was inducted which was the output signal of the sensor.

The main drawback of this version was the weight of the moving disc (*50 g*) that was too heavy to transform the pressure pulsation into an electrical signal.

In the second version [*2*] the pressure taps were positioned similarly to the first version, but the size of the measuring duct, in respect of the diameter of the disc, was reduced. In this way the oscillating weight in the sensor was reduced (*0.56 g*) thus the dynamic response was improved.

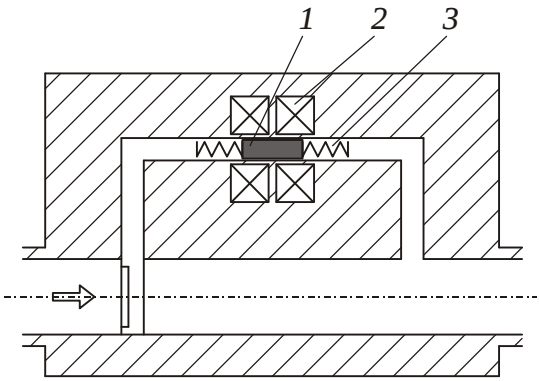

Figure 2.4: Construction of the second version of the pulsation sensor.

As *Figure 2.4* demonstrates the most significant modification was the construction of the pressure transducer. A magnet piston *(1)* was positioned in the middle of the measuring duct that was surrounded by a coil *(2)*. Just like the first version, the moving part was also supported with springs *(3)* from both sides in order to keep its position in the middle of the duct. From the dynamic point of view, a significant improvement of the design was the lower weight of the moving parts. In this sensor there was no disc, the magnet worked like a piston. Beyond this the volume of the oil in the measuring duct was reduced, as well. Nevertheless, the natural frequency of the pressure transducer was only *35 Hz*.

Another problem of both of these versions was the complex pressure distribution at the first pressure tap. Since the perpendicular tube causes a cross-section reduction, it results in, not only a pressure loss, but it also modifies the flow field; thus the measurable pulsation.

The first advantage of the optical pulsation sensor is that the two pressure taps are mounted flush on the pipe wall thus there is no resistance and disturbance in the main flow. The second benefit is the increased natural frequency (*1030 Hz*) that permits a wider range of operation compared to versions [*1*] and [*2*].

2.2 Theoretical background of the optical pulsation sensor

In order to measure the flow pulsation the OPS detects the differential pressure between two locations of an unsteady pipe flow. First, the correlation between the differential pressure and the flow pulsation is discussed which is then followed by the model of the bypass of the OPS.

2.2.1 Correlation between differential pressure and flow pulsation

An unsteady pipe stream of an incompressible medium flows through the OPS, which schematic drawing is presented in *Figure 2.5*.

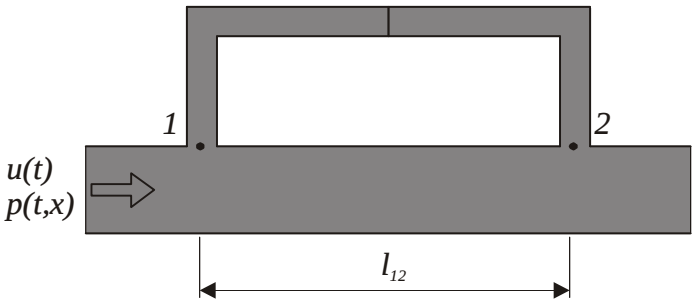

Figure 2.5: Unsteady pipe flow.

The flow velocity u, as well as the pressure p varies according to a harmonic function. Applying the unsteady energy equation [*15*] for the main flow at location (*1)* and (*2)* we get:

$$p_1(t)+\frac{1}{2}r\ u_1^{\ 2}(t)=p_2(t)+\frac{1}{2}r\ u_2^{\ 2}(t)+z\ \frac{1}{2}r\ u_2^{\ 2}(t)+r\int_1^2\frac{\partial u}{\partial t}dl\,, \qquad (2.1)$$

where r is the density of the fluid and z is the loss factor. This equation is reduced to the following form:

$$p_1-p_2=z\ \frac{r}{2}u^2+r\ l_{12}\frac{du}{dt}. \qquad (2.2)$$

The differential pressure between the taps of the OPS is the sum of two terms. The first represents the pressure loss between the two positions due to irreversible effects, such as viscosity, and the second one is the differential pressure caused by the velocity fluctuation.

Since the loss factor is proportional to the distance between the two locations l_{12}, this distance has the same effect on both terms of the right hand side of ***Equation (2.2)***. Increasing the distance results in a proportional increase of both terms. The distance between the pressure taps has effect on the maximal detectable frequency, as well. This method is accurate only if this distance is much less than the wavelength of the measured signal.

The next part deals with the comparison of the values of the first and the second part of the right hand side of ***Equation (2.2)***. The variation of the flow velocity can be written as a function of time according to:

$$u(t) = u_0 + u_A \sin(w\ t), \qquad (2.3)$$

where u_0 is the steady flow velocity and u_A represents the amplitude of the velocity pulsation. The derivative of *Equation* (*2.3*) is:

$$\frac{du}{dt} = u_A w \cos(w\ t). \qquad (2.4)$$

As ***Equation (2.4)*** shows the last term of ***Equation (2.2)*** is proportional to the pulsation frequency. The purpose of the OPS is to measure pulsation that means the frequency of the detected signal is larger than *1 Hz*. If the frequency is increased the last term of ***Equation (2.2)*** becomes significantly higher than the first one.

The ratio of the amplitude of the velocity pulsation to the steady flow velocity can be classified into the following three cases:

- $\frac{u_A}{u_0} < 1$: the steady flow velocity is higher than the amplitude of the velocity pulsation.

  The first term of the right hand side of ***Equation (2.2)*** results in a pressure loss proportional to the steady flow velocity. The differential pressure pulsation between the two locations is generated by the unsteady flow fluctuation. Detecting the first mentioned pressure loss gives the steady flow velocity while the measurement of the pressure fluctuation provides information concerning the flow pulsation.
- $u_A = u_0$: the amplitude of the velocity pulsation is equal to the steady flow velocity. As the pulsation frequency is increased the last term of *Equation* (*2.2*) becomes sufficiently higher compared to the other term. Therefore, the differential pressure is proportional to the pulsation velocity.
- $\frac{u_A}{u_0} > 1$: the amplitude of the velocity pulsation is larger than the steady flow velocity. In this case, the pressure loss caused by the first term of *Equation* (*2.2*) is also negligible compared to the second one.

If the first term of *Equation* (*2.2*) is negligible compared to the other one, it results in:

$$p_1 - p_2 = r\ l_{12}\frac{du}{dt}. \qquad (2.5)$$

Hence the differential pressure measured between location *(1)* and *(2)* is the function of the unsteady flow velocity pulsation, the fluid density and the distance between the pressure taps. This differential pressure has to be measured with the pressure transmitter to obtain information concerning the flow pulsation, defined by:

$$Q = Au = A\frac{1}{r\ l_{12}}\int (p_1 - p_2)\ dt, \qquad (2.6)$$

where A is the cross-section area of the duct.

2.2.2 Model of the bypass of the OPS

In order to determine the dynamic response of the OPS, the governing equation of the bypass is brought to a simple form. For this analysis the OPS is divided into three parts (main flow, left and right side of the bypass), illustrated in *Figure 2.6*.

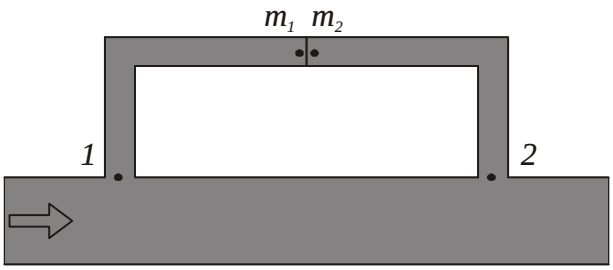

Figure 2.6: Schematic drawing of the bypass.

At position *(1)* the pressure is p_1 and at position *(2)* it is p_2. The membrane separates the bypass into two parts and due to the pressure difference between p_1 and p_2 it is deformed.

The unsteady energy equation between location *(1)* and *(m1)* can be written in the following form:

$$p_1(t) + \frac{1}{2} r\ u_1^2(t) + r\ gh_1 = p_{m1}(t) + \frac{1}{2} r\ u_{m1}^2(t) + r\ gh_{m1} + z\ \frac{1}{2} r\ u_{m1}^2(t) + r \int_1^{m1} \frac{\partial u}{\partial t} dl. \qquad (2.7)$$

The flow velocity has the same value along the bypass, thus the previous equation reduces to:

$$p_1 - p_{m1} = z\ \frac{r}{2} u^2 + r\ l_{1m1}\frac{du}{dt} + r\ g(h_{m1} - h_1). \qquad (2.8)$$

where l_{1m1} is the distance and h_{m1}-h_1 is the elevation difference between location *(1)* and *(m1)*.

Applying energy equation for the second part of the bypass, this leads to:

$$p_{m2}(t)+\frac{1}{2}r\ u_{m2}{}^2(t)+r\ gh_{m2}=p_2(t)+\frac{1}{2}r\ u_2{}^2(t)+r\ gh_2+z\ \frac{1}{2}r\ u_2{}^2(t)+r\int_{m2}^{2}\frac{\partial u}{\partial t}dl,$$

(*2.9*)

which can be written as:

$$p_{m2}-p_2=z\ \frac{r}{2}u^2+r\ l_{m22}\frac{du}{dt}+r\ g(h_2-h_{m2}).$$

(*2.10*)

On the left side of the membrane the pressure is p_{m1} while on the other side it is p_{m2}. The differential pressure acting on the membrane is:

$$dp_{m12}=p_{m1}-p_{m2}.$$

(*2.11*)

The deflection of the membrane *w* under this load is discussed in the next chapter.

Substituting *Equation* (*2.11*) into (*2.8*) gives:

$$p_1-dp_{m12}-p_{m2}=z\ \frac{r}{2}u^2+r\ l_{1m1}\frac{du}{dt}+r\ g(h_{m1}-h_1)$$

(*2.12*)

and *Equation* (*2.10*) into (*2.12*) yields:

$$p_1-dp_{m12}-p_2-z\ \frac{r}{2}u^2-r\ l_{m22}\frac{du}{dt}-r\ g(h_2-h_{m2})=z\ \frac{r}{2}u^2+r\ l_{1m1}\frac{du}{dt}+r\ g(h_{m1}-h_1).$$

(*2.13*)

After rewriting and eliminating the height difference the following equation is obtained:

$$p_1-p_2=dp_{m12}+z\ \ r\ u^2+r\ l_{1m1m22}\frac{du}{dt},$$

(*2.14*)

where l_{1m1m22} represents the length of the bypass. The differential pressure acting on the membrane is defined as the ratio of membrane force F_m and of membrane area *A*:

$$dp_{m12}=\frac{F_m}{A}.$$

(*2.15*)

F_m is the product of the spring constant k_m (a detailed description of this parameter is given in the next chapter) and the average membrane deflection w_a :

$$F_m=k_m w_a.$$

(*2.16*)

Thus, the differential pressure acting on the membrane is:

$$dp_{m12}=\frac{k_m w_a}{A}.$$

(*2.17*)

To evaluate the exact value of the loss factor *z* in case of unsteady flow in the bypass, experimental measurement is necessary. Since the dimensions of the bypass (l_{1m1m22} = *80 mm*, *d = 3 mm*) are minor, it is complicated to determine experimentally the loss factor. For this

reason, the loss factor is determined based on the steady laminar flow conditions. In a straight duct with constant cross-section it is given by [*15*]:

$$z = \frac{64m\ l}{ud^2 r}. \qquad (2.18)$$

The loss factor has a value of *0.95* in the case of a branch line where the flow is split up into two parts and *–1.2* where two parts flow together (negative sign means a gain of pressure). In case of a *90°* bend it is equal to *1.12* [*57*]. The sum of these loss factors is much smaller than the loss factor of the piping in the bypass determined by *Equation* (*2.18*). For this reason the losses by the branch lines and the bends are neglected.

Multiplying *Equation* (*2.14*) with the cross section area of the bypass *A* results in:

$$A(p_1 - p_2) = Ar\ l_{1m1m22}\frac{du}{dt} + Az\ \ r\ u^2 + Adp_{m12}. \qquad (2.19)$$

Combining *Equation* (*2.17*), (*2.18*) and (*2.19*) leads to:

$$A(p_1 - p_2) = m\frac{du}{dt} + 8pm\ l_{1m1m22}u + k_m w_a, \qquad (2.20)$$

where *m* represents the mass of the oil in the bypass. The differential pressure acting on the bypass can be considered as an excitation force, which is represented by the left hand side of *Equation* (*2.20*). The other side has three terms; the first is proportional to the acceleration, the second one to the velocity and the last to the displacement.

3 Membrane

The conversion of the pressure signal into an electrical one is completed with an opto-mechanical transducer. Its principal component is the membrane, an analysis of which is presented in this chapter. First, the theoretical background of the membrane design is performed; deflection and stresses are determined. To apply these results to the practice, the material properties of the membrane had to be known. As these parameters were not provided from the manufacturer of the membrane, they were self-measured.

When designing the membrane two important parameters have to be considered. In order to meet the requirements of sensitivity, a low stiffness of the diaphragm is preferred. In addition, the deflection should be low enough so that the membrane can sustain high-pressure differences. Low membrane stiffness reduces the natural frequency of the system. However, the detection of minor deflections is more complicated. To solve this contradiction an optimum should be found. The diaphragm is pre-tensed, but its deformation under pressure remains elastic to avoid residual damage of its material.

To check the results of the theoretical analysis of the membrane, its deflection is measured with an interferometer. The surface of the membrane is coated with silver; hence, it works like a flexible mirror. From the optical point of view the radius of the curvature of this mirror is an essential factor. This examination is presented also in this section. Finally, the natural frequency of the membrane-oil system is determined.

3.1 Membrane deflection

A membrane is basically a two-dimensional system just like a flat plate, however it can easily be bent due to its low stiffness. Based on this fact, the deflection w can be high compared to the material thickness h ($w / h > 5$). To support a lateral load, the edge of the membrane has to be clamped. In order to increase this load-supporting capacity the membrane must have initial tension.

In this work the solution of Sheplak et al. [*58*], [*59*] is used that provided the deflection w of the clamped, pre-tensed membrane in the following form:

$$w(r)=\frac{12\left(1-n_P{}^2\right)pR^4}{k_t{}^2Eh^3}\left(\frac{J_0\left(\frac{k_t r}{R}\right)-J_0(k_t)}{2k_tJ_1(k_t)}+\frac{R^2-r^2}{4R^2}\right), \tag{3.1}$$

where n_P - Poisson's ratio

p - uniformly distributed load (pressure)

R - radius of membrane

k_t - tension parameter

E - modulus of elasticity of the membrane material

h - membrane thickness

J_0 , J_1 - Bessel functions

r - radial distance.

The tension parameter is defined as:

$$k_t=\frac{R}{h}\sqrt{\frac{12\left(1-n_P{}^2\right)N_0}{Eh}}, \tag{3.2}$$

where N_0 is the initial tension.

3.2 Membrane stresses caused by differential pressure

Sheplak [*59*] defined the radial and tangential stress on the topside of the membrane as:

$$s_{rdp}(r)=\frac{3pR^2}{h^2}\left(\frac{n_P+1}{k_t{}^2}-\frac{J_0\left(\frac{k_t r}{R}\right)}{k_tJ_1(k_t)}-\frac{R(n_P-1)J_1\left(\frac{k_t r}{R}\right)}{rk_t{}^2J_1(k_t)}\right), \tag{3.3}$$

$$s_{tdp}(r)=\frac{3pR^2}{h^2}\left(\frac{n_P+1}{k_t{}^2}-\frac{n\ J_0\left(\frac{k_t r}{R}\right)}{k_tJ_1(k_t)}-\frac{R(n_P-1)J_1\left(\frac{k_t r}{R}\right)}{rk_t{}^2J_1(k_t)}\right). \tag{3.4}$$

3.3 Material properties of the membrane

To avoid any residual damage to the diaphragm material during the operation in the sensor, the stress distribution in the pre-tensed and lateral loaded membrane has to be obtained. To accomplish this, the mechanical properties of the membrane have to be determined from a tensile test [*60*].

Based on the geometry of the test material and the measured tensile force, the elastic stress s_e was determined and has a value of *59 MPa*. The strain e_e belonging to the limit of elasticity was established from the recorded displacement and is equal to *0.594 %*. According to the Hooke's law the modulus of elasticity is:

$$E = \frac{s_e}{e_e} \qquad (3.5)$$

and has a value of *10000 N/mm*^{2}. This is the upper limit that the material of the membrane sustains without any residual damage.

During the operation of the sensor the membrane has two loads, the first is from the pre-tension s_0 and the second one is caused by the differential pressure s_{dp}. The maximal differential pressure acting on the diaphragm was defined at *50 mbar*. To avoid residual deformation the following condition must be fulfilled:

$$s_e > s_0 + s_{dp}. \qquad (3.6)$$

3.4 Pre-tension of the membrane

Before determining the exact value of the initial tension, a self-developed technique is described to produce this loading. First, the membrane material was clamped between two rings to obtain a planar surface, *Figure 3.1 a*. In the second stage the membrane was loaded with a weight (*1*) to produce the required initial tension *Figure 3.1 b*. After this the membrane-supporting ring (*2*) was fixed onto the foil (*3*) with a thin layer of glue, illustrated in *Figure 3.1 c*.

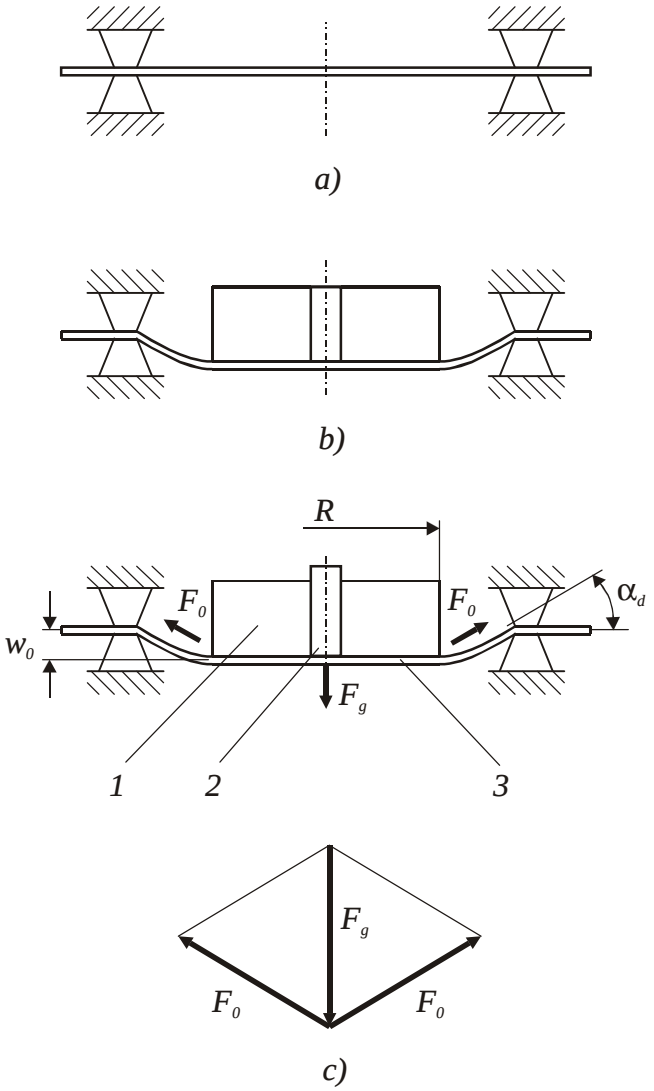

Figure 3.1: Pre-tension of the membrane.

The weight causes a distributed load on the membrane and it can be replaced with concentrated force F_g acting at the membrane centre. *Figure 7.1 c* illustrates the equilibrium of forces acting on the system. The tensile force is calculated on the basis of the following equation:

$$F_0 = \frac{F_g}{2\sin a_d}, \qquad (3.7)$$

where a_d is the angle of deflection. This force is acting on the membrane at the radius of the ring *R*, and results in a tension given by:

$$N_0 = \frac{F_0}{2Rp}. \qquad (3.8)$$

At every point of the membrane where the radial distance is smaller or equal to the radius $r \pounds R$, the stress is constant [*61*] and defined as:

$$s_0 = \frac{N_0}{h}, \qquad (3.9)$$

where h is the membrane thickness. Having the value of the initial stress, the total stress distribution of the membrane can be determined:

$$s = s_0 + s_{dp}. \qquad (3.10)$$

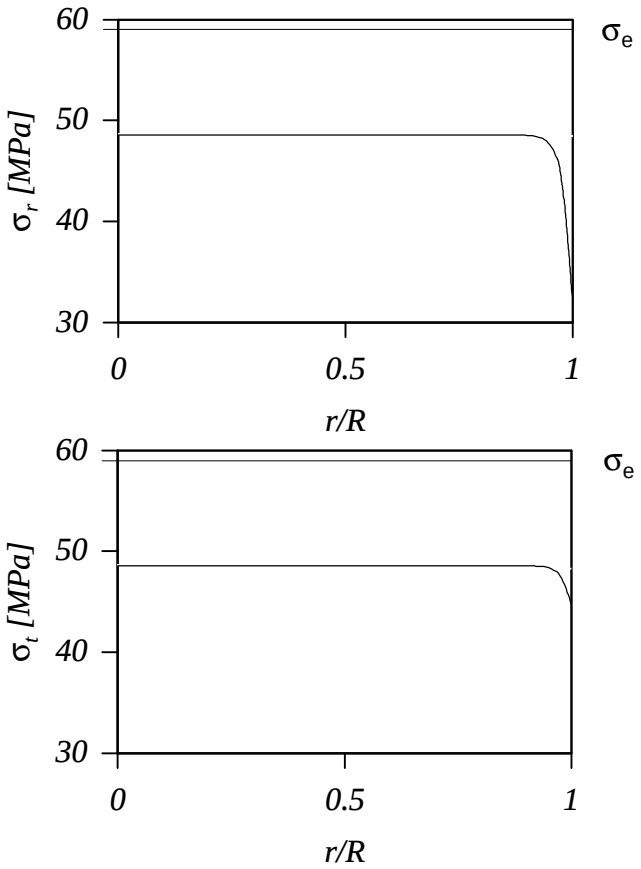

Figure 3.2: Total stress of the pre-tensed lateral loaded membrane.

As *Figure 3.2* shows, at a differential pressure of *50 mbar*, the total stress is lower than the limit of elasticity s_e.

3.5 Measurements of the membrane deflection

In the first part of this chapter the theoretical deflection of the membrane is determined. To check this result the true deformation of the diaphragm had to be measured. A method had to be found, which was suitable to detect the deflection of some *micrometers*. Interferometry proved to be the right solution. The advantage of this technique is its high resolution, hence very small displacements can be measured. With the interferometry not only the deflection of the membrane could be determined, but also the optical quality of this surface. As the membrane works also as a mirror it is important that it has symmetrical deformation and that there are no surface irregularities.

Michelson made the first basic design for an interferometer for measuring purpose [*62*], [*63*] and this method was adapted to measure the membrane deflection. The self-made set-up is illustrated in *Figure 3.3*.

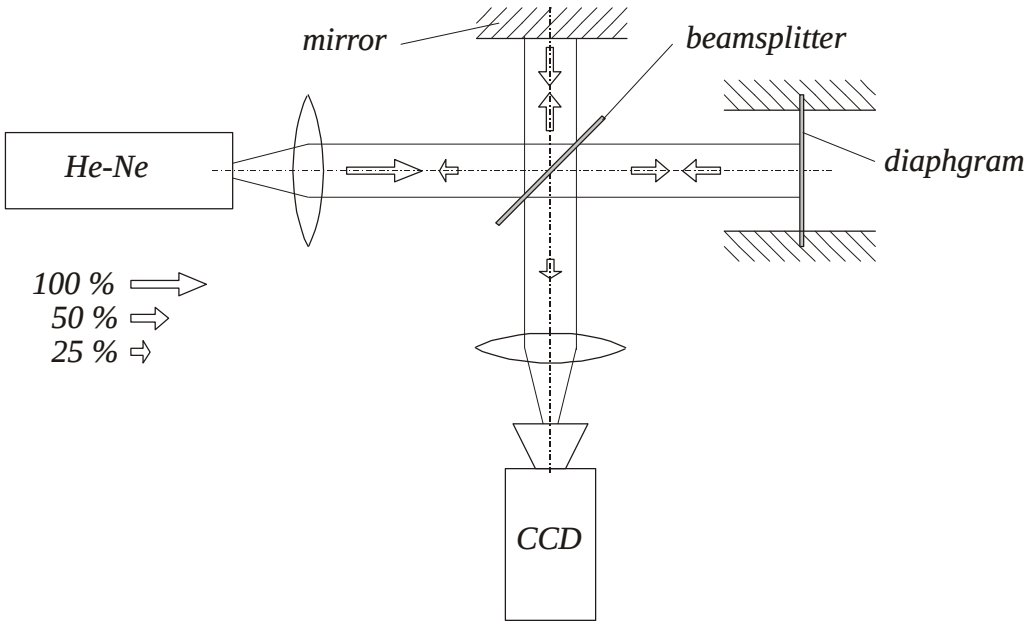

Figure 3.3: Construction of the interferometer.

The beam from the laser source is split off with a beamsplitter into two components (*50 : 50 %*). The part that passes straight through reaches the diaphragm, which reflects the light back to the splitter. The reflected beam passes again the splitter, one half passes straight through and the other half (*25 %* of the original light) is reflected. The reflected and the original beam from the laser source are combined. As the light is of a single wavelength, fringes form all along the optical axis of the combined beam, with a perpendicular orientation to the axis. A CCD

camera records the periodic intensity variation related to the phase difference of the combined waves.

In our measurement the membrane worked as a mirror, which was deflected due to differential pressure acting on its surface. The differential pressure was generated just like the static calibration of the sensor (see Chapter 5). Some typical interference pictures are presented in *Figure 3.4*.

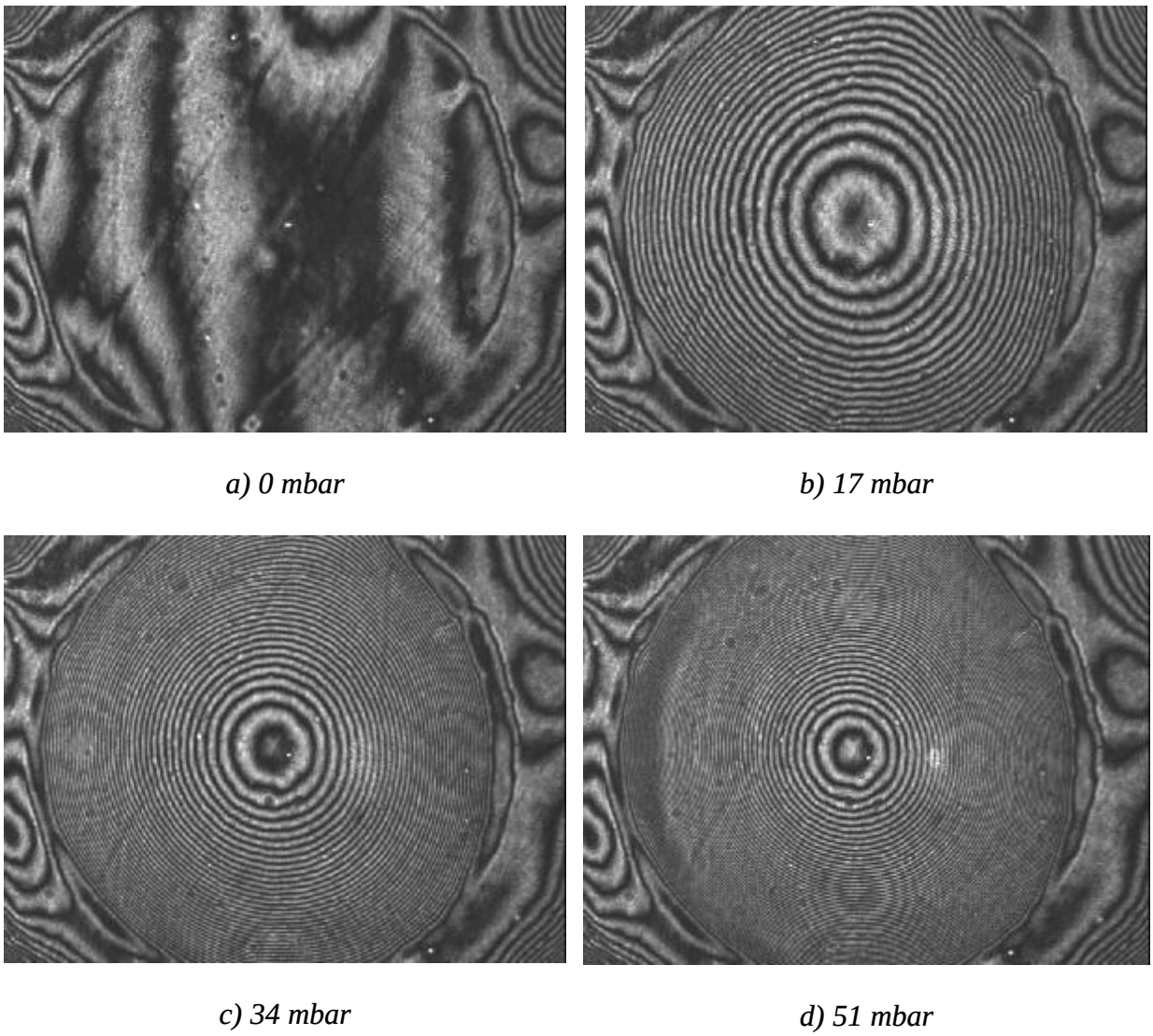

a) 0 mbar *b) 17 mbar*

c) 34 mbar *d) 51 mbar*

Figure 3.4: Images of interferometry.

As the figure shows, the fringes appear as light and dark rings surrounding the central image of the light source. The optical path difference between two dark or light rings is equal to half of the wavelength ($l/2=316.4\ nm$). If the membrane has a perfect planar surface the image would not have fringes. As this is not the case so fringes appear. Any axial deflection of the membrane causes the rings to shift. Counting the number of fringes makes it possible to measure this deformation.

With the interferometry images the whole surface of the membrane can be observed. These show some problems of the membrane and its supporting ring. During gluing the foil onto the surface of the membrane-supporting ring, it was covered with a thin layer of glue where the membrane was pressed with an appropriate force to produce an initial tension in the membrane material. Due to this load a small amount of adhesive material was pressed out from the layer between the membrane and the ring and it made the boundary region non-planar. This problem could happen even with a very thin layer of glue and it resulted in asymmetry along the edge, which disturbed the optical measurements. To avoid the disturbing effect of this boundary region it was shifted outside of the optical effective area of the membrane surface A_E illustrated in *Figure 3.5*.

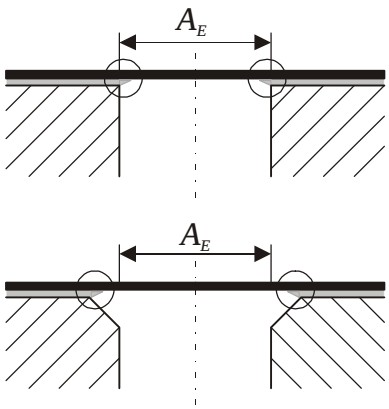

Figure 3.5: Optical effective membrane surface.

For this purpose the diameter of this ring was increased (it was larger than the diameter of the light beam), thus the optical effective membrane area had a perfect planar surface.

The results of the theoretical and experimental solutions of the deflection of the membrane at three different values of differential pressure are presented in *Figure 3.6*. As the diagram shows, the theory of Sheplak [*59*] describes the deflection exactly.

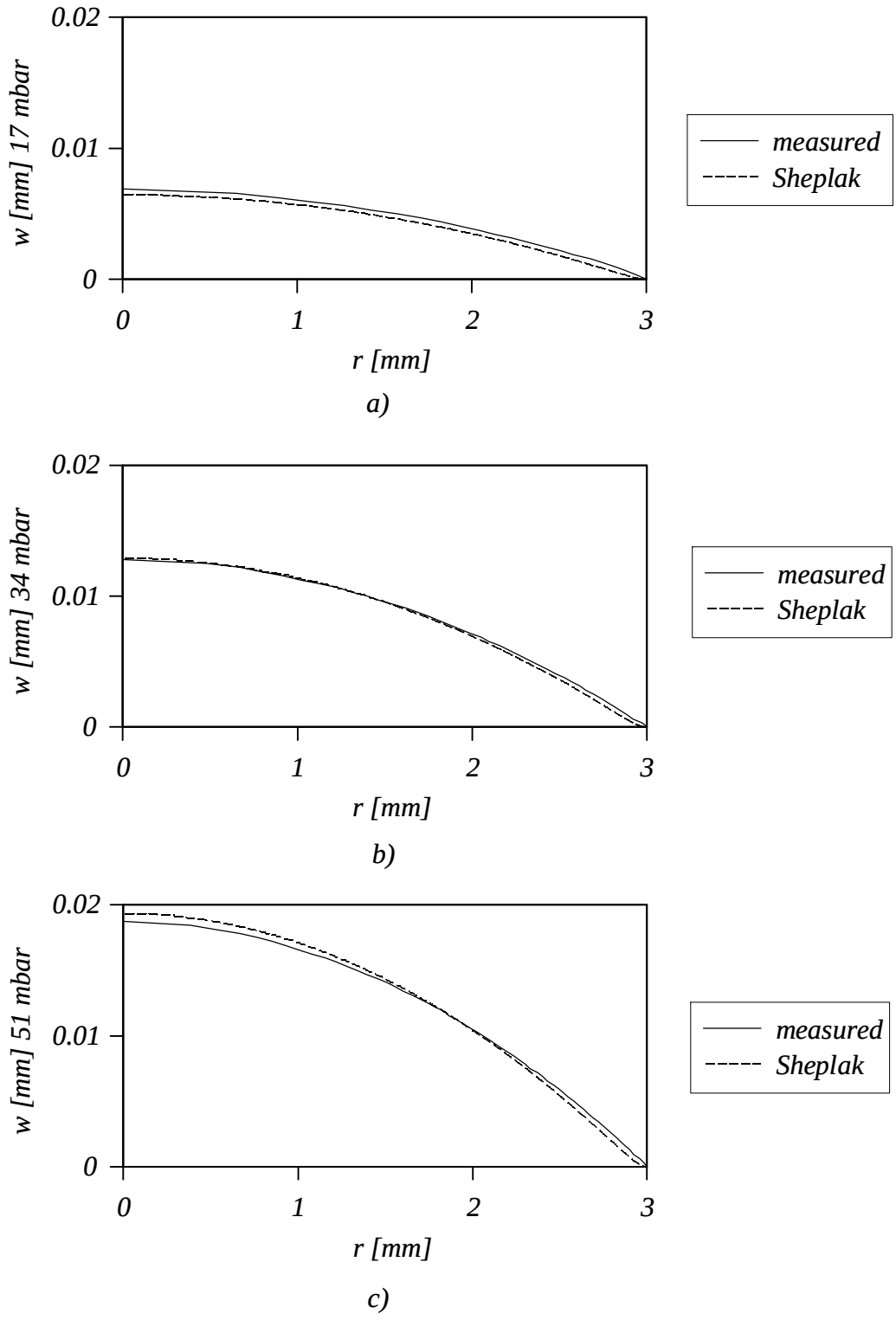

Figure 3.6: Measured and calculated membrane deflection.

3.6 Radius of curvature of the deflected membrane

In order to examine the mirroring characteristic of the diaphragm the radius of curvature was determined. The radius of curvature r_c of a function *f(x)* can be approximated applying the following equation [*60*]:

$$r_c = \frac{1}{\frac{d^2 f(x)}{dx^2}} \quad . \tag{3.11}$$

Substituting *Equation* (*3.1*) into (*3.11*) the curvature of the pre-tensed membrane can be calculated. Plotting the results by different values of the tension parameter, two effects are observed in *Figure 3.7*.

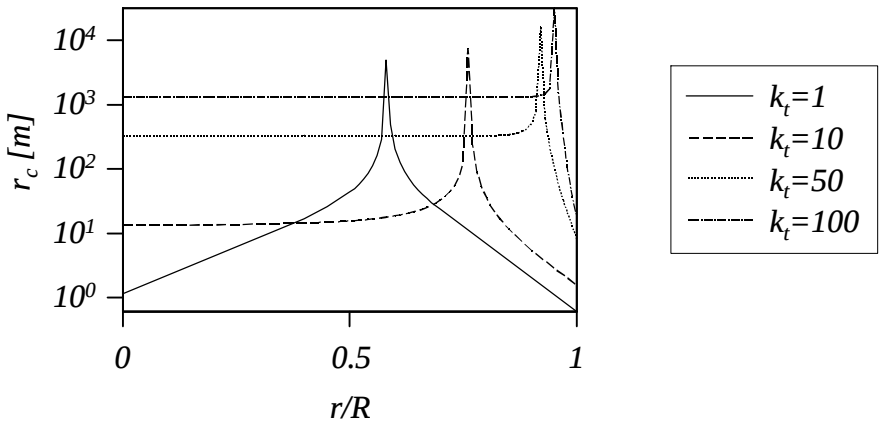

Figure 3.7: Radius of curvature as a function of the tension parameter.

Higher initial tension results not only in a larger radius of curvature, but also in the inflection points moving towards the periphery. Even for a low tension parameter ($k_t = 50$) the radius of the curvature at the central region ($r_c = 300\ m$) is much higher than the diameter of the membrane ($d = 6\ mm$). This feature, see next chapter, had an effect on the optical tracing calculation.

3.7 Natural frequency of the OPS

The governing equation of the OPS was discussed in the previous chapter. The best set-up for picking pressure pulsations is a flush mounted membrane at the pressure source, in our case on the wall of the main pipe. Connecting tubing or other fittings between the pressure source and the sensing element degrades the dynamic performance.

In this section first the natural frequency of a circular clamped membrane without tubing is determined, which is followed by the analysis of the tubing.

3.7.1 Natural frequency of the membrane

The lowest natural frequency of a circular membrane with a clamped edge is given by [*64*]:

$$f_n = \frac{10.18}{2p}\frac{1}{R^2}\sqrt{\frac{Eh^3}{12\left(1-n_P{}^2\right)}}{r\ h}. \qquad (3.12)$$

In our case this value (*1030 Hz*) is above the operation range of the OPS, however, the effect of the tubing should also be considered.

3.7.2 Natural frequency of the membrane-oil system

In the dynamical analysis of the bypass, the elasticity of the fluid and the mass of the membrane was neglected. Using the basic free vibration equation the natural frequency of the membrane-oil system is [*64*]:

$$f_{mo} = \frac{1}{2p}\sqrt{\frac{k_m}{m_o}}, \qquad (3.13)$$

where m_o is the mass of the oil, which is in the bypass of the sensor. The spring constant k_m represents the resistance of the membrane against the average value of deflection w_a:

$$k_m = \frac{F_m}{w_a}. \qquad (3.14)$$

To determine the spring constant, it is necessary to know the force acting on the membrane F_m that can be expressed as the product of the pressure p and the membrane surface A:

$$F_m = pA. \qquad (3.15)$$

For proper operation it is important that the natural frequency of the sensor should be higher than the frequency of the measured signal. To fulfil this condition the spring constant should be large and the oil mass should be as small as possible. The spring ratio can be increased by increasing the initial tension i.e. strain e_t of the membrane. The upper limit for this process is the elasticity limit of the membrane material s_e. The disadvantage of the increased initial tension is the reduced deflection, i.e. reduced sensitivity. In *Figure 3.8* the effect of the pre-tension on the deflection, spring constant and natural frequency are illustrated as a function of the pressure acting on the membrane. Without initial tension (e_t = *0 %*) the deflection at the centre of the membrane is large, the correlation between deflection and pressure is not linear. Both the spring ratio of the membrane and the natural frequency of the membrane-oil system is low. Increasing the initial tension results in a linear correlation between deflection and pressure. In addition, the

spring ratio and the natural frequency is increased as well. In the OPS the peripheral deformation is *0.36 %* and it causes a small deflection, but a high natural frequency (*1030 Hz*).

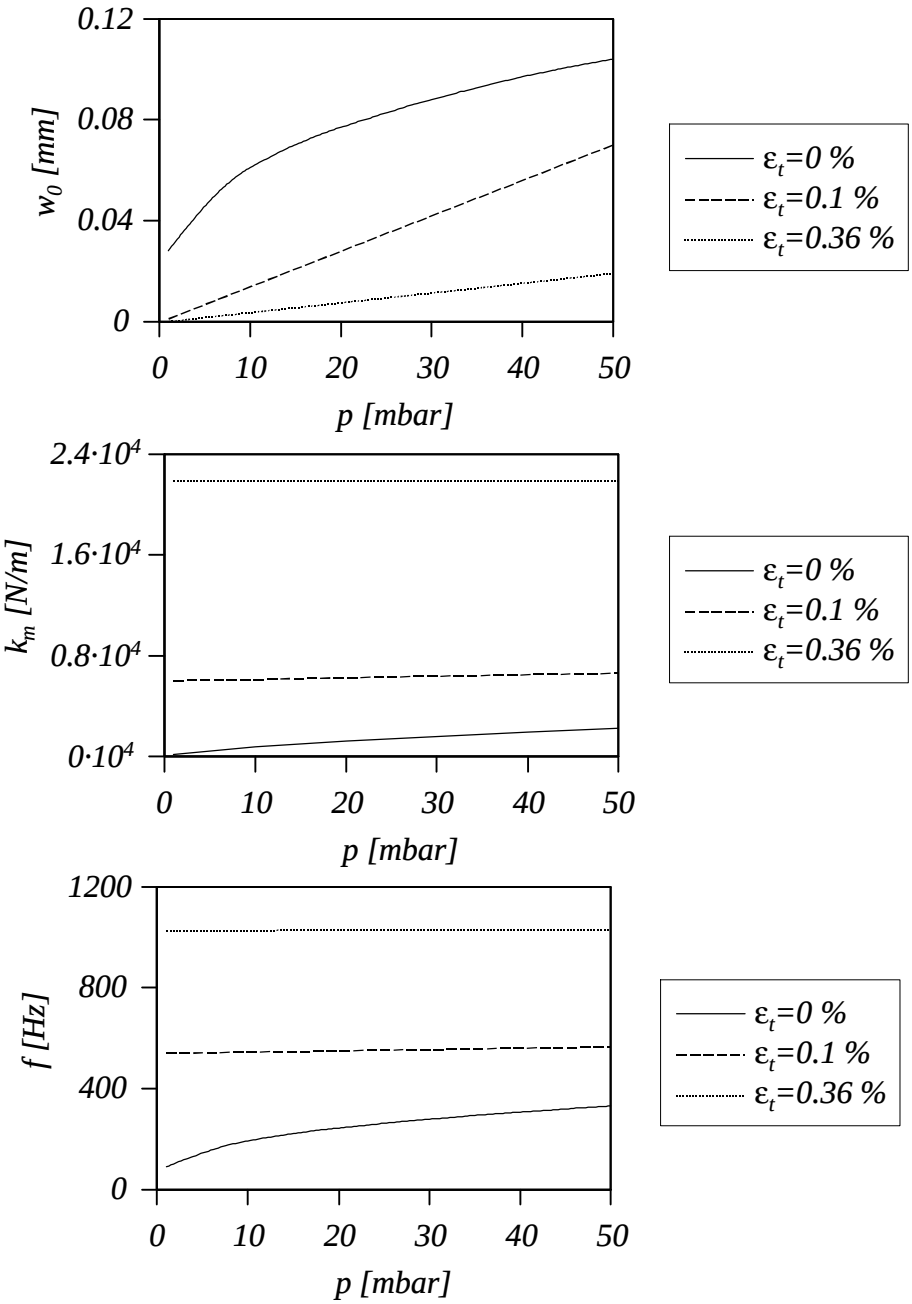

Figure 3.8: Effect of the pre-tension on the natural frequency.

Another way to increase the natural frequency is the reduction of the mass of the oil m_o that is proportional to the tubing length; hence, the tubing should be as short as possible. The probe measures the differential pressure between the pressure taps and if the distance between these points is reduced, which means that the detected differential pressure is lower, the transducer should be more sensitive.

4 Optics

This section deals with the optical design of the pressure transducer in the sensor. It is a new kind of pressure sensing element based on a simple optical method already discussed in Chapter 3. In the first part there is a detailed description of the special optical features, which should be considered to improve the performance of the optical system. The intensity distribution perpendicular to the direction of propagation is not constant which effect is also investigated in this chapter. The problem of light absorption becomes significant when the light has to pass through the oil. For this reason this problem is analysed as well. Finally, the optical characteristics of the applied optical elements are the described and optical tracing is performed.

4.1 Optical fibre

The optical sensitivity of the sensor depends inherently on the size of the light source and the size of the detector. High sensitivity was achieved by using the tips of two light fibres as a light source and a detector (its diameter is only *125 mm*). A further advantage of this procedure was that both the “true” source and the detector are placed outside of the sensor housing.

In order to couple a large amount of light into a thin optical fibre one has to use a laser. Conventional light sources cannot be focused to such a small size. To achieve high optical quality (circular beam profile and low divergence angel) a He-Ne laser was used with a wavelength of *632.8 nm*.

The light is conducted in and out of the housing with optical fibres, the construction of a fibre is illustrated in *Figure 4.1*.

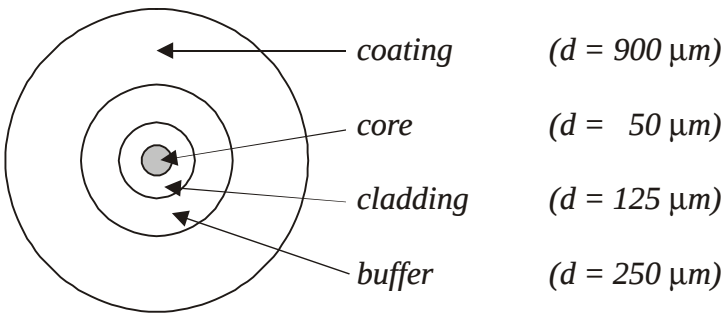

Figure 4.1: Typical fibre construction.

The optical fibre wave-guide is made of a glass core surrounded by a cladding. As the reflection index of the core is higher than the one of the cladding the light is guided by the fibre. The outer

layers of the cable protect the core against mechanical damage. Our experiments showed that the fibre should be isolated with an extra coating in order to avoid disturbances caused by external light.

While in the housing of the sensor there is no risk of mechanical damage, the two outer layers of the cable were stripped off. This way the diameter of the fibre was reduced to *125 mm*. This had a positive effect on the operation of the sensor.

The relative position of the fibres to each other had an important effect on the sensor operation. In the first version the two-fibres were placed into a tube as illustrated in the *Figure 4.2 a*. After a detailed optical analysis and experimental testing of the optics, the two-fibres were fixed into a second tube with an inner diameter which was equal to the diameter of the two-fibres, see *Figure 4.2 b*. In this way the fibres had a defined location to each other. The positioning of the source-detector unit relative to the lens is discussed in Chapter 5.

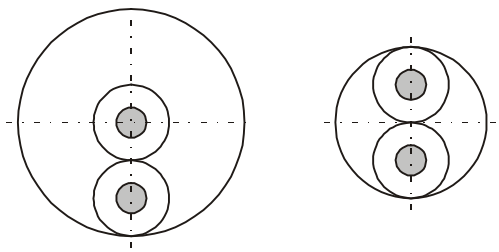

a) *b)*

Figure 4.2: Position of the optical fibres in the source-detector unit.

To increase the efficiency of the optical system the laser beam from the tube had to be focused with a condensing lens onto the optical cable. The focal distance of the lens can be determined from [*65*]:

$$l_f \approx \frac{d_f p \; d_b}{4 l}, \qquad (4.1)$$

where d_f - diameter of the optical fibre

d_b - diameter of the laser beam

l - wavelength of the laser.

Applying this equation to our case a lens with a focal distance of *10 mm* had to be used. In this manner most of the power of the laser beam was coupled into the optical fibre.

4.2 Intensity distribution in the beam

The intensity distribution within the beam of a He-Ne laser has a Gaussian profile, which means that the intensity in the beam's cross-section is not constant. The normalised intensity distribution I_b in the plane perpendicular to the direction of propagation can be expressed as [*66*]:

$$I_b(r) = e^{-\frac{2r^2}{r_b^2}}, \qquad (4.2)$$

where r is the distance from the centre of the beam and r_b is the beam radius. This beam radius is equal to the radial position; where the beam intensity falls to $1/e^2$ of its maximum value, see *Figure 4.3*.

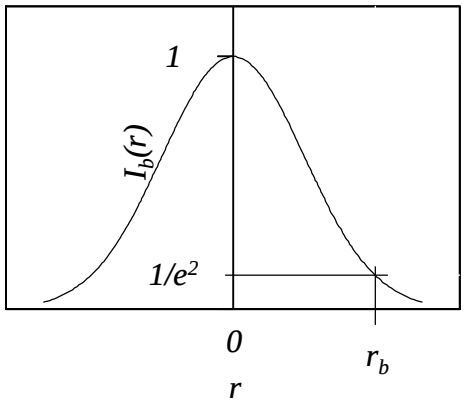

Figure 4.3: Normalised intensity distribution within the laser beam.

There are two conditions for the detection of the maximal intensity signal A_{Imax}:

- the reflected image should be mapped exactly by the sensing area of the detector and
- the image radius r_i should be smaller or equal to the detector radius r_d.

If these conditions are not fulfilled then the image is mapped in front of or behind the detector hence the image radius is larger than the radius of the detector. In this case the measured detector signal A_{Id} is lower. As *Figure 4.4* shows this can result in significant losses, which is even larger if the image is mapped to the right or to the left side of the optical axis.

When applying a one-fibre system, then there is no misalignment, the centre of the reflected beam and the detector coincide. Two-fibres system results in an unsymmetrical construction, hence, the maximum of the intensity distribution does not overlap the centre of the detector. In this case the intensity loss is even higher. The presented analysis demonstrates how important it is that the reflected image is projected to the detector.

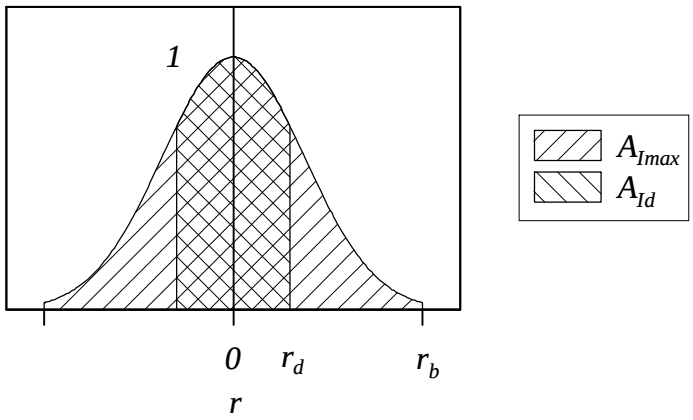

Figure 4.4: Partially detected optical signal.

4.3 Light absorption in hydraulic oil

During the operation of the sensor, the light beam leaves the optical fibre, propagates a short distance in the air and then enters into the hydraulic oil. The beam has to cover a distance of more than *60 mm* in the oil before returning back to the second optical fibre. During its path in the oil a significant part of the laser light is absorbed.

The optical properties of hydrocarbons vary from oil to oil and depend on many parameters (crude or refined oil, with or without sediment etc). In our experiments HLP *46* hydraulic oil is the working fluid that has a light brown colour. In common industrial application the optical characteristics of hydraulic oil are not important, therefore, the oil producers do not provide the optical parameters. In our application this factor has an important effect, therefore, it had to be determined.

The measurement of the light absorption coefficient was performed in two stages. In the first step the laser beam propagated in the air, it was reflected from the membrane and returned back to the detector, see *Figure 4.5 a*. The detected intensity was independent of the distance *x*. In the second stage the beam travelled in the working medium, see *Figure 4.5 b*. Due to the absorption coefficient of the oil the detected intensity decreased with increasing distance *x*.

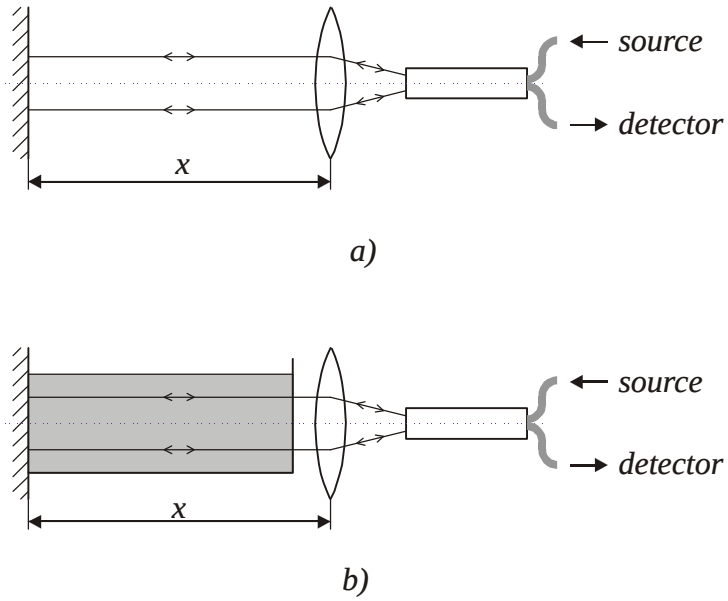

Figure 4.5: Measurement of light absorption.

The Beers´ law [*67*] describes the light absorption in a medium as:

$$I(x) = I_0 e^{-ax}, \qquad (4.3)$$

where I - light intensity

x - distance

I_0 - light intensity at $x = 0$

a - coefficient of absorption.

The result of the measurement for the coefficient of absorption was *0.022 1/mm*. *Figure 4.6* shows the light intensity versus the distance of the light in the oil. At a distance of *60 mm* a significant part (*75 %*) of the light is absorbed.

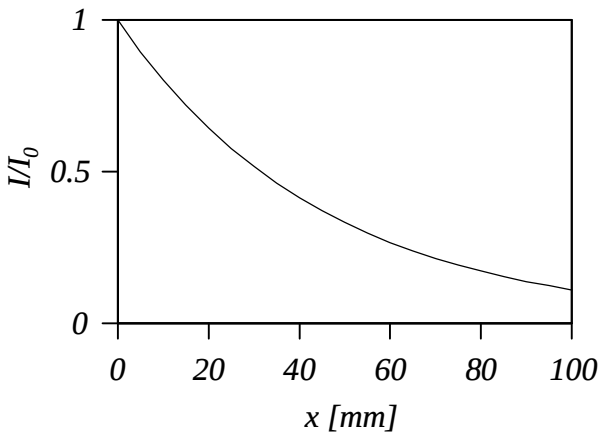

Figure 4.6: Normalised light absorption in oil.

4.4 Optical tracing

An optical analysis of the system composed of a source-lens-mirror-detector allows the determination of the optimal optical characteristic of the sensor. The term “source” and “detector” denote the tips of the optical fibres, which are fixed within the housing of the OPS.

When investigating the image position and magnitude, then there are two main equations. One of them is the well known lens equation:

$$\frac{1}{l_f} = \frac{1}{l_o} + \frac{1}{l_i}, \tag{4.4}$$

where l_f - focal distance

l_o - object distance

l_i - image distance.

The other equation defines the magnitude of the image:

$$\frac{r_i}{r_o} = \frac{l_i}{l_o}, \tag{4.5}$$

where r_i - magnitude of the image

r_o - magnitude of the object.

The radius of curvature of the deflected membrane was discussed in the previous chapter. As this value is much higher than the length and diameter of the channel, the curvature of the membrane is therefore not so significant. It is an important feature of the optical tracing because the membrane was handled as a plane mirror. When determining the optical trace of the beam, the effect of pressure was simulated with an offset of the mirror, i.e. the lens-membrane distance was modified.

First one-fibre system was studied where the source and the detector are combined. It was followed by the examination of the separate source detector system (two-fibres). Not only their axial distance relative to the focal point should have been determined, but also the position perpendicular to the optical axis, illustrated in *Figure 4.7*.

The distance between the optical axis and the centre of the source is r_s and for the centre of the detector it is r_d. The axial distance of the source and detector relative to the lens is equal and marked with l.

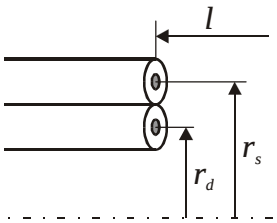

Figure 4.7: Position of the source and the detector.

As the optical fibre contained not only the core but also the cladding, the minimal distance between the centres of the two cores was *0.125 mm*.

The duct, in which the laser light propagates, had a metallic wall. Hence, it could not absorb the light. The light that reached the wall was reflected which caused a specular reflection. In order to increase the absorption and to reduce a specular reflection the wall was roughened.

In the theoretical study of the optics, many parameters were idealised. This means that the lens and the mirror were aligned perfectly perpendicular to the optical axis. For the simulation the transmission axis of the source was considered to be parallel to the optical axis. When comparing the calculated results with the measured values even a small misalignment could cause a relatively large difference.

For the intensity loss analysis the source was simulated with a finite beam diameter not only as a point source. It had a low value, but it was important to take this factor into account. For a point source the image diameter at the detector would be smaller than the detector leading to an error (the smaller the image diameter the larger is the intensity).

4.4.1 One-fibre system

The determination of the reflected image is performed in several steps. First the source and detector are handled as one-fibre, which is positioned on the optical axis. At this stage the diaphragm is modelled as a flat mirror, i.e. without the effect of differential pressure.

4.4.1.1 Source-detector on the optical axis

Positioning the source at the focal point *F*, the image is reflected to the same point. Therefore, the detected intensity was maximised. The lens, channel and mirror have a diameter of *3 mm* that limits the beams, thus limiting the intensity.

If the source is shifted further away from the lens ($l > l_f$) along the optical axis, the reflected image is positioned behind the detector and, hence, the detected intensity is reduced, illustrated in *Figure 4.8*.

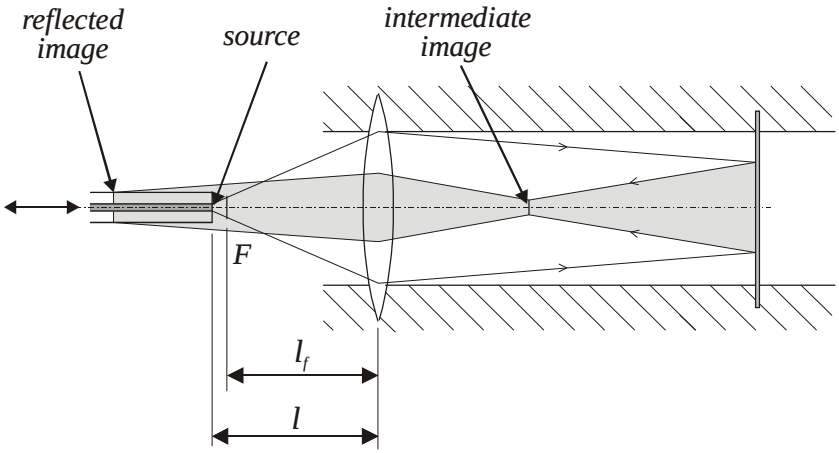

Figure 4.8: Optical tracing, one-fibre, $l > l_f$.

The same effect can be observed if the source is moved towards the lens ($l < l_f$), see *Figure 4.9*.

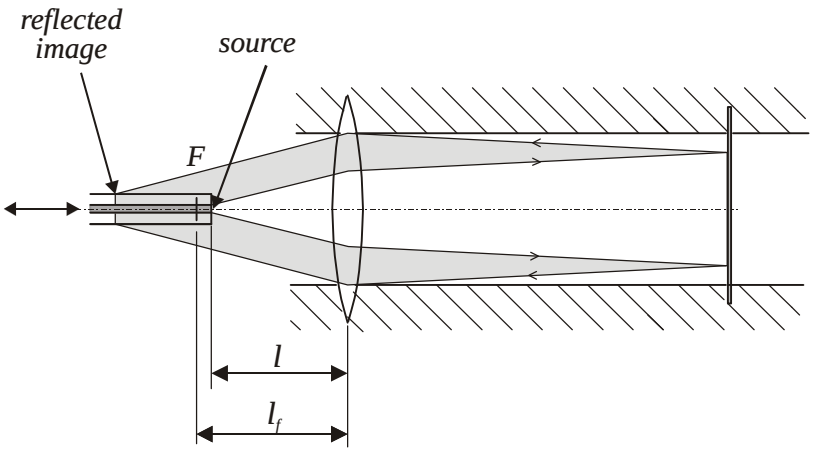

Figure 4.9: Optical tracing, one-fibre, $l < l_f$.

When plotting the product of the local beam intensity at the detector and its area for different positions of the fibre, one obtains a curve that resembles a Gaussian function, see the static calibration in the next chapter.

The total divergence angle of the beam leaving the optical fibre is 60°. Due to the geometrical parameters only the inner part of this conical beam passes the lens. However, the intensity loss is not significant, because most of the power is concentrated in the inner part of the beam.

4.4.1.2 Position of the reflected image

Figure 4.10 illustrates the optical fibre where a point P_1 is chosen to illustrate the variation of beam width at the plane of the detector after the reflection. The distance between P_1 and the optical axis remains constant and equals the radius of the core of the optical fibre (*25 mm*).

Figure 4.10: Source-detector unit with one-fibre.

The fibre is positioned on the optical axis and shifted towards the lens past the focal point. In *Figure 4.11* the radius of the beam normalised with the radius of the detector at the plane of the detector is illustrated as a function of the object distance l normalised with the focal length l_f.

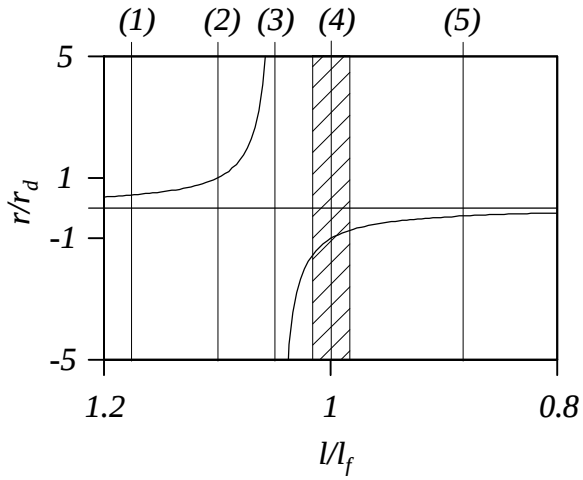

Figure 4.11: Normalised beam radius at the plane of the detector,
one-fibre on the optical axis.

First the source-detector unit is far from the focal point (*1*). Reducing the object distance l implies that the image distance on the right side of the lens and the magnification are constantly increased. The image of the lens becomes the object of the mirror that reflects it. Hence, it is the reflected image of the mirror i.e. the object of the lens. Its reflected image is projected above the optical axis on the left hand side of the lens. Shifting the unit rightwards (*2*) the image overlaps P_1, which is followed by a singularity (*3*). The reflected image of the lens is exactly mapped at the right hand side focal point. Consequently, its image is projected to infinity and that is the

reason of the singularity. Moving the source rightwards results in the reflected object of the lens is between the lens and the right hand side focal point. Therefore, its image is virtual. After this position the reflected image is under the optical axis. At the focal point of the lens (*4*) P_1 has a radial distance equal to the radial position of the source. Decreasing the axial distance of the fibre always results in projecting the image into a position closer to the optical axis (*5*).

As the diagram shows, when the source is left from position (*3*) the reflected image is projected to the same side of the optical axis where the object is settled. Right from position (*3*) the object and the image have a different sense. In the case when the source-detector is symmetrically positioned on the optical axis it does not lead to a problem. If the fibre is moved up or downwards from the axis (the radial distance is decreased or increased) the reflected image can be projected outside the surface of the detector (see later with two-fibres where the problem is more significant).

If the source is in the vicinity of the focal point the size of the image is larger than the dimension of the channel, therefore, there is an intensity loss. This region is the cross-hatched area in *Figure 4.11*.

4.4.1.3 Effect of the lens-membrane distance

The distance between the lens and the membrane l_{lm} is an important system parameter. Three distances are analysed from the optical point of view and the results are presented in *Figure 4.12*.

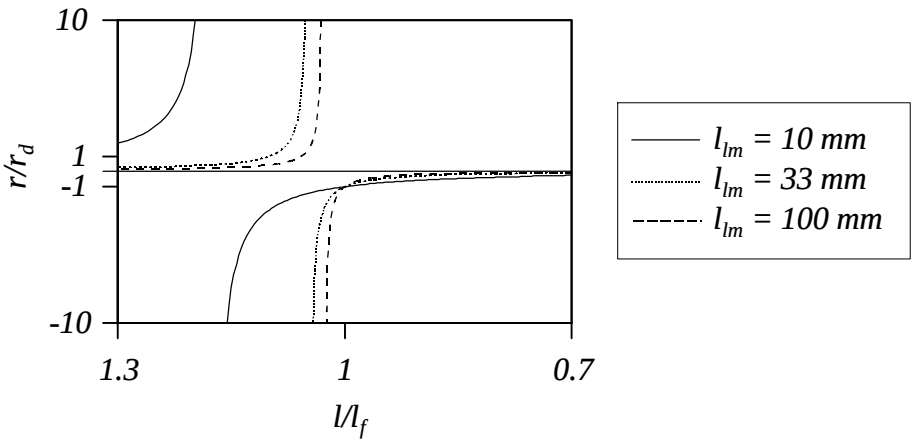

Figure 4.12: Effect of the lens-membrane distance on the radial dimension of the selected point at the plane of the detector.

In the case of a larger lens-membrane distance the position of the singularity is shifted towards the focal point. Parallel to this effect the beam diameter is always reduced. Consequently, the

measurable intensity is increased although a wider beam is more detectable. This second parameter plays an important role if the radial distance is different from the radius of the detector.

4.4.1.4 Effect of the focal distance of the lens

Three different lenses were analysed to obtain information concerning the effect of the focal distance. During this simulation the source-detector unit is shifted in the vicinity of the focal point and the radial dimension of the selected point can be seen in *Figure 4.13*.

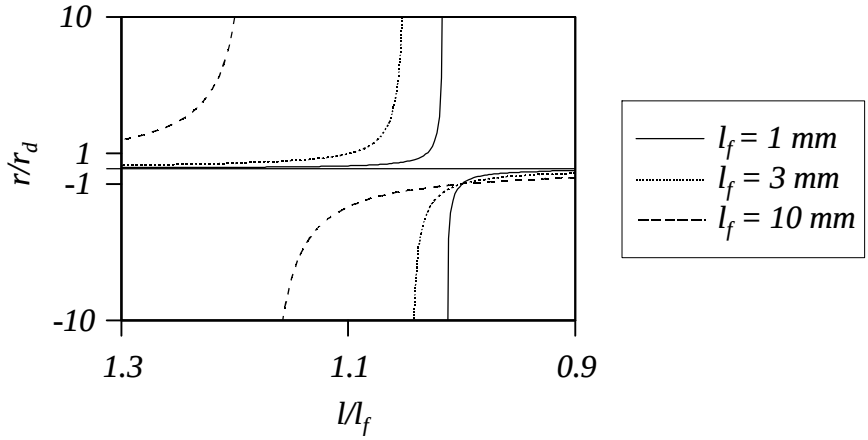

Figure 4.13: Effect of the focal distance of the lens on the radial dimension of the selected point at the plane of the detector.

The shorter is the focal distance, the closer the position of the reflected image to the focal point. The magnification of the system is proportional to the focal distance of the lens. The dual effect mentioned above also appears here; the increase of intensity infers reduced ability of detection. The focal distance also has an influence on the beam coupling into the optical fibre.

4.4.1.5 Construction of the one-fibre system

The set-up of the one-fibre source-detector unit is plotted in *Figure 4.14*. The beam from the laser tube has to pass the lens, the splitter, and after that it is coupled into the optical fibre by a lens. This fibre conducts the light into the measuring chamber where it is reflected and transmitted back to the splitter. It separates the reflected beam, which is then conducted to the photo detector.

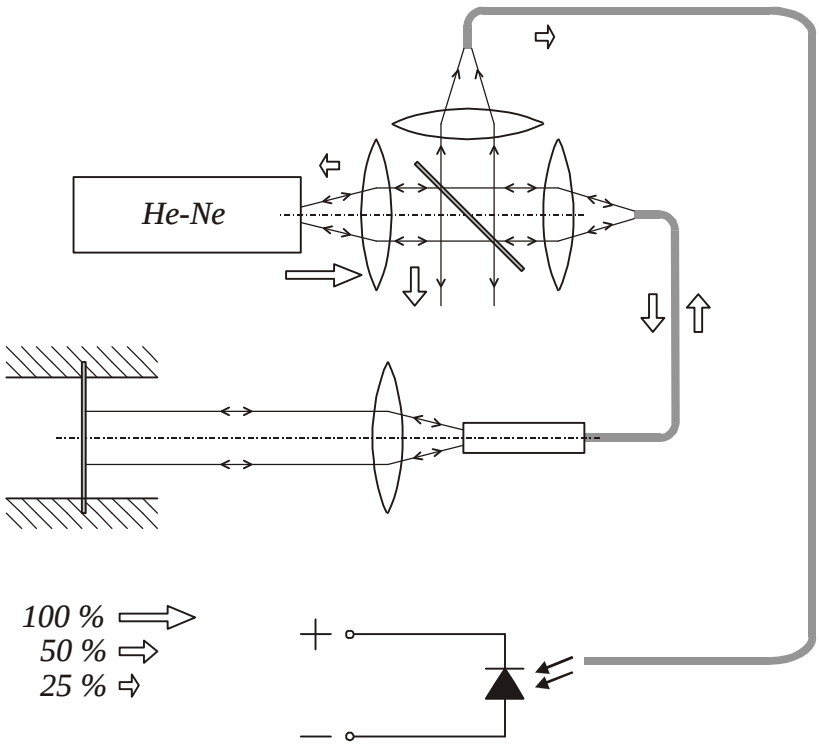

Figure 4.14: Construction of the one-fibre system.

A weak part of a single-fibre system is the beam splitter and the lenses where the forwarding and the returning beam are separated. The splitter and the lenses have to be adjusted with high precision, which is difficult to realise. Another disadvantage is the intensity loss of *50 %* every time when the beam passes through the splitter. Except for other losses only *25 %* of the original light reaches the photo detector.

4.4.2 Two-fibre system

From the optical point of view the one-fibre system would be ideal, but as the technical realization is quite complex the two-fibre system is applied, where one is the source and the other one is the detector.

In contrast to the one-fibre system, with the two-fibre unit not only the axial, but also the radial distance should be optimal. Depending on the radial position there can be the following three constructions:

- one of the fibres is in the optical axis,
- the fibres are arranged symmetrically to the optical axis,
- the fibres are arranged unsymmetrically.

Due to the miniature dimensions, it is not possible to position the fibres individually. For this reason the source and detector fibres are positioned as close to each other as possible, illustrated in *Figure 4.2 b*.

If the source is not in the optical axis non-symmetrical effects occur. Another feature is the magnification of the lens. If the source is too close to the focal point, its image is too large and the limitation of the lens diameter has a negative effect. To avoid this the source cannot be arbitrarily close to the focal point.

Figure 4.15 shows the source-detector unit with two-fibres. Two points of the source are marked (P_1 and P_2) and these projected images are analysed.

Figure 4.15: Source-detector unit with two-fibres.

If the source is on the optical axis the reflected object is projected just like that of the case of one-fibre, see *Figure 4.8* and *4.9*. The detector can be positioned either above or under the source, the effect is the same: it works only in a very narrow range.

By symmetrical construction, in the first case the light source is outside the focal point ($l > l_f$) and it is located above the optical axis, presented in *Figure 4.16*.

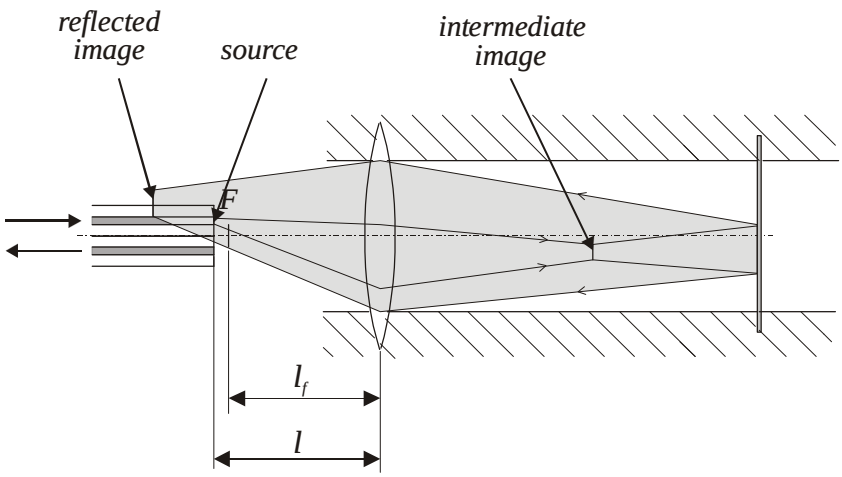

Figure 4.16: Optical tracing, two-fibres, $l > l_f$.

Just like in *Figure 4.8* the intensity loss due to the source position is not significant. A remarkable problem is that of the position of the reflected image. As it is illustrated in *Figure 4.16*, the image is in the same side of the optical axis as the source object. If the detector is under the optical axis it is possible that the detector does not detect the reflected beam.

With a non-symmetrical source-detector positioning this problem can be avoided, but the technical practicability is quite complex since the accuracy of the positioning has to be very high. It is important to know that to every l position a different r_s value belongs. The magnification of the source is limited by the diameter of the lens, channel and mirror. Increasing r_s or decreasing l (l ® l_f) the image is larger. If $l = 3.18$ mm the r_s has to be *0.057 mm* (the source and detector are beside each other) to achieve that the reflected image is at the position of the detector.

The results of the optical tracing illustrates that at a special l value (*3.15 mm*) the image of the mirror is reflected near to the right hand side focal point of the lens. Consequently, there is a singularity. In this case the reflected light breaking on the lens is parallel (the closer this image to the focal point the more parallel is the beam), hence the diameter of the beam is large. It is not positive because the diameter of the detector is small. That is why this l value should be avoided and it should be larger than *3.15 mm*.

Positioning the source inside the focal point of the lens ($l < l_f$), the reflected image is under the optical axis, *Figure 4.17*.

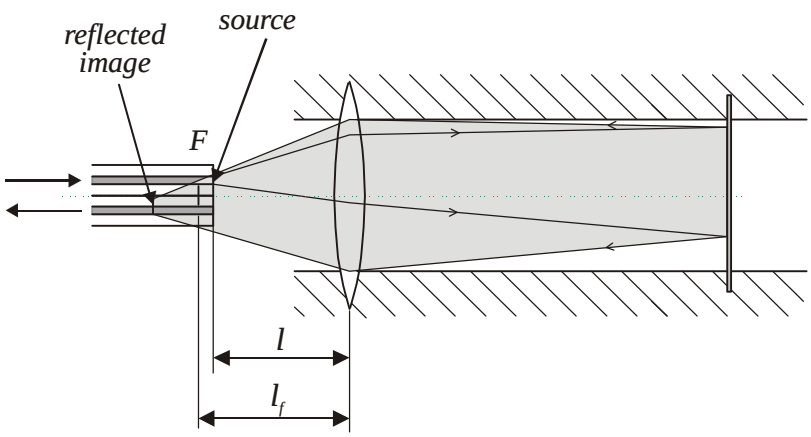

Figure 4.17: Optical tracing, two-fibres, $l < l_f$.

The limitation due to the lens diameter should also be studied here. Increasing r_s or l (l ® l_f) the image is larger and it can lead to intensity loss. That is why the object should not be very close to the focal point.

Although the source object and the reflected image are on different side of the optical axis, so in this case it can also happen, that the reflected image is not detected by the detector. Therefore, the symmetrical source-detector construction is not optimal. With unsymmetrical construction it is possible for the reflected image to be projected at the detector. If $l = 2.825\ mm$ the r_s has to be $0.012\ mm$ (the source and detector are beside each other).

Figure 4.18 illustrates the position of the reflected image as a function of the position of the source.

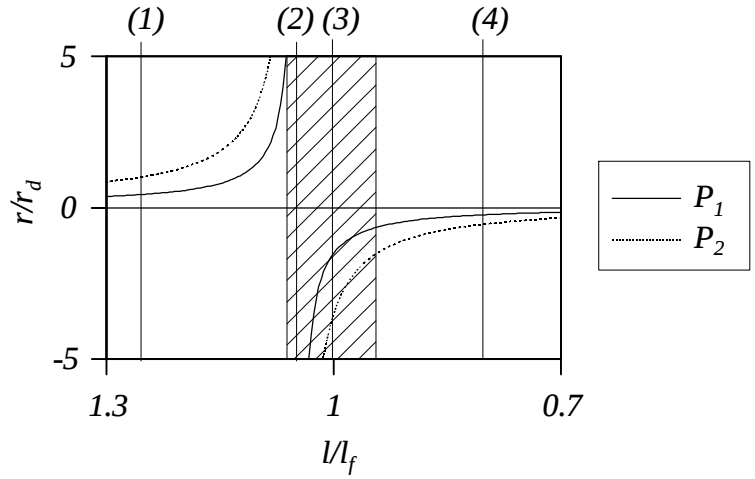

Figure 4.18: Radial dimensions of the selected points at the plane of the detector, two-fibres, symmetrical to the optical axis.

The source is above the axis and the detector is below it. If the source-detector unit is far from the focal point (*1*) the reflected image is on the source side. By shifting the unit right, a singularity is achieved (*2*) and behind this position the reflected image is on the side of the detector. As the diagram shows, close to this singularity the reflected image is outside of the detector. At a certain position (*3*) the beam is projected to the detector so its maximal output signal is increased. Achieving its maximum the signal is decreased as the detector is shifted towards position (*4*).

Limitation of the diameter of the lens results in an intensity loss in a region marked with cross-hatch. Compared to the one-fibre unit, it is wider as the distance between the optical axis and the selected point (P_2) is larger.

Shifting the source perpendicular to the optical axis results in the radial distance of the reflected image is increased.

The results of the parameter analysis of the one-fibre system (effect of the lens-membrane distance and the effect of the focal distance of the lens) can be applied to the two-fibre system, as well.

As this optical tracing analysis shows using two-fibres has many dangerous features, but it is the only solution. With an appropriate positioning, see next chapter, these problems can be avoided.

4.4.3 Optical tracing with the effect of pressure

In this part of the optical analysis the effect of the membrane deformation is analysed. During the optical analysis the membrane deformation is simulated as a shift i.e. the modification of the lens-membrane distance. Lower pressure means that the lens-membrane distance is decreased, when the pressure is increased the lens-membrane distance is increased as well.

In the real membrane a differential pressure of *50 mbar* causes a very small membrane deformation (*0.02 mm* in the centre of the membrane) and the corresponding radius of curvature is more than *300 m*. As *Figure 4.19* shows even a large deformation causes a relatively small modification of the reflected image.

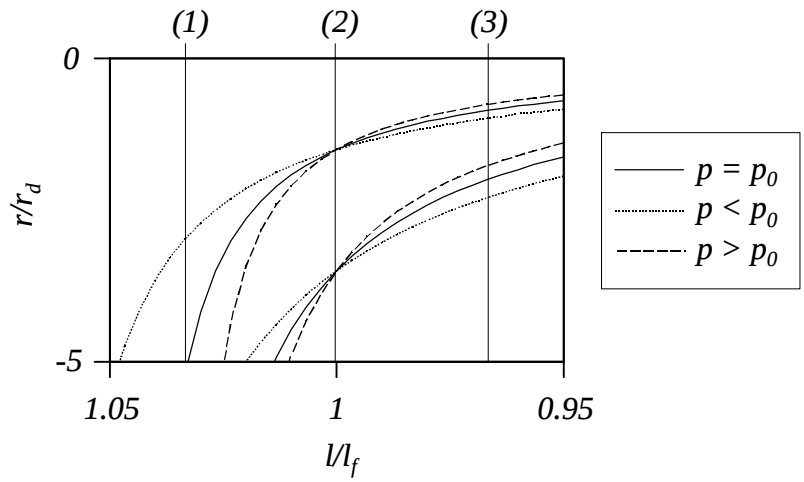

Figure 4.19: Effect of the membrane deformation on the radial dimensions of the selected points at the plane of the detector.

The effect of the lower pressure (dotted line) is that the membrane behaves like a convex mirror. Therefore, the image diameter is increased. A higher pressure (dashed line) results in the membrane behaving like a concave mirror, thus the image diameter is decreased.

Left from focal point (*1*) the pressure change causes a larger image modification than on the other side of the focal point. The disadvantage of the left hand side position is the fact, that the beam diameter is larger than the diameter of the detector. Hence, the sensitivity is decreased. Right from the focal point (*3*) the pressure change causes a relatively small image modification, but the beam diameter is relatively small, therefore, it is more detectable.

As *Figure 4.19* shows the pressure change has no effect if the source-detector is positioned at focal point (*2*). In the real system the operating point is not the focal point.

This analysis provides a good theoretical basis to solve the problem of the measurement of the membrane deflection. The most important conclusion of this examination is the importance of the accuracy of the positioning system. The source-detector unit should have a very precise adjustability because even a small deviation from the optimal position leads to an enormous signal loss. Above all, the positioning should be rigid, as well, to avoid misadjustment due to vibration.

5 Experimental results

The primary aim of the experimental work was the study of the dynamical response of the newly developed sensor, however a detailed analysis of the hydraulic loop was also necessary. With increasing performance of the sensor, the weak points of the experimental apparatus were detected and improved. It was a long process with two parallel paths, one was the improvement of the performance of the sensor and the other was the simplification of the test loop.

In the experimental apparatus, used by the tests of the previous versions of the pulsation sensor [*1*] and [*2*], the resulted pulsations were quite complex especially for the test of such kind of new measuring device. Consequently, the author constructed a simple test loop.

In an ideal case, during the dynamic tests of a new method the natural frequencies of the components of the experimental apparatus should be outside of the examined domain. If it is not possible the understanding of the disturbing frequencies are necessary. In addition, the method of how to tune the above mentioned frequencies is important, as well.

For the flow pulsation measurement in hydraulic systems it is a serious difficulty to produce high frequency excitation with a simple frequency spectrum. The fastest hydraulic components are the servo valves that are capable of producing a defined pulsation up to approximately *250 Hz* [*68*]. In many cases this range is lower than the frequency series of interest hence other methods had to be found to generate pulsation. Pumps also create flow vibration containing the pumping frequency and its harmonics. By varying the pump speed the pulsation frequency can be modified, nevertheless this pulsation is too complex. Due to these reasons, these hydraulic elements cannot be applied to perform a detailed investigation of the newly developed pulsation sensor.

To produce a high frequency pulsation, with adjustable frequency and amplitude, the excitation source was chosen to be a shaker, which can generate pulsations up to *1000 Hz*. The main drawback of this method is the fact that the operation of the shaker is only optimal at a low system pressure (at a higher pressure the shaker does not have enough force to move the piston). Hence, the measurements described in this chapter were performed at atmospheric pressure (*1 bar*).

The source of excitation, in this case is a shaker, which generates not only a flow pulsation but also a mechanical vibration. This mechanical vibration in the piping acts on the flow pulsation and vice versa. In order to reduce the disturbing effect of the mechanical vibration the coupling between the shaker and the piping was performed with a solution which is discussed later.

Before starting with the presentation of the experimental results of the OPS, the analysis of the positioning of the source-detector unit is presented and that is followed by the results of the static calibration performed in a test apparatus and in the housing of the sensor.

In order to design a hydraulic system the dynamic behaviour of the whole circuit, i.e. the behaviour of the fluid filled piping, should be examined. The actual resulting pressure pulsation in the system depends on the combination of the spectrum generated by the sources (pumps, valves etc.) and the acoustic resonance effects of the piping. Not only rigid bodies, but also the compressible fluid column has natural frequency that affects the response of the circuit. For designing a system it is important to identify these frequencies and to know how they might affect the response of the whole structure. Before the results of the pulsation measurements are presented there is a short introduction to hydro-acoustics.

Since the knowledge of the speed of sound is an important parameter from the hydro-acoustical point of view, its value was measured. The explanation of the low value of the speed of sound led to an extensive experimental investigation of the test circuit. The effect of air contamination of the working fluid was investigated, that then was followed by the influence of the structure born vibration. After that the resonance frequency of the fluid as a function of the length of the column was determined.

In the next step the measurement of sinusoidal pulsation was carried out at different frequencies and amplitudes. These results are compared to the theoretically expected values.

Finally, the OPS was mounted into a hydraulic circuit in order to measure the flow pulsation of a gear pump. To be able to compare the measured and the expected flow pulsation there is an introduction into the operating principles and flow delivery of gear pumps.

In order to record the flow pulsation with other techniques than the OPS, measurements were carried out with a hot film anemometer. By means of the available anemometer instruments the detection of the pulsation was not possible, since the output signal was very low with a high

noise level. Consequently, pressure transducers were applied in order to obtain information concerning the dynamic behaviour of the fluid.

5.1 Positioning of the source-detector unit

There were two conditions, which had to be fulfilled by the design of the positioning of the source-detector unit. The first was the precise adjustability, already discussed by the optical tracing. The second criterion was the rigidity, as the optical system is very sensitive to mechanical vibrations, which are common in hydraulic systems.

The need to improve the operating principle of the OPS resulted in the set-up of a simple test loop, illustrated in *Figure 5.1*, where the sensor analysis could be made more accurately than in the housing of the sensor. The most significant advantage of this test apparatus was the fact that there was no housing of the sensor; hence, the system could be observed during its operation. Not only the membrane deformation, but also the laser beam on the membrane and the operation of the positioning system of the source-detector unit could be examined as well.

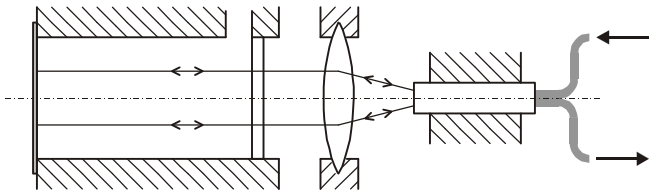

Figure 5.1: Apparatus for optical testing.

As *Figure 5.1* shows, the measuring duct with the reflective membrane on its left hand side, the lens and the source-detector unit are composed of three individual elements. They could be positioned and oriented independently from each other, which was not possible within the housing of the sensor.

The first version of the positioning is presented in *Figure 5.2*. The adapter *(1)* has a fix mounting in the housing of the sensor and holds the lens and the screw *(2)* where the source-detector unit *(3)* is installed. Turning the screw *(2)* in the adapter *(1)* the optical fibres are shifted in an axial direction. These parts are connected with fine thread that allows for fine positioning. The source-detector unit can be rotated in the screw and so consequently it has another degree of freedom (the first of which is the shift parallel to the optical axis).

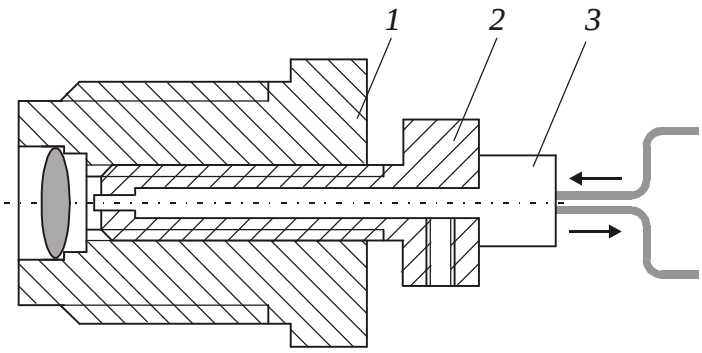

Figure 5.2: First version of the positioning of the source-detector unit.

When comparing the test measurements in the optical bench with the measurement in the housing of the sensor, the level of the output signal of the second version was quite low. In the optical bench the position of the individual elements of the optics (membrane, lens and source-detector unit) were adjustable not only in an axial direction, but also perpendicular to this direction (*3D* positioning). With the positioning system in the housing of the sensor this second condition could not be fulfilled. To solve this problem a new system had to be developed, where the available space was the main limitation. For this reason the commonly applied positioning in optical systems was too large, a compact unit was developed, presented in *Figure 5.3*.

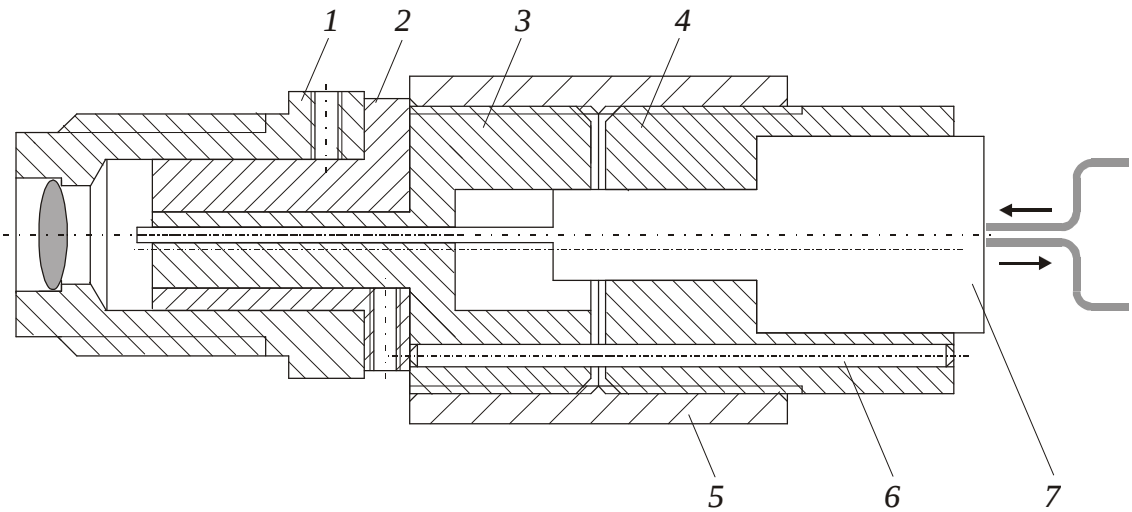

Figure 5.3: Second version of the positioning of the source-detector unit.

The positioning unit is fixed by an adapter *(1)* into the housing of the sensor similar to the first version, but in this case it is without an inner thread. Into this piece a sleeve *(2)* is fitted. This part has an excentric bore wherein the second sleeve *(3)* is assembled. It has also an excentric bore wherein the source-detector unit *(7)* is installed. Parts *(2)*, *(3)* and *(7)* can be turned relative to each other and they can be adjusted due to the excentric bores to every arbitrary position perpendicular to the optical axis.

The side view of part *(2)*, *(3)* and *(7)*, *Figure 5.4*, demonstrates once more the excentric setting of the different parts. Turning them relative to each other the centre of the source-detector unit can be positioned in a circular area marked grey in *Figure 5.4*.

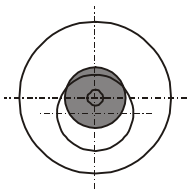

Figure 5.4: Positioning area perpendicular to the optical axis.

With the above-described way the positioning in one plane is possible, but the source-detector unit should also be shifted in an axial direction. This problem was solved with a system containing right hand and left hand screws. The sleeve *(3)* has a right hand thread, but the other one *(4)* has a left hand thread. These two parts are installed into a nut *(5)* having a right hand thread in the left side and a left hand thread in the other end. Turning the nut results that the gap between part *(3)* and *(4)* is adjustable, hence the positioning problem in an axial direction is solved. Part *(3)* and *(4)* are connected with a pin *(6)* that fixes the relative position of element *(3)* to *(4)*.

Applying this positioning system, the source-detector unit can be shifted in an axial direction and also positioned perpendicular to the optical axis. If it is necessary it can also be rotated around its axis.

5.2 Static calibration

Static calibration of the OPS was performed in order to determine the correlation between the pressure difference at the membrane and the output signal of the OPS. Before the calibration was completed the operating point of the optical system was determined. Both of these steps were performed in a test apparatus and in the housing of the sensor.

5.2.1 Calibration in a test apparatus

To study the operation of the optics its parts were mounted onto an optical bench, where some test measurements were carried out. The duct, the lens and the source-detector unit could be positioned individually. The benefit of this option was a very high output signal of the optical system.

A fluid column connected to one side of the measuring duct generated the static displacement. Varying the height of the liquid by *dh* altered the applied differential pressure, thus the deflection of the membrane, see *Figure 5.5*.

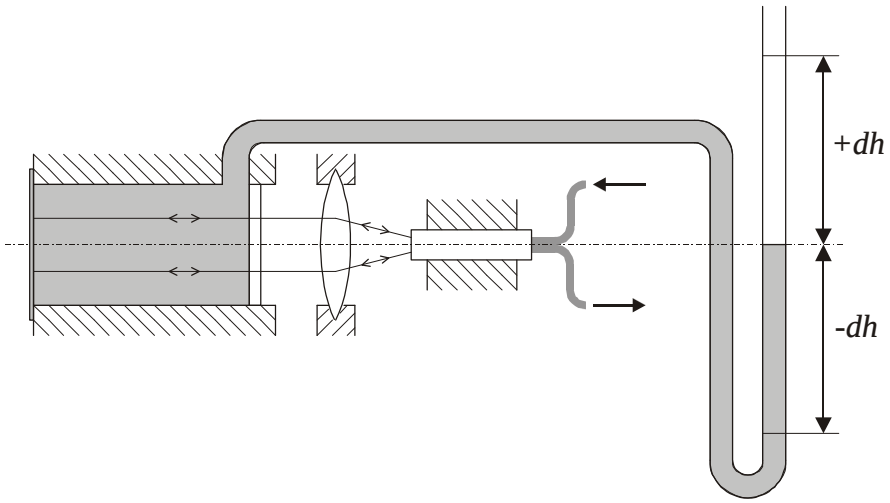

Figure 5.5: Static calibration in the test apparatus.

The differential pressure *dp* is proportional to the density r, acceleration due to gravity *g* and the height difference *dh*:

$$dp = r \; g \; dh \, . \qquad (5.1)$$

The calibration factor was determined with the knowledge of the differential pressure acting on the membrane and the corresponding output voltage of the sensor *U*.

The first step of the calibration process was to adjust the maximal output signal. It means that the laser source-detector unit was positioned in an axial and a radial direction until the peak of the output voltage was achieved. By this location the output signal had a value of *8.5 V*. Shifting the source-detector unit in an axial direction *x* a voltage distribution was obtained, illustrated in *Figure 5.6*.

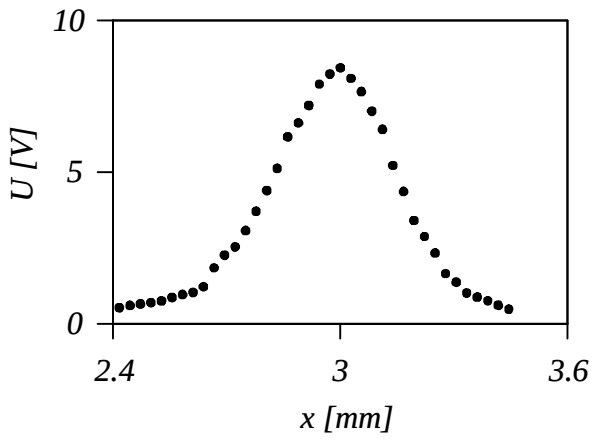

Figure 5.6: Voltage vs. position measured in test apparatus.

Based on this function the operating point could be determined. If this point would be placed at the maximum, a positive or a negative pressure change resulted in the same effect and the output signal decreased. To avoid this, the working point was moved right or leftwards from the maximum.

The working point should be selected in a way, that the same pressure changes in positive and negative direction (± *50 mbar*) caused the same output voltage modification. In addition the variation of the input and output signals should be symmetrical.

According to these criteria one point could be chosen on both sides of the curve. First the working point right from the maximum was studied whereto the source-detector unit was positioned. By means of the fluid column a differential pressure was produced and the output signal U_{twp1} was recorded. As *Figure 5.7* shows, a pressure change of ± *50 mbar* causes a signal modification of ± *2.8 V*.

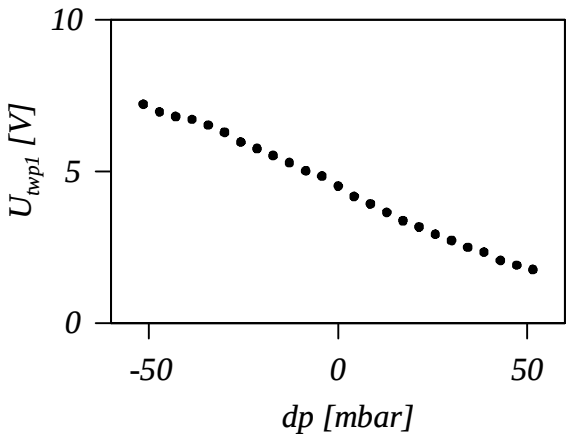

Figure 5.7: Result of the static calibration in test apparatus, working point *1*.

In the next step the source-detector unit was moved to the working point left from the maximum. At this location the same process was produced, as described above, and the measurement results are presented in *Figure 5.8*. At this position the same pressure change resulted in a signal modification of ± *0.8 V*, which was less than in the other position. The reason for this is the unsymmetrical image formation, discussed in the previous chapter.

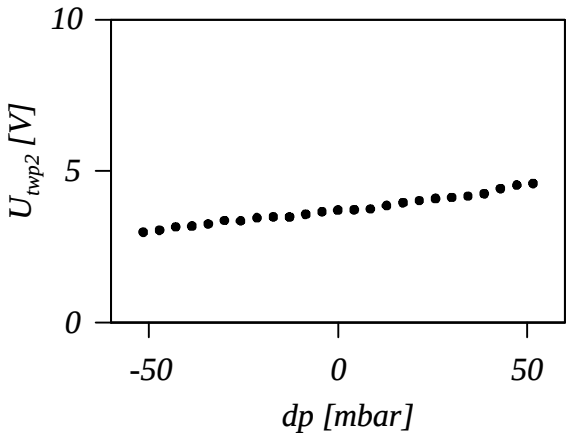

Figure 5.8: Result of the static calibration in test apparatus, working point *2*.

5.2.2 Calibration in the housing of the sensor

After the calibration of the sensor in the test apparatus the transducer was mounted into its housing in order to determine the correlation between the differential pressure and the output voltage of the sensor in the real operating environment. The dimensions of the housing defined the relative position and orientation of the components. The only variable geometrical parameter was the position of the source-detector unit. In *Figure 5.9* this configuration is depicted.

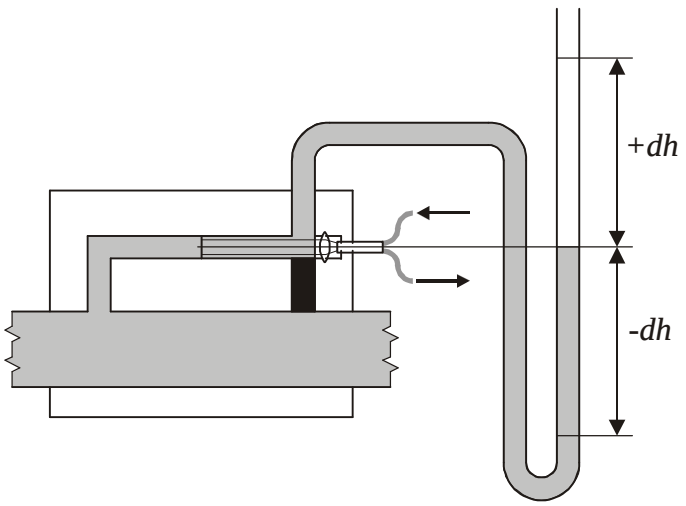

Figure 5.9: Static calibration in the housing of the sensor.

The left hand side of the duct was connected to the hydraulic system where the pressure was kept constant (atmospheric pressure). The tubing between the right hand side of the measuring duct and the main flow was closed. In order to generate a differential pressure it was connected to an external tube. By varying the height of the fluid column in the tube the differential pressure acting on the membrane was modified.

The first step of the calibration process was to achieve a maximal output signal that was *7 V*. After that, the source-detector unit was shifted in an axial direction and the voltage distribution, presented in *Figure 5.10*, was recorded. Comparing this diagram to the one measured in the test apparatus (*Figure 5.6*), the intensity distribution in the sensor housing is lower. The reason of the lower signal is the geometrical inaccuracy of the housing compared to the test apparatus and the misalignment of the optical axis. The same effects cause the unsymmetrical distribution of the measured data.

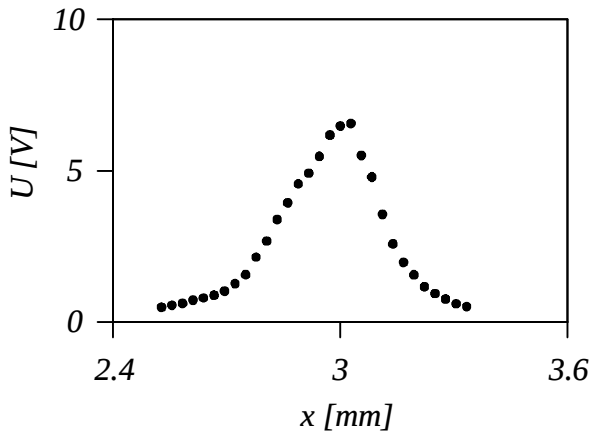

Figure 5.10: Voltage vs. position measured in the housing of the sensor.

The determination of the working point in the housing of the sensor was analogous to the method described above. The calibration curve at the operation point right from the maximum is plotted in *Figure 5.11*.

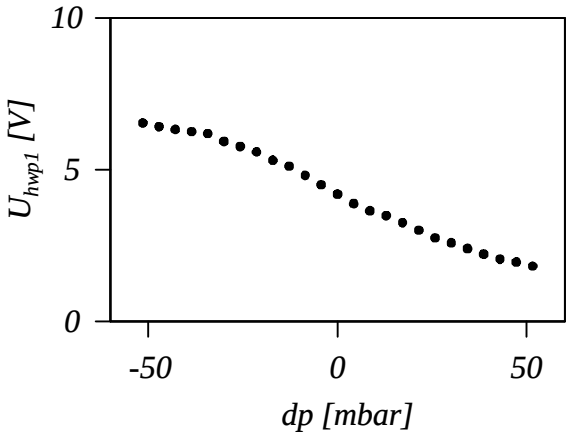

Figure 5.11: Result of the static calibration in the housing of the sensor, working point *1*.

As the diagram shows pressure change of ± *50 mbar* causes a signal modification of ± *2.4 V*. By the operation point left from the maximum the corresponding variation is ± *0.7 V*, illustrated in *Figure 5.12*.

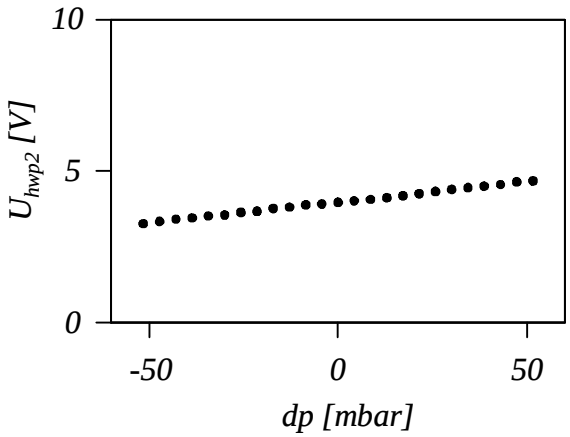

Figure 5.12: Result of the static calibration in the housing of the sensor, working point *2*.

The first point was chosen as a working point because of the higher sensitivity. The response is monotone with a slope of *0.02 mbar/mV*. This parameter was used when the pulsation measurements were taken.

5.3 Hydro-acoustics

This part is a short introduction to hydro-acoustics [*69*], [*70*], [*71*] as it had a significant effect on the experimental investigation of the OPS. The aim of this study is to determine the resonance frequencies of a fluid column and which are the parameters that influence the dynamic behaviour of the test loop.

Considering a circular rigid-walled duct whose length l is many times greater than its diameter d. The tube is filled with a compressible fluid with density r and the pressure inside the tube is p_0. When introducing a disturbance at one end of the duct with a piston, the disturbance propagates towards the other end at a velocity c, called the speed of sound. The pressure increase dp caused by the disturbance is proportional to the density of the medium, the speed of sound and the increase of the piston velocity:

$$dp = r\ c\ du\,, \tag{5.2}$$

where $r\ c$ is noted as acoustic impedance Z of the fluid in a tube with constant cross-section. Involving the cross-section area A the characteristic acoustic impedance was obtained given as:

$$Z_c = \frac{r\ c}{A}\,. \tag{5.3}$$

As long as the impedance is constant the propagation of the wave is not disturbed. To satisfy this condition, the diameter of the circular tube should remain constant. Any modification of the cross-section of the pipe has major effect on the wave propagation. By such kind of cross-section

variation waves can be partially or completely reflected, the transmission or reflection depends on the local wave resistance (impedance).

In practice there is no infinitely long tube, the boundary condition of the tube can be classified into three groups:

a. perfect sound absorber, which means that the travelling wave is totally absorbed, there is no reflection at the end termination,
b. perfectly rigid termination, where the incident waves are perfectly reflected,
c. partially absorptive termination, which means, that one part of the travelling wave is absorbed and the other part is reflected.

5.3.1 One-dimensional wave equation

The one-dimensional wave equation for the propagation of acoustic pressure within a tube [*72*], defines the pressure fluctuation with respect to space as a function of the coordinate distance *x* and with respect to time *t* given by:

$$\frac{\partial^2 p}{\partial x^2} - \frac{1}{c^2}\frac{\partial^2 p}{\partial t^2} = 0, \qquad (5.4)$$

where the speed of sound *c* is the function of the bulk modulus of the fluid E_f and the density:

$$c = \sqrt{\frac{E_f}{r}}. \qquad (5.5)$$

The solution of *Equation* (*5.4*) in case of harmonic excitation depends on the boundary conditions of the tube. One end is considered to be rigid, while the second one at *(x = l)* can be classified into the three groups [*70*]:

a. Open end: by this termination the acoustic pressure is zero *p(l,t)=0,*

   the acoustic pressure is: $p(x,t) = ir\ c\ u\ \frac{\sin(k(l-x))}{\cos(kl)} e^{iw\ t}$. (*5.6*)

   If *cos(kl)=0* the field variables becomes unlimited, hence resonance occurs. The corresponding frequencies are:

   $f_n = \left(n - \frac{1}{2}\right)\frac{c}{2l}$ *n = 1, 2, 3 …* (*5.7*)

b. Closed end: in this case the particle velocity at *x = l* must be zero *u(l,t)=0,*

   the acoustic pressure is: $p(x,t) = -ir\ c\ u\ \frac{\cos(k(l-x))}{\sin(kl)} e^{iw\ t}$. (*5.8*)

Similar to the previous case resonance can also appear at frequencies given by:

$$f_n = n\frac{c}{2l} \qquad n = 1, 2, 3 \ldots \tag{5.9}$$

c. Partially absorptive termination: the reflection depends on the impedance of the termination:

$$Z(l) = \frac{p(l)}{u(l)}, \tag{5.10}$$

the acoustic pressure is: $p(x,t) = r\ c\ u\ \dfrac{\cos(k(l-x)) + i\left(\dfrac{r\ c}{Z}\right)\sin(k(l-x))}{\left(\dfrac{r\ c}{Z}\right)\cos(kl) + i\sin(kl)} e^{iw\ t}$. (5.11)

The resonance criterion depends on the impedance of the termination

a. $Z \to \infty$: closed end criterion

b. $Z \to 0$: anechoic end termination

c. $Z = r\ c$: open end criterion.

The wave number k is the spatial equivalent of the angular frequency w and given by:

$$k = \frac{2p}{l}, \tag{5.12}$$

where l is the wavelength.

In real hydraulic systems there is a pump at the pipe beginning, hence it is a closed termination [*73*]. If the system has an open or closed end on the right hand side, then this defines the condition of resonance given by *Equation* (*5.7*) and (*5.9*), illustrated in *Figure 5.13*. Resonance occurs with open line termination if the pipe length is a quarter of the wavelength ($l = l/4$). In case of closed end resonance is generated if the pipe length is half of the wavelength ($l = l/2$). As the plot shows not only the first natural frequency appears, but also its harmonics, therefore, the resulted pressure distribution is fairly complex.

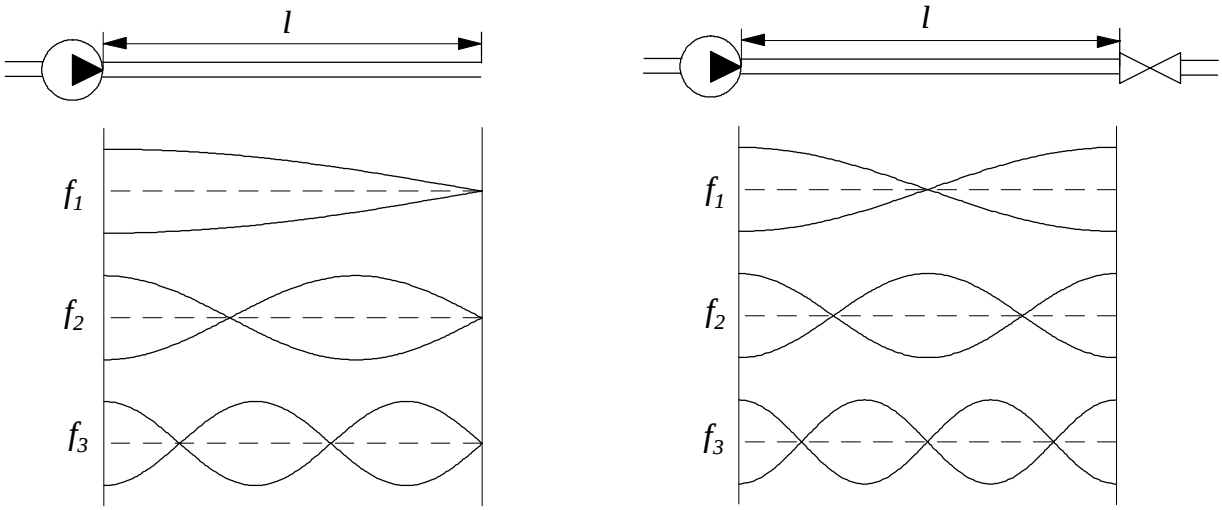

Figure 5.13: Pressure distribution in hydraulic line with open or closed line termination [*73*].

5.3.2 Transmission line theory

In this work measurements were carried out with the pulsation sensor in a hydraulic loop. As the source of the pulsation and the measuring position are different the dynamic behaviour of the hydraulic line had to be studied. The one-dimensional wave equation describes the field variables in the case of the wave propagation, but does not include viscous losses, which are frequency dependent and distributed throughout the length of the transmission lines. To describe the dynamic behaviour of the system the viscous compressible model was used [*74*]. The basic equations of this model are the continuity equation and the Navier-Stokes equation, where losses are introduced with the viscous friction loss factor *N*. The theoretically exact expression for *N* contains Bessel functions of order zero J_0 and two J_2 and has a form of:

$$N_{exact} = -\frac{J_0\left(ir\sqrt{s/n}\right)}{J_2\left(ir\sqrt{s/n}\right)}. \qquad (5.13)$$

An approximate analytical solution for the friction loss factor is given in the following equation:

$$N = 1 + \frac{1}{i\Omega} + \frac{0.1515}{1+0.303i\Omega} + \frac{0.162}{1+0.04i\Omega} + \frac{0.02}{1+0.001i\Omega}, \qquad (5.14)$$

where the non dimensional frequency is:

$$\Omega = \frac{w}{a_P} \qquad (5.15)$$

and the Poiseuille coefficient is given as:

$$a_P = \frac{32n}{d^2}. \qquad (5.16)$$

The friction loss factor is a complex function; the real part is related to the resistance due to viscous losses in the fluid while the imaginary part of N expresses the damping caused by the viscosity of the fluid.

Pressures are measured at the input p_i and output p_o of the pipe, the flow pulsation Q at these locations can be determined based on the four-pole approach written in matrix form:

$$\begin{bmatrix} Q_o \\ p_o \end{bmatrix} = \begin{bmatrix} \cosh\left(Ts\sqrt{N}\right) & -\frac{1}{Z_c\sqrt{N}}\sinh\left(Ts\sqrt{N}\right) \\ -Z_c\sqrt{N}\sinh\left(Ts\sqrt{N}\right) & \cosh\left(Ts\sqrt{N}\right) \end{bmatrix} \begin{bmatrix} Q_i \\ p_i \end{bmatrix}, \tag{5.17}$$

where s is the Laplace operator and T is the inviscid propagation time, given by the ratio of the pipe length to the speed of sound:

$$T = \frac{l}{c}. \tag{5.18}$$

This model is valid only for simple pipelines with laminar flow and with rigid pipe walls.

5.3.3 Effects of fluid and pipe parameters

The speed of sound has an important effect on the dynamic characteristic of the fluid. In hydraulic systems its value depends on the fluid (pressure, elasticity, density, temperature and air contamination) and piping parameters (geometry, elasticity of the pipe material, variation of the cross-section, end terminations, pipe clamping). In hydraulic circuits the pressure is not constant, it varies from low values up to some hundreds of *bar*. The larger the system pressure, the greater is the speed of sound [*75*].

A fluid wave can propagate in a free surface without significant disturbance, however, in a pipe it is reduced due to the damping effect of the pipe material [*35*], [*44*], [*76*], [*77*]. In hydraulic systems a hydraulic hose is often used, which results in a reduced speed of sound. In this case there is a strong dependence of the speed of sound on the system pressure (the higher the pressure, the larger the stiffness of the hydraulic hose). In most cases the effect of elasticity of the pipe material is small compared to the impact of the air contamination.

5.3.3.1 Air contamination of the hydraulic oil

Gas is more compressible than fluid, therefore gas contamination of the hydraulic fluid has an immense influence on the dynamic behaviour of the system [*78*], [*79*]. The advantage of gas

contamination is the increased attenuation; therefore, unwanted pressure peaks are reduced. On the other hand, mineral oil is used as a working fluid because of its low compressibility. This property is eliminated by gas contamination. The compressibility of the hydraulic fluid, trapped in a volume V at a given pressure p is:

$$\frac{dV}{V} = -\frac{dp}{E_f}, \tag{5.19}$$

where E_f is called bulk modulus of the fluid and has a typical value of $1600\ N/mm^2$. In practice this value is much lower, mainly due to a small percentage of trapped air, which in fact cannot be avoided. The bulk modulus of the fluid-air mixture E_{fa} is defined as [79]:

$$E_{fa} = E_f \frac{1+\frac{V_a}{V_f}}{1+\frac{p_0}{p}\frac{V_a}{V_f}\frac{E_f}{p}}, \tag{5.20}$$

where V_a - volume of the air at p_0

V_f - volume of the fluid

$\frac{V_a}{V_f}$ - volumetric air contamination

p_0 - atmospheric pressure

p - system pressure.

The dependence of the speed of sound on the system pressure is presented in *Figure 5.14 a* by a volumetric air contamination of *0.1 %*. As the diagram shows especially at low pressures ($p < 10\ bar$) the air contamination results in a significant reduction of the speed of sound.

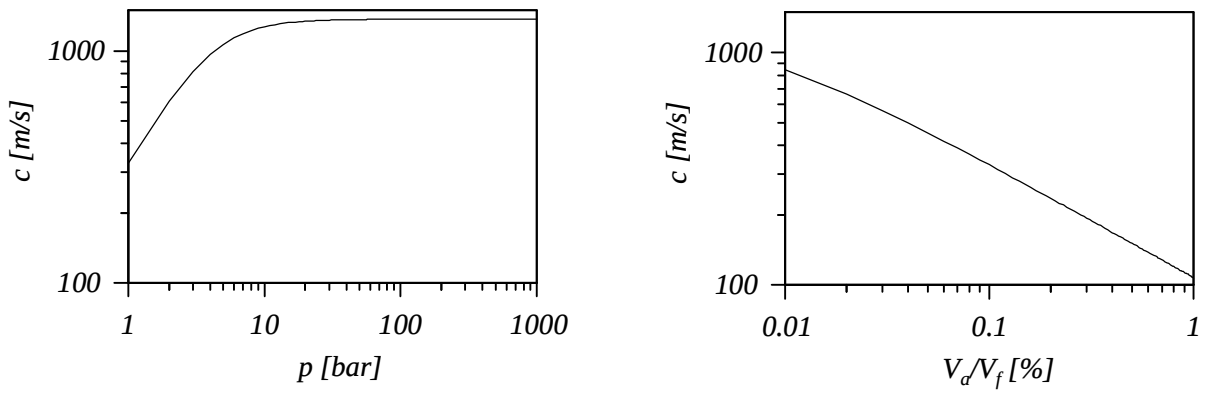

Figure 5.14: Dependence of the speed of sound.

In our measurements the system pressure was near to the atmospheric one. By this condition increasing air contamination leads to reduced speed of sound, illustrated in *Figure 5.14 b*.
A practical problem is that the percent of trapped air in an operating hydraulic system is nearly impossible to determine accurately, moreover it varies from minute to minute. For this reason experimental measurements are necessary to determine the exact value of the bulk modulus. Heisel et al. [*80*] studied the effect of gas bubbles on the propagation of a pulse in a hydraulic system. The speed of sound was determined from the measurement of the propagation time of a pressure pulse. According to these measurements the amplitude of the pulse had an effect on the speed of sound. The smaller the pulse amplitude, the lower was this speed. Air contamination less than *1 %* results in a significant reduction of the speed of sound.

Even a small amount of air in the fluid causes two effects, on one hand the speed of sound is reduced, and on the other, the dynamic behaviour is modified. Smereka [*81*], Wilson [*82*] and Brennen [*83*] investigated this topic in the case of water, however, the attenuation is not so well understood. The speed of sound at room temperature had a value of approximately *1500 m/s* in pure water and *340 m/s* in air. Considering a low frequency excitation through a uniform suspension of air bubbles in water, where the wavelength was much larger than both the bubble size and spacing. In this case, the mixture could be treated as a homogenous fluid with the compressibility of air and density of water. Having *0.5 %* of air in the water, then the sound speed of the mixture was only *160 m/s*, which was lower than either water or air alone. The bubbles could be considered as simple oscillators. To predict the acoustic behaviour of the fluid-gas mixture, it is necessary to know the void fraction, the number, the size respectively and the distribution of the bubble sizes.

5.3.3.2 Anechoic line termination

To avoid hydro-acoustical resonance in the test loop, the reflecting waves have to be eliminated. The simplest way, however is not very practical, which is to avoid reflection by the application of a very long pipe, where the friction in it decreases the reflecting waves. Gössele [*84*] studied the effect of the piping length on the wave reflection. As long as the ratio of the piping length to the wavelength was smaller than *0.1*, there was no resonance. Another method by which to reduce reflection at the piping end is to absorb the travelling wave. Hoffmann [*41*], [*42*] and Haarhaus [*43*] described a method, where an orifice was positioned at the end of the measuring section. If the resistance of this orifice was equal to the characteristic impedance of the line upstream of the orifice, then the travelling wave was transmitted without reflection. To avoid waves coming from

behind the orifice Theissen [*85*] placed a volume behind the orifice. Larsson et al. [*86*] completed the line termination of Theissen with a second orifice located behind the volume. With this orifice the required flow rate could be adjusted, as well. The reflection at the end of a line depends not only on the geometrical and acoustical parameters, but also on the operating point of the system (e.g. pressure and flow rate). As these parameters are normally not constant, the above described methods work only at discrete operating points. Schellinger et al. [*87*] developed an automated device for anechoic line termination. A characteristic sign of a reflection free operation was analogous (apart from phase and amplitude) pressure signals, measured at two different positions in the line. By the previous versions of the anechoic line termination, the opening of the end termination was adjusted manually to achieve the similar pressure devolution at both locations. This manual adjusting process was then replaced by an automated system that adjusted the orifice based on the analysis of the pressure signals. Perfect adjusted termination prevents reflection, but an unadjusted orifice has either low or high pass characteristics. If the opening is too small, then low frequency pulsations are reflected to a greater extent than high frequencies. High pass characteristics occur when the gap is too large resulting in the reflection of high frequencies rather than low ones. In practice it is difficult to achieve good and reliable reflection-free line termination over a broad frequency range.

5.4 Measurement of the speed of sound

As the previous section points out, the understanding of the speed of sound is an essential factor for the determination of the resonance frequencies of the experimental set-up. The measurement of the speed of sound seemed to be a simple problem; nevertheless, in the real tests it required a detailed investigation of the system.

Several literature examples deals with the measurement of the speed of sound [*35*], [*44*], [*75*], [*76*], [*77*], however there is none, in which the effect of the air contamination of the hydraulic oil is described. In our case this factor had a significant effect.

The speed of sound in a fluid filled pipe can be determined by the measurement of a pressure pulse in two different positions. The excitation is generated at the beginning of the pipe and measured by two pressure sensors. In order to increase the accuracy of this method, the distance between the two sensors should be as large as possible.

The experimental apparatus used for the measurement of the speed of sound is illustrated in *Figure 5.15*. The pipe was a standard hydraulic steel pipe, the fluid was hydraulic oil, its density, viscosity and bulk modulus were obtained from the manufacturer. On the left hand side of the pipe there was a piston-cylinder unit that was used to excite the system. The fiction between the piston and its cylinder was very low, consequently this factor had only a minimal effect on the experiment. Before the measurement was performed, the piping of test loop was rotated from its original horizontal position in order to get the trapped air out of the fluid.

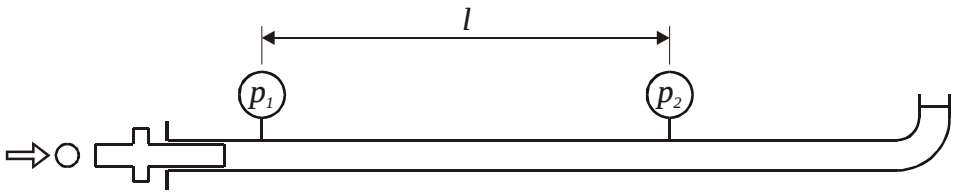

Figure 5.15: Experimental apparatus for the measurement of the speed of sound.

The excitation signal was produced by a ball, which was shot onto the free end of the piston. This signal was transformed into fluid fluctuation that was measured by means of two pressure transducers, illustrated in *Figure 5.16*. The comparison of the recorded pressure signals shows that the signals at the locations of the transducers are completely different. Not only the amplitude, but also the frequency of the first signal is greater.

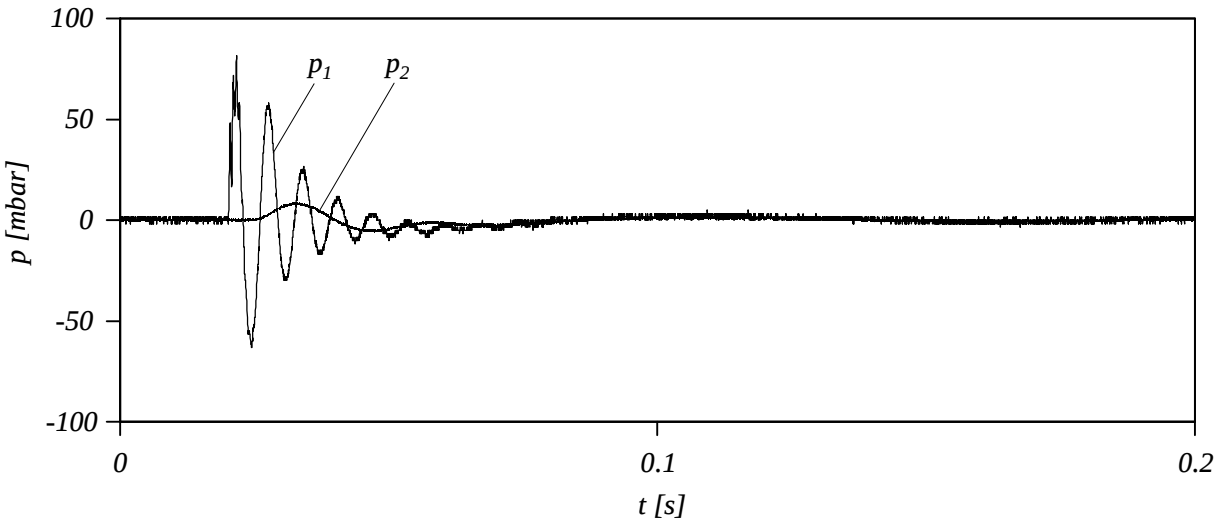

Figure 5.16: Pressure signals for the measurement of the speed of sound.

Nevertheless, based on these two pressure curves the speed of sound can be determined. Having the pressure signals in time domain the measured speed of sound c_m is calculated as a ratio of the distance l and the time difference dt:

$$c_m = \frac{l}{dt} \tag{5.21}$$

and the result is *434 m/s*. Although, one part of the air was removed before the experiment, there was still trapped air in the fluid. As discussed by the introduction to hydro-acoustics even a small amount of air has a significant effect on the dynamic behaviour of the fluid. It resulted not only in a lower speed of sound, but also the pulse amplitude at the second location was damped, as well.

Beside the amplitude the form of the pressure signal was also modified. Other authors dealing with the measurement of the speed of sound do not mention such a kind of signal deformation. The reason for this is that the system pressure of these measurements is much higher than the atmospheric one, hence the effect of the air is not significant. With our measurement the system pressure was equal to the atmospheric one for this reason the trapped air in the oil had a significant effect.

5.4.1 Filtering the measured signals

As the recorded pressures show, the fluid attenuates the signal and it behaves like a filter, due to the air contamination. In order to understand the measured signals and eliminate erroneous information it is recommended to analyse the signals with mathematical filtering tools. To suppress frequencies above a certain value a low pass filter is applied. This filtering process had three steps

- first the original signal was transformed into frequency domain,
- then amplitudes above the limit frequency were reduced to zero
- and finally the filtered signal was recalculated.

The filtered signals are presented in *Figure 5.17*.

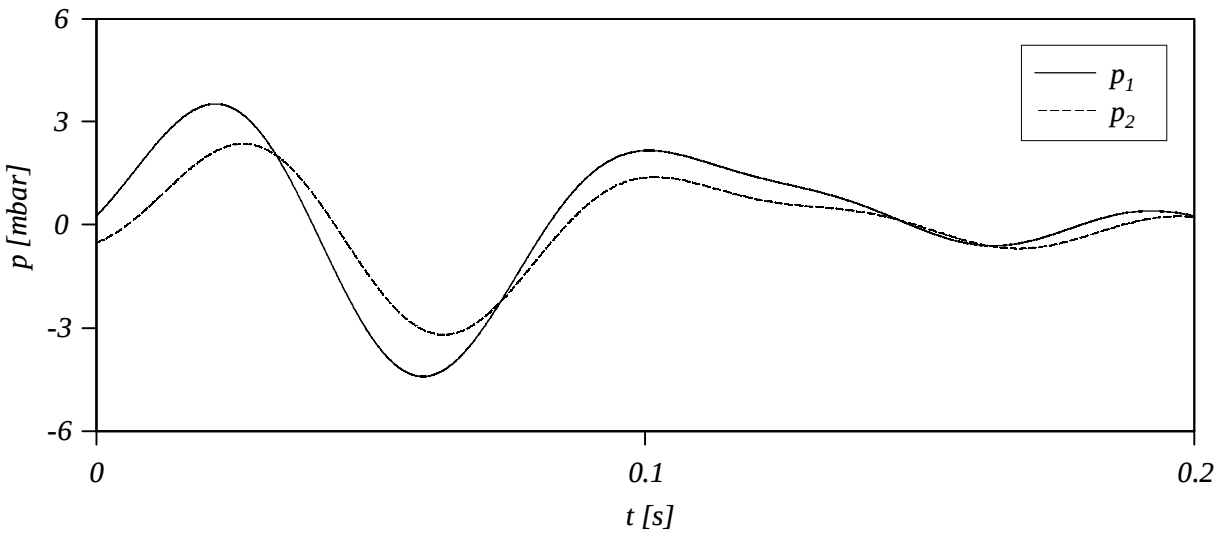

Figure 5.17: Filtered pressure signals for the measurement of the speed of propagation.

The form of both pressure signals has now the same characteristics, which confirms the assumption that the fluid column behaves like a filter.

5.4.2 Effect of the air contamination

It is important to perform the measurements in such a manner that the results are reproducible. In our case the most critical factor was the air trapped into the hydraulic oil. By filling the oil into the system a small amount of air was always introduced. To study the effect of the air contamination of the liquid the previous measurements were carried out in the following way. First the working fluid was oil, which was filled several times into the apparatus. During the filling and the empting processes more air was continuously introduced into the oil. These measurements were repeated with hydraulic oil that had not been used before. As *Figure 5.18* shows, air contamination has a significant effect on the damping characteristic of the fluid. At the first location the signals are still very similar (results with new oil are marked with *no*), however, at the second pressure transducer the damping effect of the used oil is significant. Not only the amplitude, but also the frequency is reduced that confirms the damping effect of the trapped air.

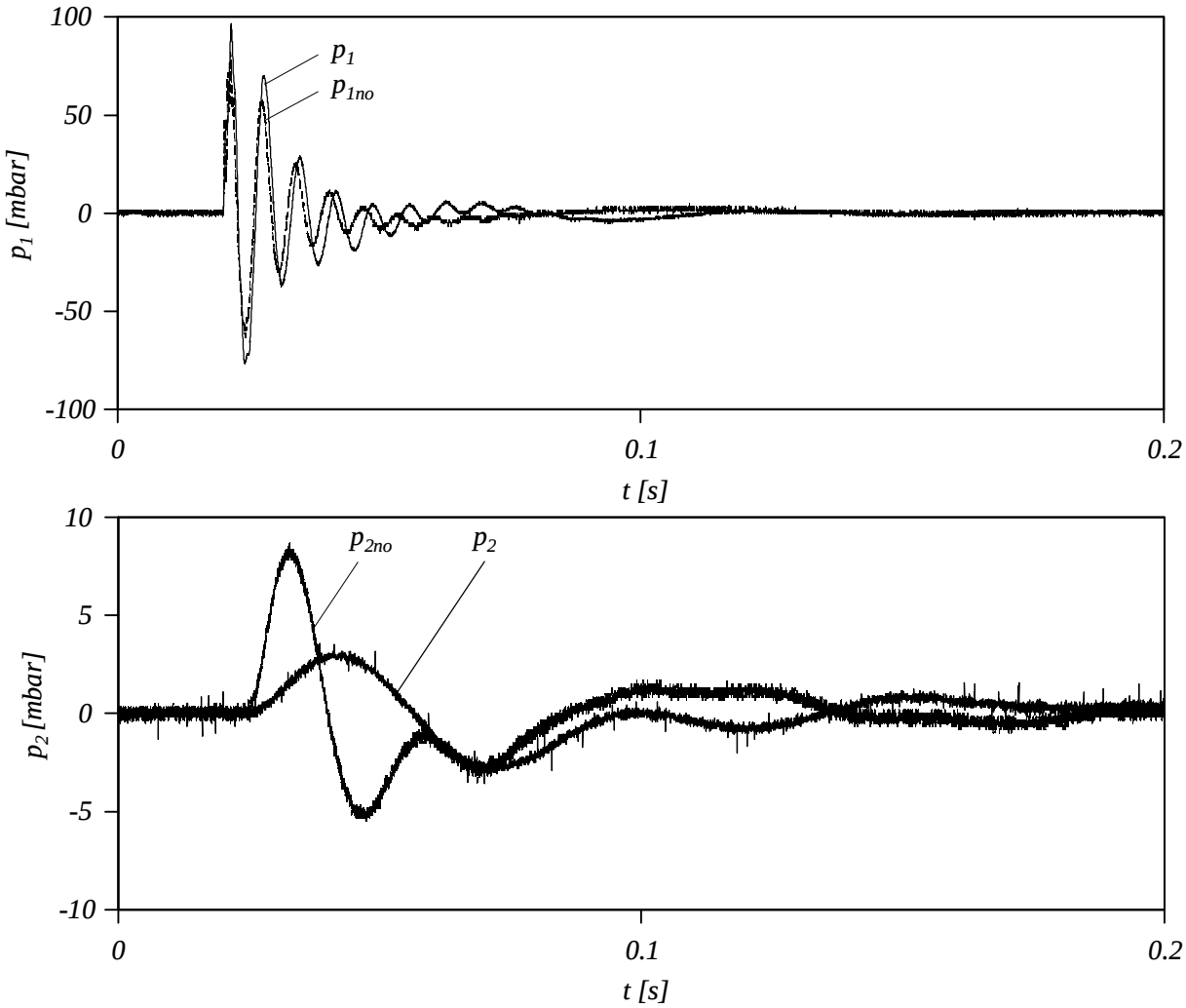

Figure 5.18: Pressure signals for used and new hydraulic oil.

5.4.3 Structure born vibration

Besides the air contamination, mechanical vibration can have an influence on the experiment. To study this second effect structural vibration was measured as well. The piston was shifted towards the cylinder until there was a mechanical contact between them, which is illustrated in *Figure 5.19*.

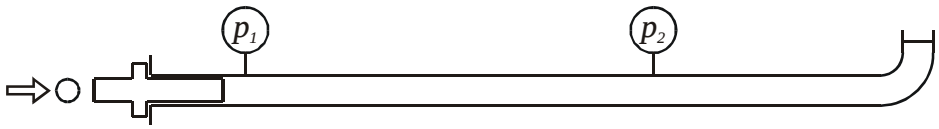

Figure 5.19: Structure born excitation.

The piston had a collar that transformed the mechanical excitation made by the ball to the piping. The right hand side end of the piston generated the excitation of the fluid, however, this signal was too small to detect it with the second pressure transducer. The direct fluid born and structure

born signals (marked with *str*), presented in *Figure 5.20*, are similar, but the amplitude is reduced. It means that although the piston creates more structure born vibration, fluid born vibration also exists.

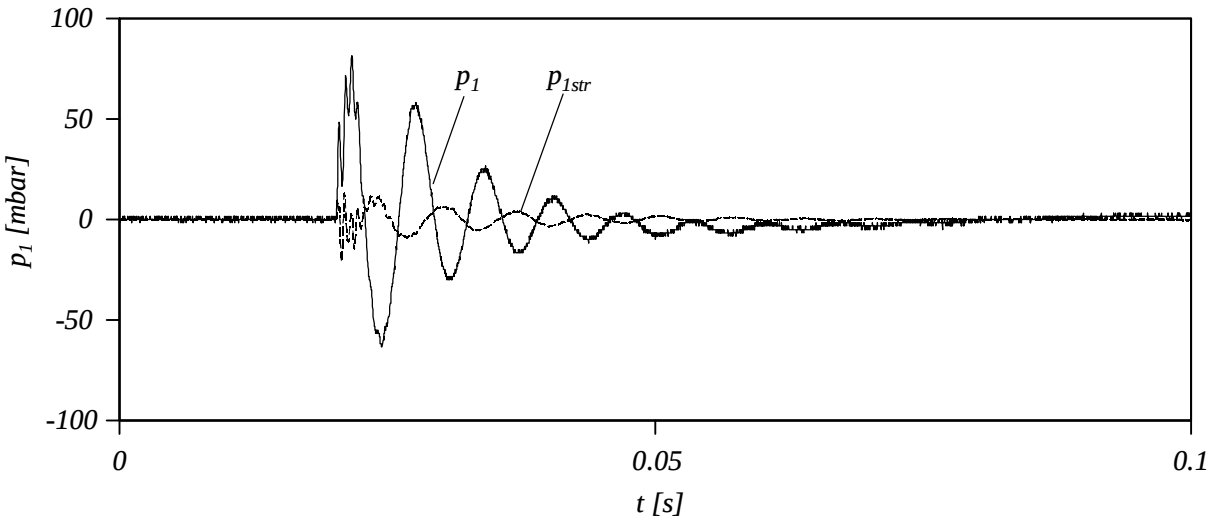

Figure 5.20: Fluid and structure born pressure signals.

During the measurements, the pipe of the loop had one clamp in the middle and one at both ends. Neither the increase of the fastening torque of the screws of the clamps, nor the increase of the number of the clamps resulted in a variation of the dynamic behaviour of the loop. Kurr [*88*] also studied this effect with similar results. Consequently, an incorrectly fixed pipe was not the reason of the dynamic behaviour of the system.

In order to find out if any other mechanical vibration had an effect on the experiment, the measurement was repeated without the working fluid. In this case only mechanical vibration was generated, but the pressure transducers could not detect it. Consequently, mechanical vibration of the piping is not the reason of the unexpected fluid pulsation. The characteristics of the fluid born and structure born vibrations are similar, hence it is a parameter of the fluid. In order to obtain more information concerning this unexpected dynamic behaviour the correlation between the resonance frequency and the length of the fluid column was studied.

5.4.4 Resonance frequency of the fluid column

In this section of the experimental work the fluid length was modified (l_{fl} = *1.4 m, 1.78 m, 2.71 m, 3.66 m, 5.22 m*) in order to study the effect of the length of the fluid column on the dynamic behaviour of the system. The measurements process was the same as described in the measurement of the speed of sound.

As discussed in the introduction of the hydro-acoustics, the natural frequency of the compressible fluid column depends on the speed of sound, the length of the fluid and the boundary condition at both ends. The experimental apparatus is already presented in *Figure 5.15*, at the left hand side there was a piston, therefore, this acoustical boundary condition was closed. The other end of the pipe was open, which corresponds to an open acoustical boundary condition. The natural frequency f_m is proportional to the measured speed of sound c_m and inversely proportional to the length of the fluid column l_{fl}, which was varied during these measurements, and given as:

$$f_m = \frac{c_m}{4\ l_{fl}}. \qquad (5.22)$$

The theoretical value of the natural frequency f_t is:

$$f_t = \frac{c_t}{4\ l_{fl}}, \qquad (5.23)$$

where the theoretical value of the speed of sound c_t is *1330 m/s*.

The resonance frequency f_r is determined from the recorded pressure signals. *Figure 5.21* illustrates the three different natural frequencies as a function of the inverse of the length of the fluid column l_{fl}. The correlation between the natural frequency and the length of the fluid column is proportional. The theoretically expected values of f_t are higher than the measured natural frequency f_m, but the resonance frequencies f_r obtained from the recorded pressure signals are even smaller.

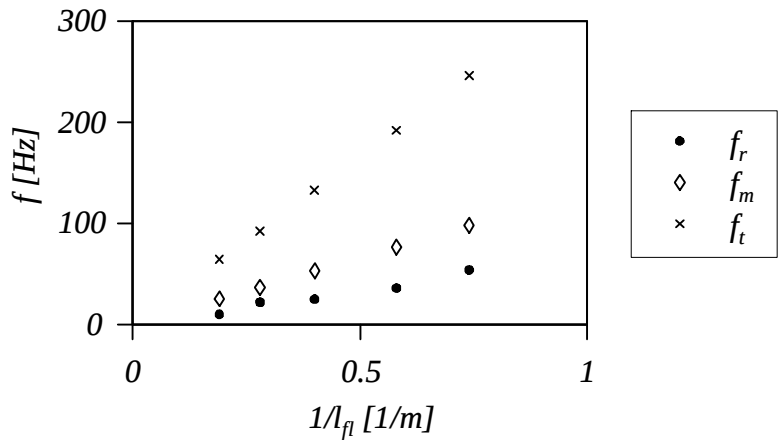

Figure 5.21: Calculated and measured natural frequency of the fluid column.

The results presented in the last sections represent that the dynamic behaviour of the experimental set-up differs from the expected one. The disturbances caused by the complex apparatus of [*1*] and [*2*] could be reduced, however, they still caused difficulties with the dynamic tests of the new technique. It is a very important point to note, because if one would

like to test a new measuring technique, then the detailed understanding of the test loop is necessary.

5.5 Pulsation measurement

As has already been mentioned, the experimental loops of the previous versions of the pulsation sensor were too complex. Such a kind of system is dangerous, because if one would like to investigate the dynamic behaviour of a new technique, the disturbance of the experimental loop should be kept as small as possible. In addition, a simple excitation signal is recommended for the dynamic test.

To reduce the disturbing effects, the piping was constructed as simple as possible, which is presented in *Figure 5.22*.

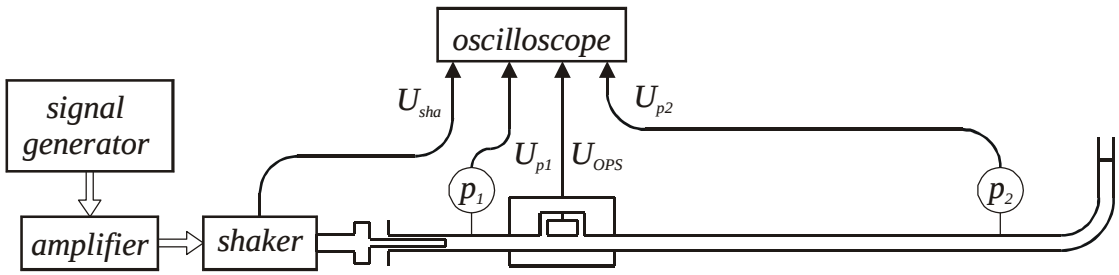

Figure 5.22: Experimental apparatus to measure the amplitude and frequency response of the OPS.

The pulsation source was chosen to be a shaker, whose pulsation did not contain as much harmonics as the pulsation of a pump. The frequency and the amplitude of the shaker was adjustable. To the moving part of the shaker a piston was fixed and its cylinder was connected to the piping. The piston-cylinder unit should have two important characteristics; first the friction between the moving parts had to be as small as possible, in order to generate pulsations with a wide range of frequency and amplitude. Secondly, air-seep into the fluid had to be avoided, because it damps the pulsations. The construction of the piston-cylinder unit is illustrated in *Figure 5.23*.

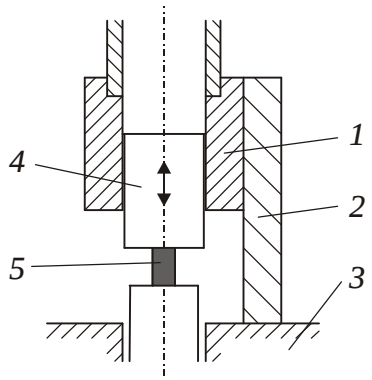

Figure 5.23: Piston-cylinder unit of the experimental apparatus.

The cylinder *(1)* was mounted with an adapter *(2)* onto the stationary body of the shaker *(3)*. To perform a perfect operation, the moving part of the shaker and the cylinder should be centralised. In practise it can be solved with high precision manufacturing, however in our case it was not possible. To compensate the existing misalignment, the coupling between the shaker and the piston (*4*) was performed with a magnetic one, part (*5*). In this way there was misalignment compensation, hence the unwanted pulsations were reduced. The advantages of this solution compared to the one used in [*2*] is that the friction between the moving parts were reduced and pulsation under *100 Hz* could be generated, as well.

The air contamination of the liquid caused many problems during the measurements. As the air is much more compressible than the oil it damps the pulsations. Another advantage of this simple experimental apparatus was that the air contamination could also be reduced.

5.5.1 Amplitude response of the OPS

During the test of the amplitude response of the OPS, sinusoidal oscillations were generated between *20 Hz* and *350 Hz*. At every frequency the velocity amplitude of the shaker was modified and the signals were recorded by the OPS. The flow pulsation measured by the OPS was evaluated by means of the static calibration factor and by means of *Equation (2.6)* and *(2.20)*. Two typical signals are illustrated in *Figure 5.24*.

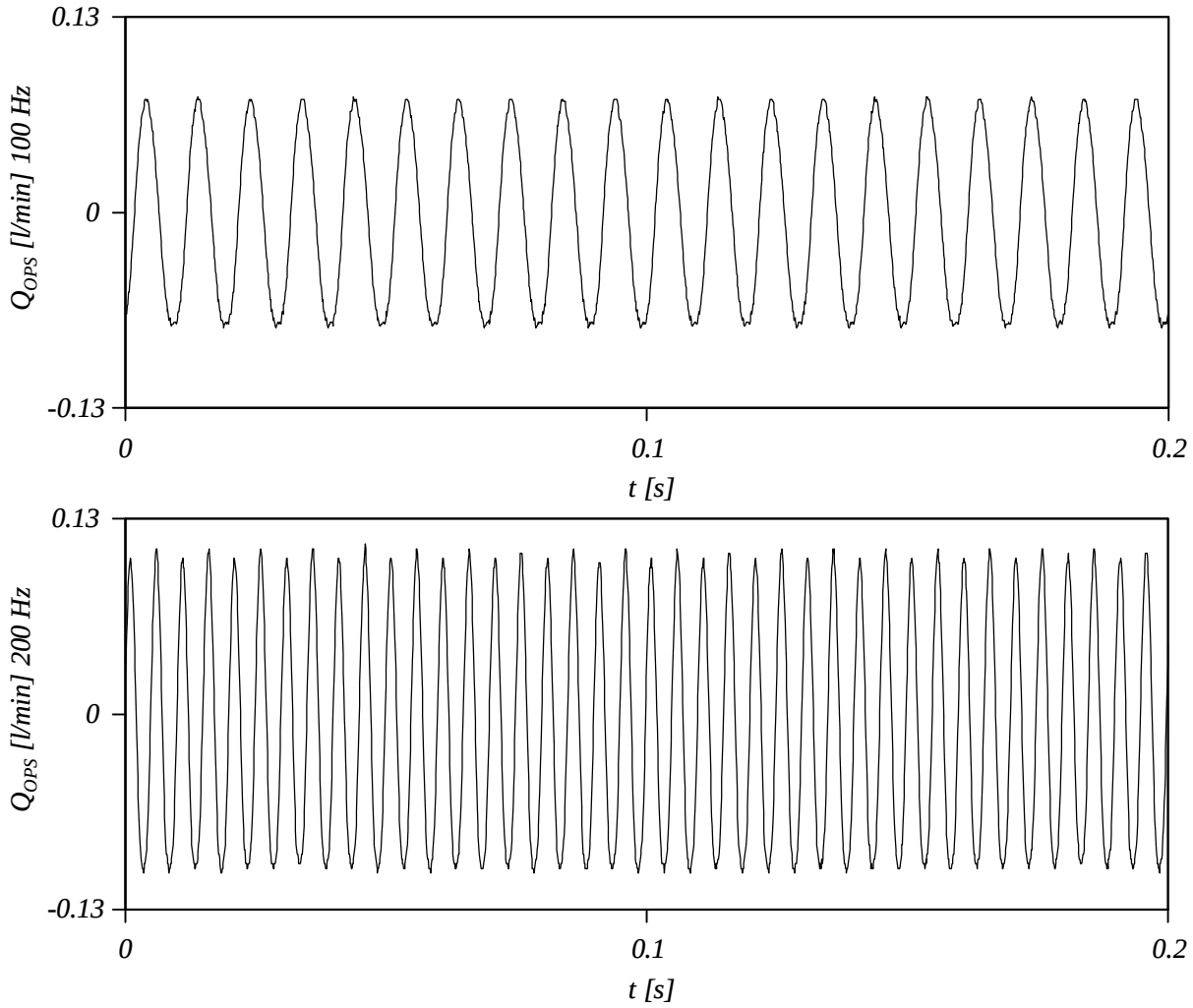

Figure 5.24: Flow pulsation signals of the OPS.

The output of the OPS has a sinusoidal form, the frequency of the excitation can always be detected; however, the amplitude depends on the frequency of the pulsation. Root mean square values of the signals of the OPS at two frequencies at different flow pulsation amplitudes of the shaker are plotted in *Figure 5.25*. At each frequency the increase of the amplitude of the excitation signal is easily detectable by means of the OPS. In the whole range the output signal is proportional to the input, but the slopes are different at different frequencies due to the resonance frequencies of the experimental loop.

In order to obtain information concerning the linearity of the OPS, the measured data were analysed with a linear regression technique [*89*]. In case of perfect correlation, i.e. all points lie along a straight line; the value of the correlation coefficient C_{cor} is one.

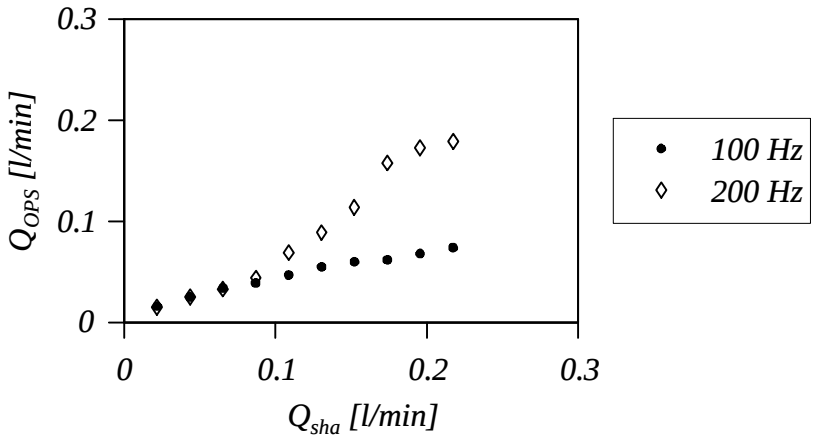

Figure 5.25: Amplitude response of the OPS.

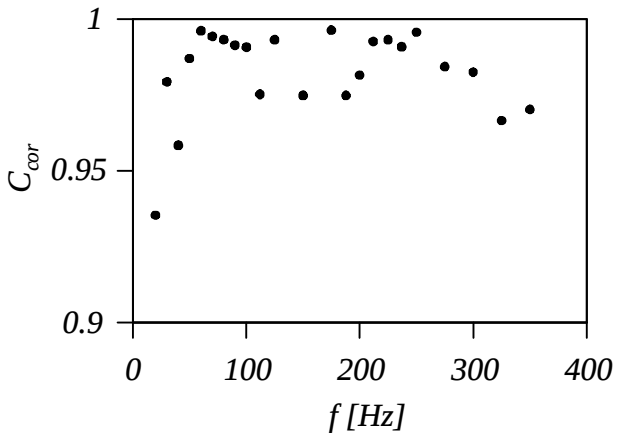

Figure 5.26: Correlation coefficient.

As *Figure 5.26* shows, in the total frequency range, the correlation coefficients are very close to one and it means that the linearity of the sensor is very good.

5.5.2 Frequency response

After the test of the amplitude response of the OPS, sinusoidal pulsations were generated in a frequency range between *10* and *2000 Hz*. During the tests the length of the fluid column was varied just like in the determination of the resonance frequency of the fluid. The experimental apparatus was already presented in *Figure 5.22*; the generated flow pulsation was detected with an accelerometer, which was fixed onto the moving part of the shaker. Its signal was used to determine the flow pulsation, illustrated in *Figure 5.27* at three different lengths of the fluid column.

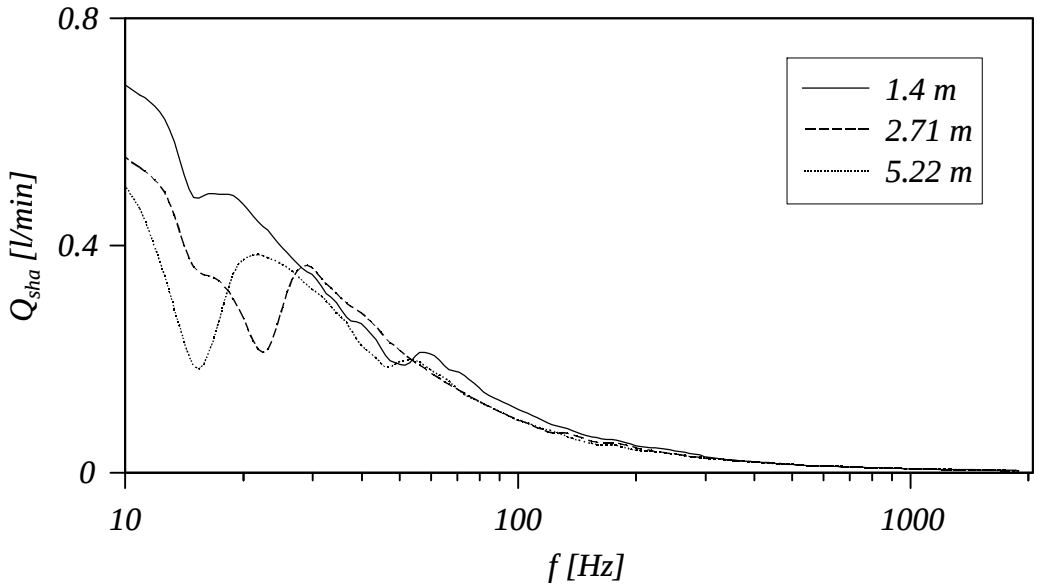

Figure 5.27: Sinusoidal excitation, flow pulsation of the shaker.

Although in all cases the output of the signal generator and the amplifier was the same, the pulsations of the shaker have different characteristics. It means that the fluid had an effect on the signal excitation depending on the length of the column. In case of a short fluid column (*1.4 m*) the curve has no significant peaks, increasing the length results in local minima, which corresponds to the resonance frequencies f_r presented in *Figure 5.21*.

In order to obtain information concerning the amplitude of the pulsation at different locations of the pipe, the generated pulsation was recorded by means of two pressure transducers. The first was located near to the excitation source and the second at the end of the piping. The recorded signals are presented in *Figure 5.28*. If the two transducers were located near to each other (thick lines) the signals had similar characteristics, but the amplitude was reduced. As the distance between the pressure probes was increased, the attenuation was higher, therefore the amplitude at the second transducer was continuously reduced. This damping effect can also be observed in *Figure 5.16*. Nevertheless, the first resonance frequencies can be detected at both locations. These peaks are equal to the resonance frequencies f_r presented in *Figure 5.21*, consequently they depend on the length of the fluid.

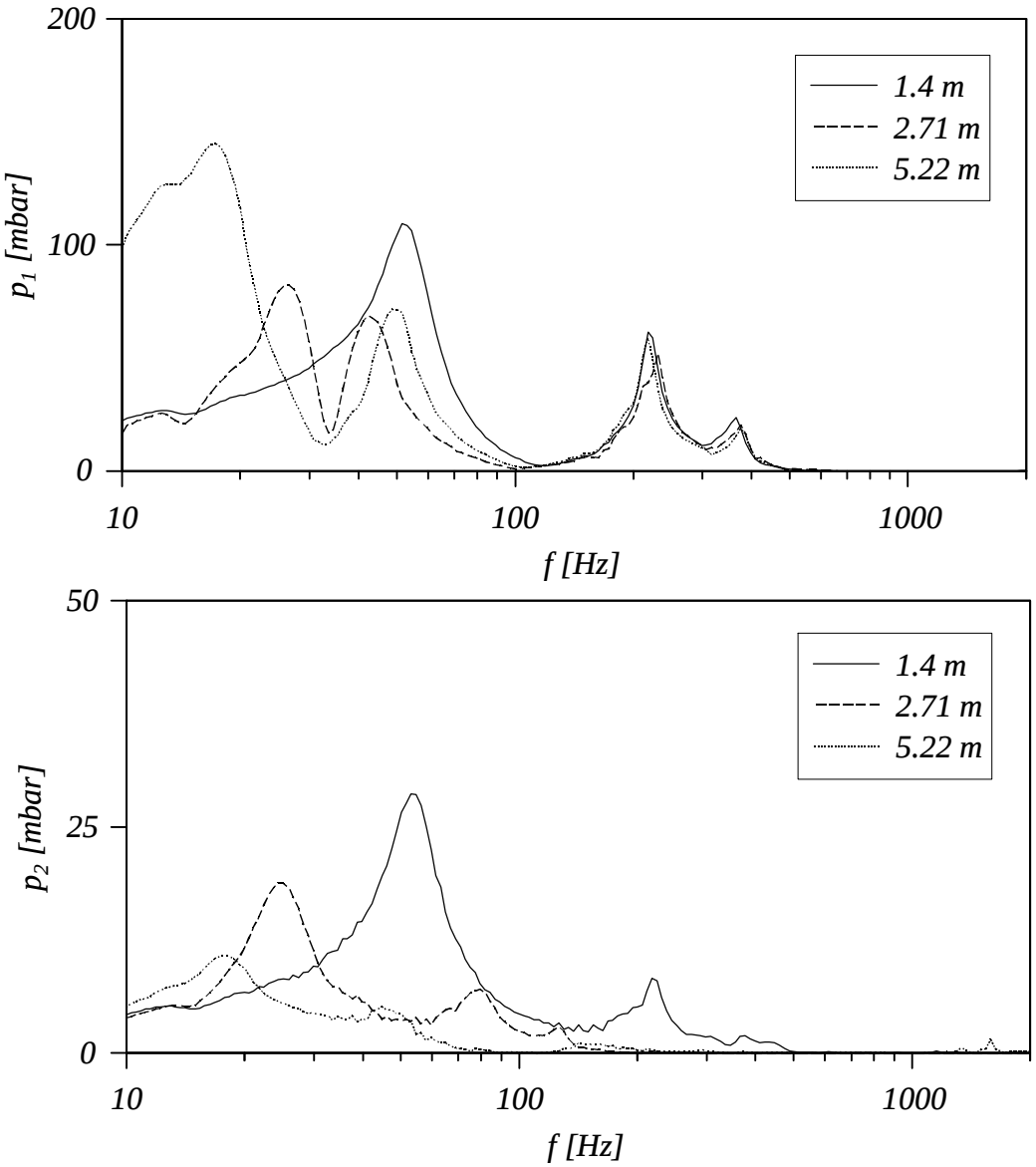

Figure 5.28: Sinusoidal excitation, pressure signals.

As *Figure 5.28* shows there are two peaks between *200* and *400 Hz* at the location of the first pressure transducer, independent from the length of the fluid. These maximums could also be detected by the second pressure transducer in case of the shortest piping and by the OPS, illustrated in *Figure 5.29*.

The same characteristic recorded with two different sensors located near to each other means that this was an attribute of the studied system and it had always an effect on the pulsation measurement. Above *400 Hz* the generated pulsation could be detected neither by the first transducer nor by the OPS. Consequently, in this experimental loop this was the maximal frequency that could be used to test the performance of the OPS.

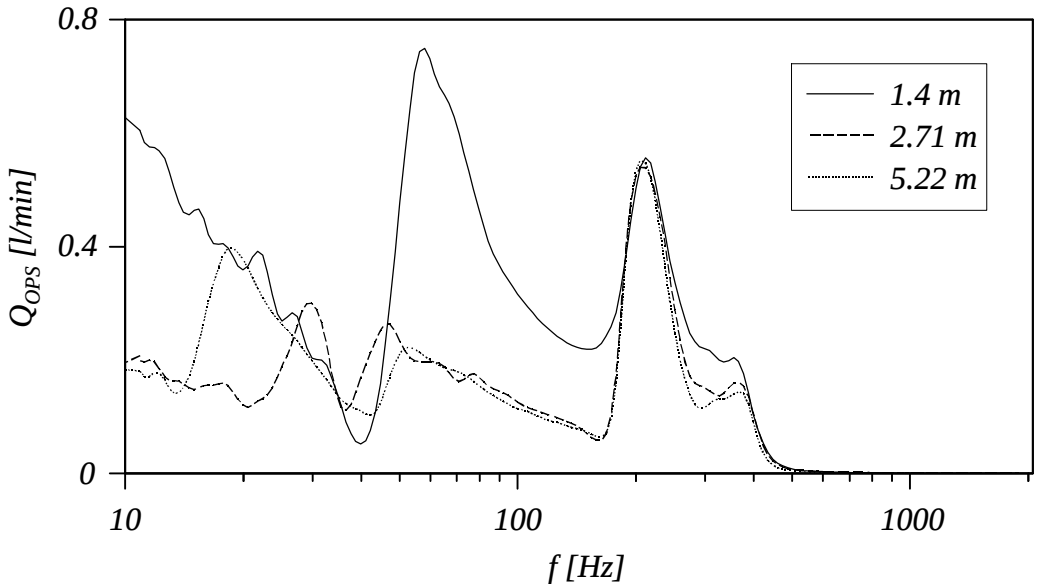

Figure 5.29: Sinusoidal excitation, signal of the OPS.

5.5.3 Comparison of the theoretical and experimental results of the transmission line

With the purpose of testing the frequency response of the developed sensor, sinusoidal pulsations were generated and recorded by pressure transmitters and by the OPS. As the experimental results show, not only the outputs of the OPS, but also the pressure signals are different from the expected ones. Therefore, the pressure distribution in the experimental apparatus is simulated based on the solution of Crocker [*70*] and Viersma [*74*]. *Figure 5.30* presents the comparison of the measured and calculated pressure distribution at the first pressure transducer at three different lengths of piping.

The theoretical solution, *Equation (5.17)*, predicts the first resonance frequencies, however the frequencies of the harmonics differ from the measured values. Besides this, the theoretical attenuation disagrees with the measured one. Another limitation of this theory is that it gives no information concerning the reason of the peaks between *200* and *400 Hz*.

With the calculation of the signal of the OPS the differential pressure between the taps is evaluated just like as with the pressure transducers. Its output is used to determine the deflection of the membrane from the static calibration factor. Having this value the differential pressure acting on the membrane can be calculated based on *Equation (3.1)*. The differential pressure between the two pressure taps is derived from *Equation (2.20)*. Finally the theoretical flow pulsation is determined from *Equation (2.6)*. These simulation results are compared to the experimental ones in *Figure 5.31*.

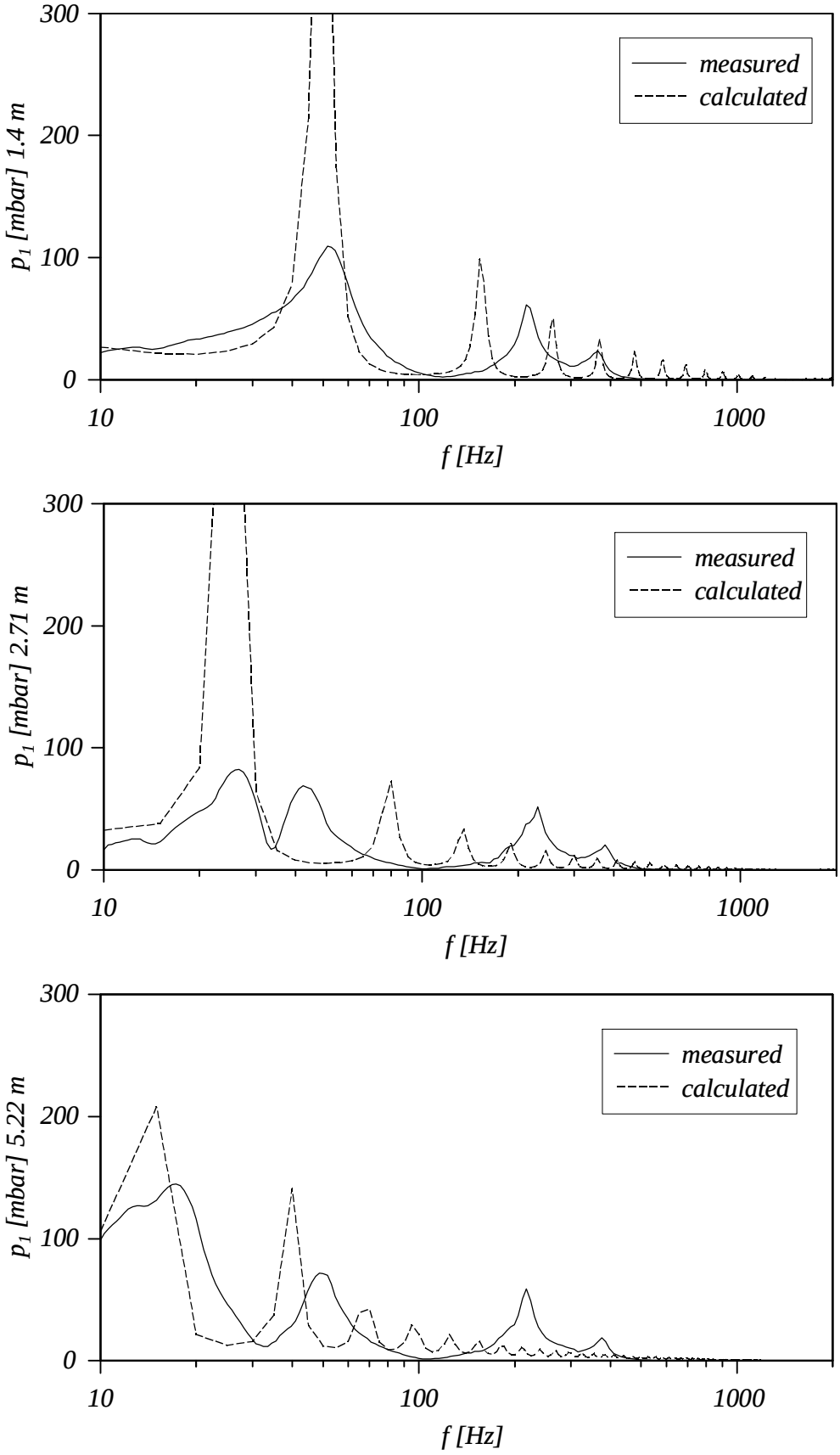

Figure 5.30: Comparison of measured and calculated pressure.

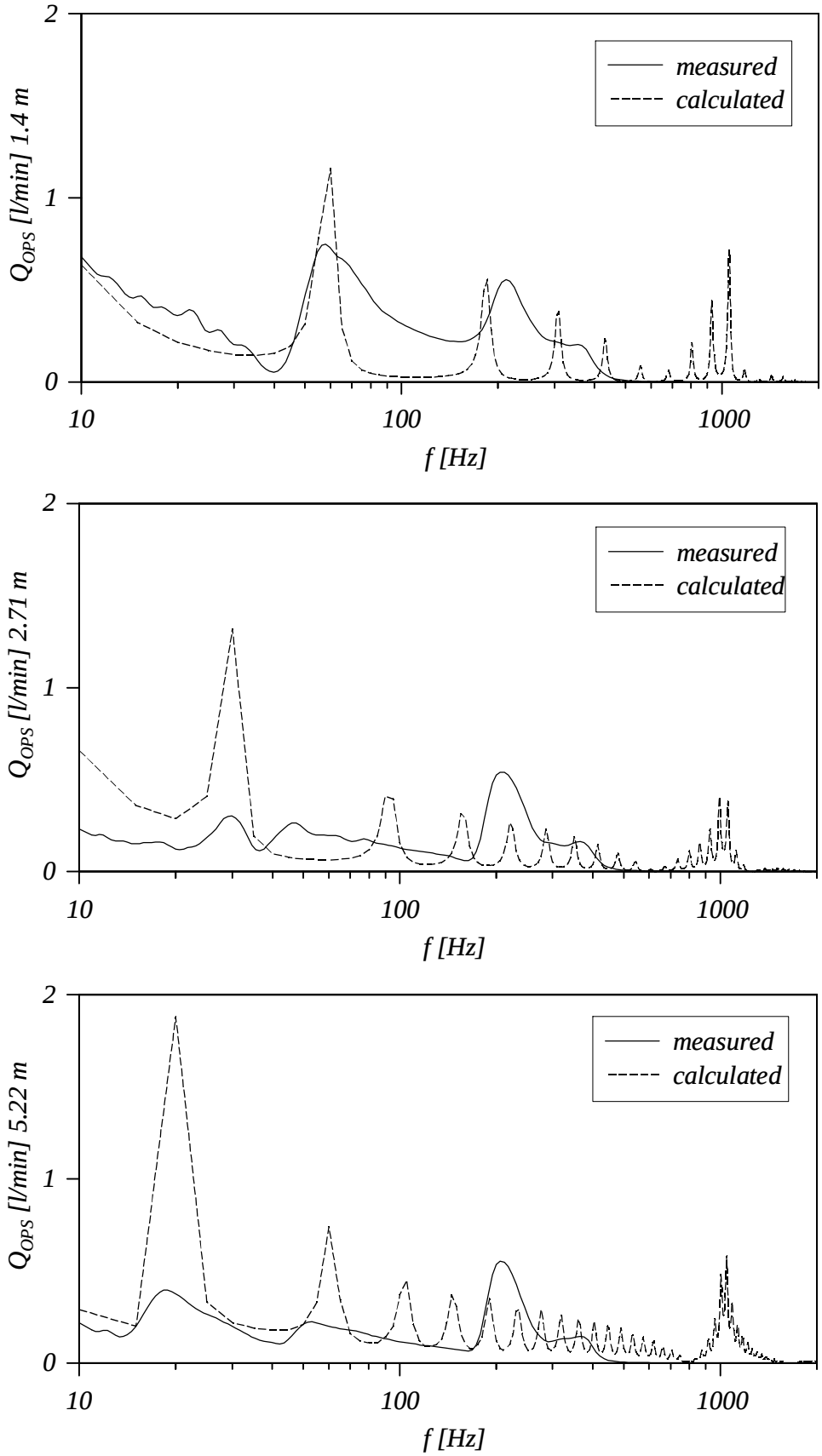

Figure 5.31: Comparison of measured and calculated flow pulsation.

The first natural frequencies of the measured flow pulsations are accurately predicted by the theoretical solution, however the resonance frequencies disagree just as the result of the simulation of the pressure signal.

5.6 Flow delivery of gear pumps

The pulsations sensor was developed in order to detect flow pulsations in real hydraulic systems. A typical unsteady signal is the flow ripple of the gear pump that was used to test the operation of the sensors. The main drawback of the application of the pump as a signal source was the complex waveform with major components at harmonics of the pumping frequency. However, with the test of a circuit the sensor proved its applicability to detect machinery failures.

To be able to compare the measured and the theoretical flow ripple, the understanding of the flow pulsation characteristic of the pump was necessary. Since from the pump manufacturer there was no documentation concerning this parameter, the pump operation had to be simulated.

In order to understand the flow pulsation of the gear pump, this section starts with a short introduction of this kind of pump. It is then followed by the theoretical determination of the flow delivery of a gear pump. Finally, some experimental results are presented.

5.6.1 Operating principle of gear pumps

The German astronomer and mathematician Johannes Kepler patented the first gear pump in *1604* [*90*]. Because of the simple construction and low cost, these kinds of pumps are widely used in hydraulic systems. Their main drawback is the noise and pulsation that originates from the kinetics of the rolling process within the meshing gear pairs [*39*], [*91*], [*92*], [*93*], [*94*], [*95*], [*96*], [*97*]. This noise is transmitted and amplified by other system components (fluid, piping).

Gear pumps are positive displacement rotary pumps in which two or more gears mesh to provide the pumping action, illustrated in ***Figure 5.32***. As the teeth disengage, suction pressure delivers liquid into the cavities between the teeth. The teeth then carry the liquid around to the discharge side of the pump. As the teeth engage, the fluid is pressed into the discharge. Based on this process the gear pumps have a pulsating output whose detailed description is presented later.

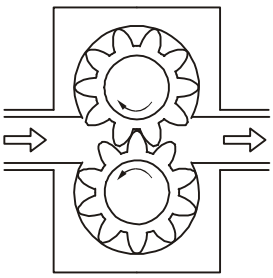

Figure 5.32: Schematic drawing of a gear pump.

The basic frequency f_b of the flow pulsation is the product of the number of gear teeth z and the revolution speed n of the pump shaft:

$$f_b = zn\,. \tag{5.24}$$

Two meshing gears generate a single pulsation frequency. The geometric flow of the pump is the superimposed flow from all pumping volumes. However, this theory is not sufficient alone to explain the pump flow pulsation. Each time a pumping volume meets the output port of the pump there is a rapid backflow into the suction side. The seal between suction and delivery is the mechanical contact of the teeth driving each other. As the backflow is very fast, there are also a number of harmonics. If the system pressure is equal to the pressure in the suction side, the backflow is reduced; hence, the geometric flow pulsation is dominant. The size of the backflow also depends on the system pressure.

Variation of the tooth pair stiffness during meshing is other source for the generation of vibrations. It can be reduced with the variation of the gear geometry, for example profile correction, optimisation of the profile and overlap ratio.

Normally not only one pair of teeth meshes each other at the same time (overlap ratio is larger than one), thus a small amount of fluid is closed between these two pairs. The fluid closed in this gap is called “trapped oil”. As the volume of the gap is not constant the oil inside it is compressed so it also results in vibration. With special design features it can be achieved that the pressure peaks caused by trapped oil are reduced.

5.6.2 Geometrical flow delivery of gear pumps

Different solutions for the flow delivery can be found in [*92*] [*98*] [*99*], however in this work the flow delivery of the applied gear pump was determined by the method of Ivantysyn [*100*].

The input parameters of the calculation were the geometrical dimensions of the gear pump:

r_{h1}, r_{h2} - outside radius

r_1, r_2 - pitch radius

b - tooth width

z_1, z_2 - number of teeth

a_k - centre distance.

The solution of Ivantysyn [*100*] has a form of:

$$Q_g(t) = bp\ \ n\frac{1+e_o}{2}\left(r_{h1}{}^2 + \frac{r_1}{r_2} r_{h2}{}^2 - r_1 \frac{a_k{}^2}{a} - \left(1+\frac{r_1}{r_2}\right)\left(r_1 \sin(2p\ \ nt)\right)^2 k_g \right). \qquad (5.25)$$

where n represents the revolution speed of the pump shaft, e_0 is the overlap ratio ($e_0 = 1.193$) and k_g is the modified trapped oil factor ($k_g = 1.23$). The frequency of the flow pulsation is defined in *Equation* (*5.24*). As *Equation* (*5.25*) shows the frequency and the amplitude of the pulsation is proportional to the pump speed ($n_1 > n_2 > n_3$) illustrated in *Figure 5.33*.

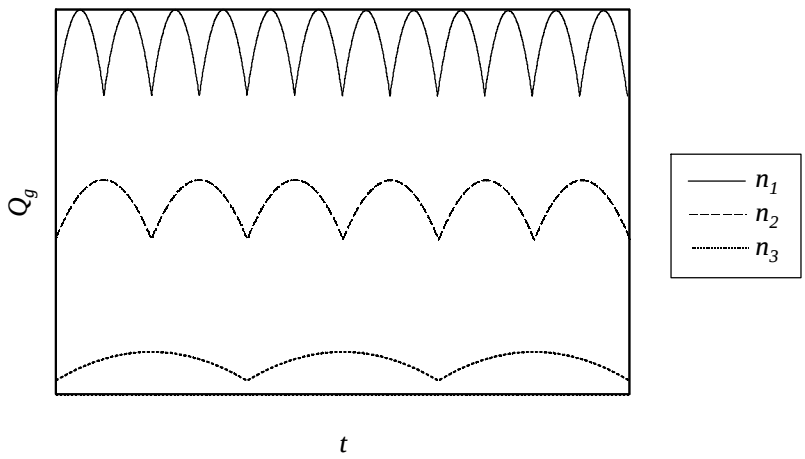

Figure 5.33: Flow delivery of a gear pump at different speeds.

The average geometrical flow rate Q_{ga} can be determined from the following equation:

$$Q_{ga} = \frac{1}{t_2 - t_1}\int_{t_1}^{t_2} Q_g(t)dt\,. \qquad (5.26)$$

In order to compare the pulsation of different kinds of pumps a parameter is defined, which represents the ratio of the pulsation magnitude (the difference between the maximal Q_{gmax} and minimal flow rate Q_{gmin}) to the average flow rate Q_{ga}:

$$d = \frac{Q_{g\max} - Q_{g\min}}{Q_{ga}}\,. \qquad (5.27)$$

The parameter d defined above is called “pulsation factor” or “flow deviation”. The lower its value the smoother is the flow delivery of the studied pump. In the case of gear pumps its value

depends on the number of teeth, respectively the teeth geometry and has a typical value between *9 %* and *24 %* for a teeth number of *24-8* [*93*]. Ivantysyn defined the pulsation factor as a function of the teeth number and in case of a pump with *10* teeth the value of the pulsation factor was *20 %*.

Determining the flow delivery of the applied pump with *Equation* (*5.25*) the pulsation factor d is almost twice as much as expected. To reduce the pulsation, a correction factor is applied, hence the flow pulsation is:

$$Q_g(t) = bp\ n\frac{1+e_o}{2}\left(r_{h1}{}^2 + \frac{r_1}{r_2} r_{h2}{}^2 - r_1 \frac{a_k{}^2}{a} - \left(1+\frac{r_1}{r_2}\right)\left(r_1 \sin(2p\ nt)\right)^2 k_g k_d \right), \qquad (5.28)$$

where the value of the pulsation correction factor is $k_d = 0.564$. Calculating the pulsation factor based on the flow delivery defined in *Equation* (*5.28*), a value of *20 %* is obtained.

The data sheet of the applied pump contains only one parameter regarding to the flow delivery, the average flow rate is *18 l/min* at a revolution speed of *25 Hz* (system pressure is *1 bar*). According to the flow delivery determined by *Equation* (*5.28*) this value is higher, hence, another correction factor is necessary that reduces the flow rate. The value of the flow rate correction factor is $k_f = 0.9$ and the flow delivery function is defined as:

$$Q_g(t) = bp\ n\frac{1+e_o}{2}\left(r_{h1}{}^2 + \frac{r_1}{r_2} r_{h2}{}^2 - r_1 \frac{a_k{}^2}{a} - \left(1+\frac{r_1}{r_2}\right)\left(r_1 \sin(2p\ nt)\right)^2 k_g k_d \right) k_f . \qquad (5.29)$$

In this way the flow delivery of the applied gear pump is modelled. It should be mentioned, that this model expresses the geometrical flow rate. Loss factors, compression and the damping effect of the system pressure are not included within this model.

The flow fluctuation, based on the geometrical parameters of the pump, is determined using *Equation* (*5.29*). From the dynamic point of view the pulsation amplitude and frequency are two important parameters. *Figure 5.34* illustrates the maximal, minimal and average flow rate as a function of the pump speed. As the diagram shows the pulsation amplitude has a linear correlation with the revolution speed of the pump shaft.

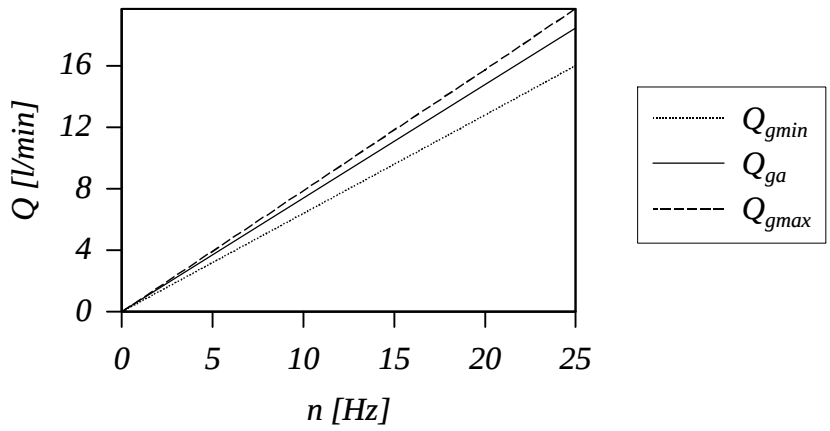

Figure 5.34: Flow rate as a function of the pump speed.

5.6.3 Measurement of the flow delivery of the gear pump

At the beginning of this work some test measurements were carried out with the version of the pulsation sensor presented in [*2*]. This version was built into an experimental apparatus, illustrated in *Figure 5.35*, to measure the flow ripple of a gear pump.

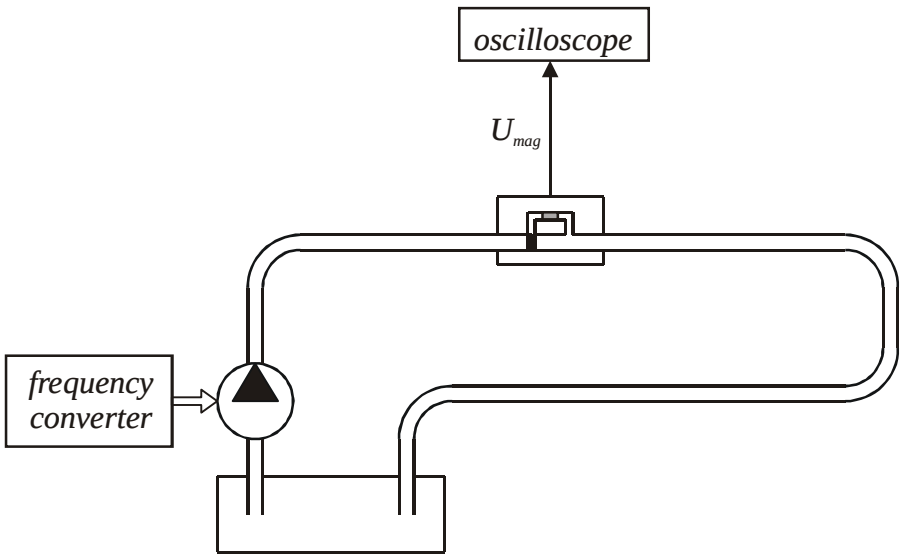

Figure 5.35: Flow ripple measurement of the old gear pump.

The single adjustable system parameter was the pump speed that resulted in a pulsation at discrete frequencies. As discussed by the theoretical study of the flow delivery of the gear pump the pulsation frequency is the product of the pump speed and the number of teeth. This was the expected frequency although the experiments delivered some surprising results, plotted in *Figure 5.36*. Since the perpendicular tube of the sensor alters the flow field the correlation between the flow pulsation and the output signal of the second version is not determined. For this reason the output voltages U_{mag} are plotted in the diagram.

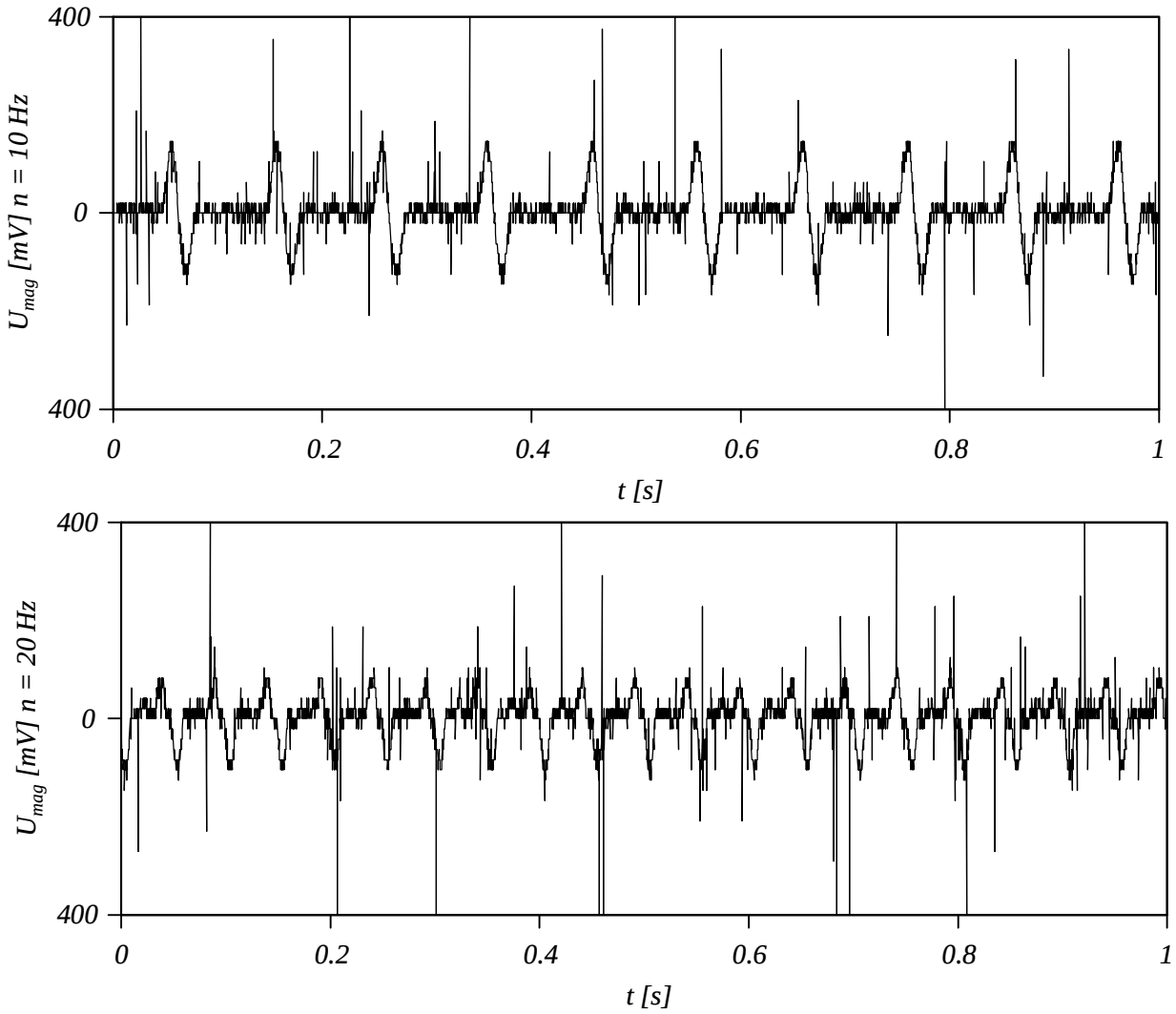

Figure 5.36: Flow ripple of the old gear pump.

As the graphs show, the electro-magnetic disturbance and the high noise level reduces the quality of the magnetic transducer. These disturbances were eliminated by the application of the optical pressure transducer.

The recorded signals of the second version were periodic, however the frequencies were lower than the basic frequency determined by *Equation (5.24)*. Measurements were carried out at different flow rates and the frequencies of the measured signals were always equal to the revolution speeds of the shaft of the pump. The search for the reason of this unusual signal led us to open the pump. It proved to be a good decision, because one tooth of the pump was broken.

This failure was detected by the pulsation sensor, which indicated that this method works well in practice. This fact encouraged us to continue the development of the new pulsation measurement technique.

After the detection of the failure, a new pump was substituted for the old one. As the pump manufacturer did not provide a detailed description of the flow delivery of the pump this characteristic had to be simulated to be able to compare the theoretical and experimental measured pulsations. The input parameter of this model was the tooth geometry. Before the pump was built into the loop, it was opened to measure its geometrical dimensions. The geometrical flow delivery of the gear pump was determined based on *Equation (5.29)* and is illustrated in *Figure 5.37*. As the chart illustrates the flow ripple always has sharp tips, when the delivery of one pair of teeth is finished. In the real pump these sharp tips were damped, therefore, the curve should be smoother. In addition, the fluid was compressible which resulted in a reduced amplitude, as well.

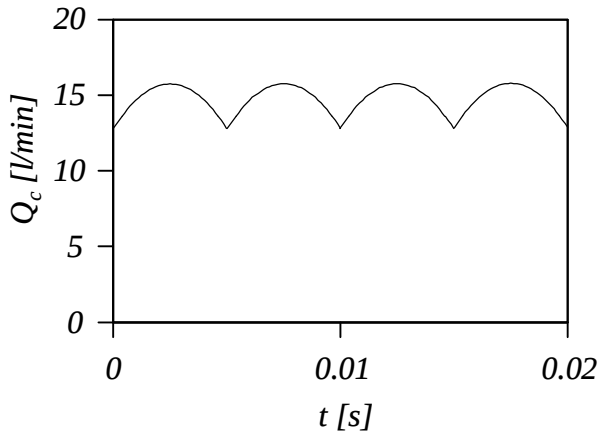

Figure 5.37: Calculated flow pulsation, n_p = *20 Hz*.

To measure the flow ripple of the new gear pump, the OPS was mounted into a simple hydraulic loop, illustrated in *Figure 5.38*.

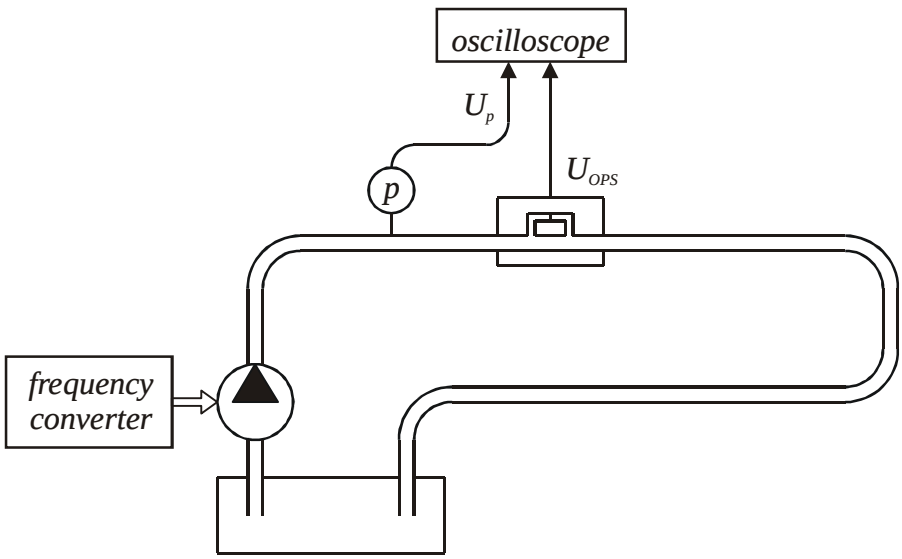

Figure 5.38: Experimental apparatus, flow ripple measurement.

The circuit also contained a pressure transducer in order to measure the system pressure and obtain information concerning the form of the pressure pulsation.

Measurements were carried out at different revolution speeds of the pump shaft, between *2.5 Hz* and *20 Hz*. *Figure 5.39* illustrates a signal measured at a revolution speed of *20 Hz*.

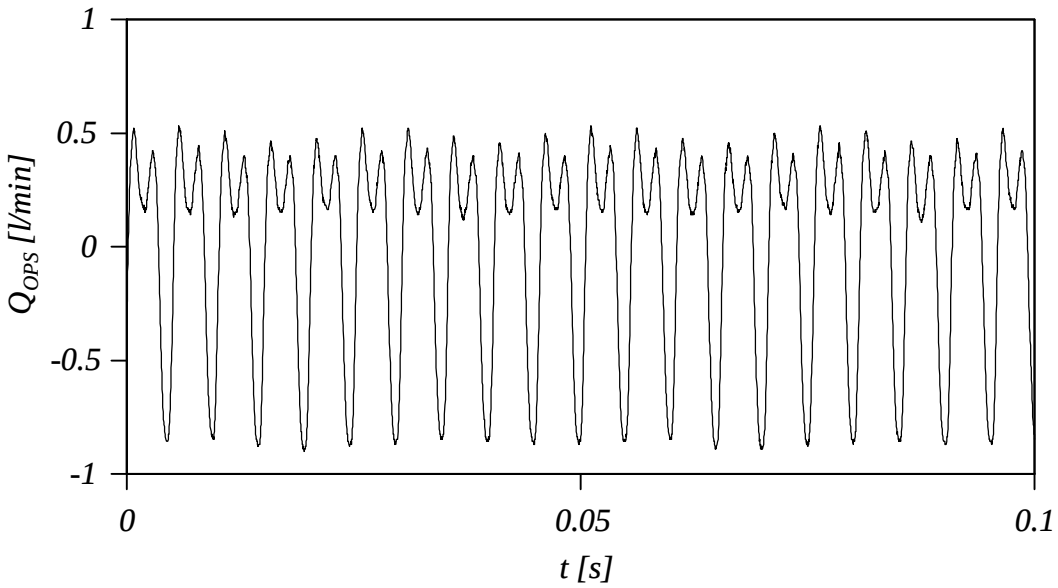

Figure 5.39: Flow pulsation measured by the OPS, n_p = *20 Hz*.

The flow pulsation measured by the OPS differs from the result of the flow delivery calculation. One of its reasons is the theoretical model of the pump, which defines only the pure geometrical flow delivery but does not include the dynamic effects caused by the pressure difference between the suction and the delivery side. Another trouble source is the compressibility of the working fluid, which is even increased by the air contamination.

In order to detect the pulsation a pressure transmitter was built into the circuit and the recorded signal is presented in *Figure 5.40*. As the diagrams represent, the pressure pulsation is also a complex signal just like the flow pulsation recorded by the OPS.

The spectral distributions of the measured signals were obtained by feeding the data into a spectrum analyser (Fast Fourier Transformation). The amplitude distributions (normalised by the maximal amplitudes) as a function of frequency are illustrated in *Figure 5.41*. The basic pumping frequency (pump speed multiplied with the number of teeth, *200 Hz*) is visible with both of the instruments.

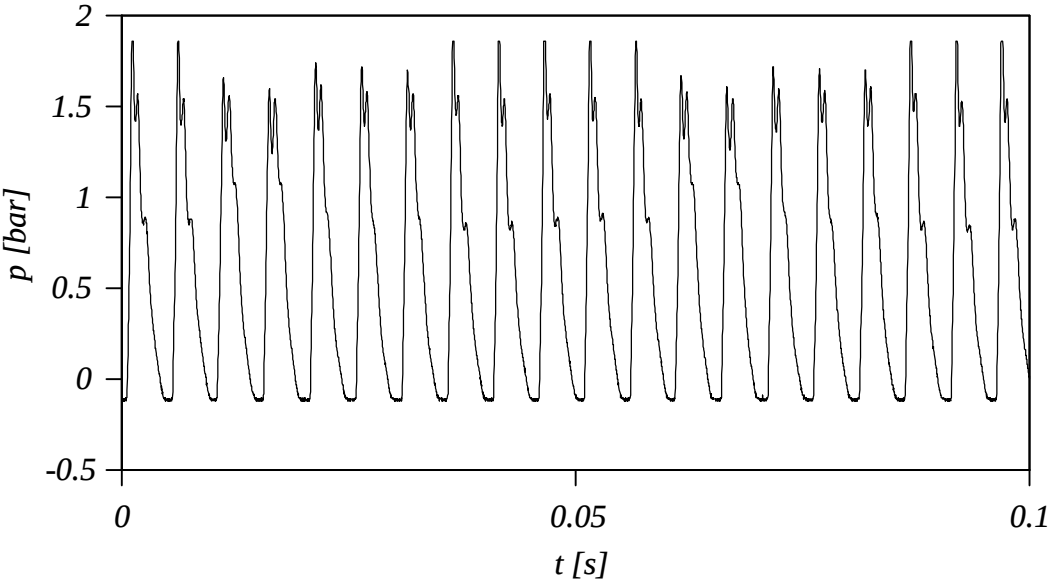

Figure 5.40: Pressure pulsation measured by the pressure transducer, n_p = *20 Hz*.

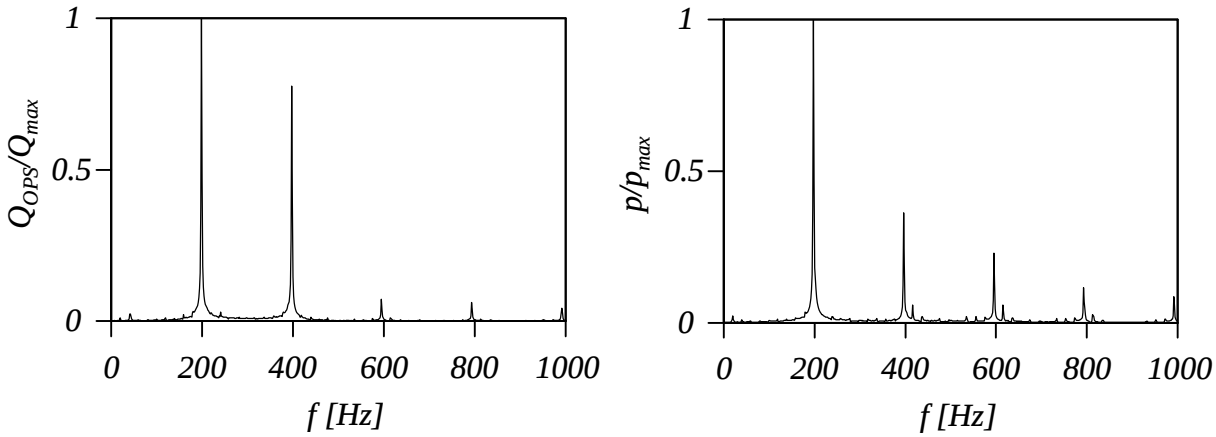

Figure 5.41: FFT signals of the OPS and the pressure transducer, n_p = *20 Hz*.

The comparison of the calculated *Equation (5.29)* and measured flow pulsations are plotted in *Figure 5.42*. Increasing the pump speed results in increased pulsation amplitude, which is also detected by the OPS. As the diagram shows the amplitude of the measured signals are lower than the theoretical ones. Its reason is that loss factors, compression and the damping effect of the system pressure are not included within the theoretical model. Nevertheless, the two curves have the same slope that indicates that the measured signals are proportional to the calculated ones.

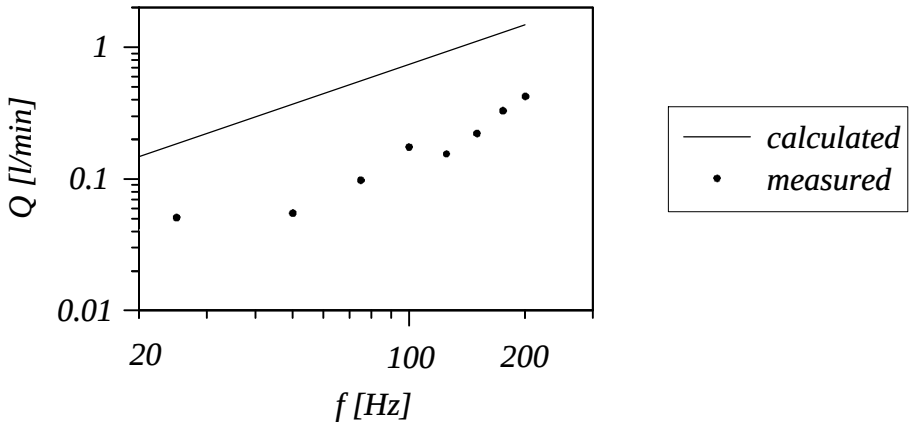

Figure 5.42: Calculated and measured flow pulsation of the pump.

5.7 Summary of the experimental results

In the hydraulic industry there is a demand for a simple method that can measure flow pulsation in a wide bandwidth. As the results presented here show besides the development of the pulsation sensor, the test facility also needs a detailed investigation. The simpler is the set-up the easier the analysis.

The flow ripple of a gear pump is too complex to study the dynamical behaviour of a new technique at the early stage of the development. The application of a shaker as a pulsation source with a simple piping was a good decision. Based on the measurements it is clear that with this experimental apparatus the maximal pulsation frequency is approximately *400 Hz*. This upper limit is higher than the one of other techniques, in addition the form of the excitation signal is simple and it has a discrete frequency component.

An important point to note is the low value of the speed of sound caused by the air contamination. With the understanding of this speed the first resonance frequency of the fluid could be predicted, however, the theory fails by the determination of the harmonics.

Although much effort has been put into the study of the dynamic behaviour of the experimental apparatus, the understanding of the flow pulsation and its damping under such conditions is far from complete.

Recommendation for further woks is to apply an even simpler experimental apparatus which dynamic characteristic is known. With the understanding of this behaviour one could focus on the true development of the sensor.

6 Conclusions

In this study, a method is presented to measure flow pulsation in hydraulic systems. The experimental results demonstrate that the optical pulsation sensor is an effective device for this purpose. When developing a new technique for the measurement of unsteady flow parameters, one must understand the physical characteristics of the test apparatus and be especially aware of the resonant frequency and the damping effects.

The main conclusions can be summarised as follows:

Differential pressure measurement is suitable to detect flow pulsation. For industrial applications a wide operating pressure range is welcomed. If one would detect differential pressure by means of two individual pressure transmitters, the system pressure would be limited by the range of the individual instruments. Applying only one unit has the advantage that the system pressure can be arbitrarily high.

During the design of the optical pulsation sensor an important aim is to achieve a compact construction of the sensor without introducing appreciable manufacturing difficulties. To minimize the distortion of the flow field from the presence of a probe, the pressure taps are mounted flush on the wall. In order to improve the dynamic performance of the pressure sensing system a fast transducer is applied and the length of the tubing is made as short as possible. By means of two tubes the trapped air can be removed.

In common industrial applications the pressure sensors are operating in a very noisy environment with many electrical and magnetic disturbances. Applying the optical transducer has a benefit that these disturbances do not influence the performance.

The pressure sensing element must be produced as one unit, which guarantee a fixed position of the individual components to each other. Thus, it has a low sensitivity to mechanical vibrations that allows the operation in vibrating systems.

With this optical technique a very small displacement can be detected permitting high sensitivity. The reflecting membrane is appropriate for the transformation of the differential pressure into mechanical motion and the applied theory describes the true deformation well.

The compact positioning unit fulfils the requirements of the sensitive optics and allows the adjustment of the position of the source-detector unit in three directions with high precision.

Concerning the experimental setup it is essential to mention that a simple excitation signal is required for the test of such a kind of new measuring device. Besides this the apparatus should be as simple as possible, in order to eliminate parameters disturbing the analysis of the pulsation sensor.

The low value of the speed of sound has a significant effect on the dynamic behaviour of the system. The first resonance frequency can be determined with the transmission line theory, but the harmonics do not match.

The resonance peaks are recorded, not only by the optical pulsation sensor, but also by the applied pressure transducers. It demonstrates that it is the real system behaviour, not a measuring failure.

Due to the dynamic response of the fluid and the piping system, the dynamic calibration of the sensor in this experimental apparatus is limited. Owing to the acquired experience, the dynamic calibration should be done only for the bypass-membrane part of the sensor without the main flow. It would provide the dynamic response of this measuring technique independent from the disturbing effects.

Bibliography

[*1*] Nagy, R.: Beitrag zur Dimensionierung, Simulation und Kalibrierung eines elektrohydraulischen Pulsationssensors sowie seine Erprobung, Diplomarbeit, TU Bergakademie Freiberg, *2000*

[*2*] Pál, Á.: Beitrag zur Weiterentwicklung eines Volumenstromssensors für Drucköle, Diplomarbeit, TU Bergakademie Freiberg, *2001*

[*3*] Backer, R. C.: Flow Measurement Handbook, Industrial Designs, Operating Principles, Performance, and Applications, Cambridge University Press, *2000*

[*4*] Schäfer, R.: Durchflussmessungen von Flüssigkeiten mit Differenzdruckverfahren bei kleinere Nennweiten, Dissertation, VDI Verlag Düsseldorf, *1999*

[*5*] DIN-Taschenbuch *229* Durchflussmessung von Fluiden in geschlossenen Leitungen mit Drosselgeräten, Beuth Verlag Berlin, *1993*

[*6*] Bonfig, K. W.: Technische Durchflussmessung, Vulkan Verlag, Essen, *1987*

[*7*] Lipták, B. G.: Instrument Engineers´ Handbook: Process Measurement and Analysis, Chilton Book Company, Randor, Pennsylvania, *1995*

[*8*] Schrüfer, E.: Elektrische Messtechnik, Cals Hanser Verlag München Wien, *1995*

[*9*] Harland, P. H.: Pressure Gauge Handbook, Ametek U.S. Gauge division, Sellerville, Pennsylvania, *1985*

[*10*] Miller, R. W.: Flow Measurement Engineering Handbook, McGraw-Hill, *1996*

[*11*] Pathak, M. M., Rediniotis, O. K.: A simple technique for frequency response of the miniature pressure probes, AIAA Journal, Nr. *37*, pp. *897-899*, *1999*

[*12*] Johansen, E. S., Allen, R. D., Rediniotis, O. K., Zeiger, M. D.: Embedded-Sensor, Fast-response, Multi-hole probes, *41st* Aerospace Sciences Meeting and Exhibit, January *6-9*, *2003*, Reno, Nevada, USA

[*13*] Schäfer, R.: Durchflussmessungen von Flüssigkeiten mit Differenzdruckverfahren bei kleinen Nennweiten, Dissertation, VDI Verlag Düsseldorf, *1999*

[*14*] Weddfelt, K.: Measurement of Pump Source Characteristics by the Two-Microphone Method, *2nd* Tampere International Conference on Fluid Power, Tampere Finland, *1991*

[*15*] Czibere, T.: Áramlástan, Nemzeti Tankönyvkiadó, Budapest, *2001*

[*16*] Uchida, S: The pulsating viscous flow superposed on the steady motion of incompressible fluid in a circular pipe, Z. angew. Math. Phys. *7*, pp. *403-421*, *1956*

[*17*] He, S., Jackson, J. D.: A study of turbulence under condition of transient flow in a pipe, Journal of Fluid Mechanics, Vol. *408*, pp. *1-38*, *2000*

[*18*] Durst, F., Kikura, H., Lekakis, I., Jovanovic, J., Ye, Q.: Wall shear stress determination from near-wall mean velocity data in turbulent pipe and channel flows, Experiments in Fluids *20*, pp. *417-428*, *1996*

[*19*] Durst, F., Jovanovic, J., Sender, J.: LDA measurements in the near-wall region of a turbulent pipe flow, Journal of Fluid Mechanics, Vol. *295*, pp. *305-335*, *1995*

[*20*] Mao, Z-X., Hanratty, T. J.: Studies of the wall shear stress in a turbulent pulsating flow, Journal of Fluid Mechanics, Vol. *170*, pp. *545-564*, *1986*

[*21*] Yamanaka, G., Kikura, H., Takeda, Y., Aritomi, M.: Flow measurement on an oscillating pipe flow near the entrance using the UVP method, Experiments in Fluids *32*, pp. *212-220*, *2002*

[*22*] Poggi, D., Porporato, A., Ridolfi, L.: An experimental contribution to near-wall measurements by means of a special laser Doppler anemometry technique, Experiments in Fluids *32*, pp. *366-375*, *2002*

[*23*] Schlichting, H., Gersten, K.: Grenzschichttheorie, Braun Verlag Karlsruhe, *1997*

[*24*] Mochizuki, S., Nieuwstadt, F. T. M.: Reynolds-number-dependence of the maximum in the streetwise velocity fluctuation in wall turbulence, Experiments in Fluids *21*, pp. *218-260*, *1996*

[*25*] Akhavan, R., Kamm, R. D., Shapiro A. H.: An investigation of transition to turbulence in bounded oscillatory Stokes flow, Part 1. Experiments, Journal of Fluid Mechanics, *225*, *1991*

[*26*] Wachel, J. C., Bates, C. L.: Techniques for Controlling Piping Vibration and Failures, Joint Petroleum Mechanical Engineering and Pressure Vessels and Piping Conference, Mexico City, Mexico, pp. *11-20*, *1976*

[*27*] Watchel, J.: Piping vibration and stress, Machinery vibration monitoring and analysis, Vibration Institute, New Orleans USA, pp. *1-20*, *1981*

[*28*] Keiper, W.: Schall und Schwingungen am Hydraulikantrieb, O+P Ölhydraulik und Pneumatik *37*, Nr. *8*, pp. *622-624*, *1993*

[*29*] Breuer, D., Goenechea, E.: Lärmbekämpfung in der Hydraulik, O+P Ölhydraulik und Pneumatik, pp. *8-21*, Konstruktions Jahrbuch *2002/2003*

[*30*] Sinimbari, G. R., Fallen, M.: Ingenieurakustik, Friedr. Vieweg & Sohn Verlagsgesellschaft mbH, Braunschweig, *1984*

[*31*] Fritsch, H.: Druckpulsationen und Resonanzerscheinungen in Rohrleitungen oszillierender Verdrängerpumpen, *3*R International *21*, Heft *3*, pp. *99-105*, *1982*

[*32*] Fritsch, H.: Hydraulische Schwingungen und ihre Dämpfung in Rohrleitungen oszillierender Verdrängerpumpen, Chemie-Technik, *13*. Jahrgang, Nr. *10*, *1984*

[*33*] Lang, S. M., Pokorny, P.: Körperschall- und Flüssigkeitsschallausbreitung in verzweigten Rohrleitungssystemen, O+P Ölhydraulik und Pneumatik *32*, Nr. *1*, pp. *23-29*, *1988*

[*34*] Schweinfurter, F.: Beitrag zur rechnerischen Bestimmung von Druckschwingungen in Rohrleitungssystemen bei Erregung durch ein- und mehrzylindrige oszillierende Verdrängerpumpen, Dissertation, Technische Fakultät der Universität Erlangen-Nürnberg, *1988*

[*35*] Brodin, E.: Small amplitude pulsatile flow in hydraulic transmission line, Dissertation, Norvegian University of Science and Technology, Trondheim, *1998*

[*36*] Breuer-Stercken, A.: Systematische Untersuchung von Strukturschwingungen im Hinblick auf die Entwicklung geräuscharmer Kolbenpumpen, Dissertation, RWTH Aachen, *1999*

[*37*] Müller, B.: FEM-Schwingungsberechnung zur Geräuschanalyse und –optimierung von Hydropumpen, O+P Ölhydraulik und Pneumatik *44*, Nr. *1*, pp. *37-42*, *2000*

[*38*] Kozminesky, R.: Hydraulische Schwingungen in Rohrleitungen durch Drehkolbenpumpen, Dissertation, Technische Fakultät der Universität Erlangen-Nürnberg, *2001*

[39] Jarmer, R.: Zur Erregung mechanischer Rohrleitungsschwingungen durch oszillierende Verdrängerpumpen – Numerische Berechnung und experimentelle Verifikation, Dissertation, TU Erlangen-Nürnberg, *2002*

[*40*] Leslie, D. J., Vardy, A. E.: Practical Guidelines for Fluid-Structure Interaction in Pipelines, A review, *10th* International Meeting of the Work Group on The Behaviour of Hydraulic Machinery Under Steady Oscillatory Conditions, Trondheim, Norway, pp. *1-8*, *2001*

[*41*] Hoffman, D.: Dämpfung von Flüssigkeitsschwingungen in Hydraulikleitungen, O+P Ölhydraulik und Pneumatik *24*, Nr. *1*, pp. *32-37*, *1980*

[*42*] Hoffman, D.: Dämpfung von Flüssigkeitsschwingungen in Hydraulikleitungen, O+P Ölhydraulik und Pneumatik *24*, Nr. *2*, pp. *102-105*, *1980*

[*43*] Haarhaus, M.: Minderung von Druckschwingungen in Flüssigkeitsrohren, O+P Ölhydraulik und Pneumatik *25*, Nr. *10*, pp. *802-806*, *1981*

[*44*] Wacker, K.: Flüssigkeitsschall in ölhydraulischen Leitungssystemen – Die Berechnung der Schallausbreitung und des Dämpfungsverhaltens von Flüssigkeitsschalldämpfern bei reflektierenden Randbedingungen, Dissertation, Universität Stuttgart, *1986*
[*45*] Esser, J.: Adaptive Dämpfung von Pulsationen in Hydraulikanlagen, Dissertation, Rheinisch-Westfälischen Technischen Hochschule Aachen, *1996*
[*46*] ISO/TC *108* Mechanical Vibration and Shock
[*47*] ISO *10816* Bewertung der Schwingungen von Maschinen durch Messung an nicht-rotierenden Teilen, Beuth-Verlag, Berlin, *1997*
[*48*] ISO *2954* Mechanical Vibration of Rotating and Reciprocating Machinery – Requirements for Instruments for Measuring Vibration Severity
[*49*] ANSI/ASME Standard OM-*3* Preoperational and Initial Start-up Vibration Testing of Nuclear Power Plant Piping System, ASME, New York, USA, *1987*
[*50*] API Standard *674* Positive Displacement Pumps – Reciprocating, Second Edition, American Petroleum Institute, Washington D. C. USA, *1995*
[*51*] Schwarz, T.: Schallanalyse in der Schadensdiagnose: Erkennung von Defekten an Hydraulikpumpen, O+P Ölhydraulik und Pneumatik *3*, Nr. *4*, pp. *313-319*, *1989*
[*52*] Mundry, S., Stammen, C.: Condition Monitoring for Fluid Technology, O+P Ölhydraulik und Pneumatik *46*, Nr. *2*, pp. *120-127*, *2002*
[*53*] Navy Engine Mechanic, Fluid Power Manual, Integrated Publishing, *2003*
[*54*] Nagy, R.: Pulsation Measurement in Hydraulic Systems MicroCAD International Scientific Conference, Miskolc, Hungary, *2003*
[*55*] Chaves, S. H., Meier, G. E. A., Stasicki, B.: Optischer Weg- und Verformungsmesser, Patent DE *410 52 70*, München, *27.08.1992*
[*56*] Hein, S., Nagy, R.: Ergebnisse einer neuen Messmethode hydraulischer Pulsationen, Vortrag, GÉP, LI. Évfolyam *8*. szám, *2000*
[*57*] Bauer, G.: Ölhydraulik 7. Auflage, B. G. Teubner Stuttgart, *1998*
[*58*] Sheplak, M., Dugundji, J.: Large Deflections of Clamped Circular Plates Under Initial Tension and Transitions to Membrane Behaviour, Journal of Applied Mechanics, Vol. *65*, pp. *107-115*, *1998*
[*59*] Saini, R., Bhardwaj, S., Nishida, T., Sheplak, M.: Scaling Relations for Piezoresistive Microphones, Proceedings of IMECE, International Mechanical Engineering Congress and Exposition, Orlando, Florida, pp. *1-8*, *2000*
[*60*] Beitz, W., Küttner, K.-H.: Dubbel Taschenbuch für den Maschinenbau, *18*. Auflage, Springer, *1995*
[*61*] Altenbach, H., Altenbach, J., Naumenko, K.: Ebene Flächentragwerke, Grundlagen der Modellierung und Berechnung von Scheiben und Platten, Springer, *1998*
[*62*] Hering, E., Martin, R., Stohrer, M.: Physik für Ingenieure, VDI Verlag, *1995*
[*63*] Williams, D. C.: Optical Methods in Engineering Metrology, Chapman & Hall, London, *1993*
[*64*] Fischer, U., Stephan, W.: Mechanische Schwingungen, VEB Fachbuchverlag Leipzig, *1981*
[*65*] Präzisionsoptik, Spindler & Hoyer, *1989*
[*66*] Young, M.: Optics and Lasers, Springer, Berlin *2000*
[*67*] Gerthsen, C., Kneser, H. O., Vogel, H.: Physik, Springer Verlag Berlin, *1992*
[*68*] Findeisen, D., Findeisen F.: Ölhydraulik, *4*. Auflage, Springer Verlag Berlin, *1994*
[*69*] Fahy, F. J., Walker, J. G.: Fundamentals of Noise and Vibration, E & FN Spot, London, *1998*
[*70*] Crocker, M. J.: Handbook of Acoustics, John Wiley & Sons, New York, *1998*
[*71*] Zoebl, H.: Rechenverfahren zur Verwertung physikalischer Gesetze in der Fluidtechnik, O+P Ölhydraulik und Pneumatik *45*, Nr.*4*, pp. *228*, *2001*

[*72*] Henn, H., Sinambari, G. R., Fallen, M.: Ingenieurakustik, Friedr. Vierweg & Sohn Wiesbaden/Braunschweig, *1984*

[*73*] Fritsch, H, Müller, F., Schwarz, J.: Hydraulische Schwingungen und ihre Dämpfung in Rohrleitungen oszillierender Verdrängerpumpen, Pumpen, Bauelemente der Anlagetechnik (Hrsg. G. Vetter), Vulkan-Verlag, Essen, *1987*

[*74*] Viersma, T. J.: Analysis, Synthesis and Design of Hydraulic Servosystems and Pipelines, Elsevier, Amsterdam, *1980*

[*75*] Harms, H. –H., Prinke, D.: Messverfahren zur Bestimmung der Schallgeschwindigkeit in Mineralölen, O+P Ölhydraulik und Pneumatik *23*, Nr.*3*, pp.*191-194*, *1979*

[*76*] Schmidt, H.: Schalltechnisches Taschenbuch, VDI-Verlag GmbH, Düsseldorf, *1989*

[*77*] Nguyen, D. L.: Schallgeschwindigkeit und kritischer Massendurchsatz in ein- und zweikomponentigen Gas-Flüssigkeits-Strömungen, Dissertation, Technische Universität München, *1981*

[*78*] Kröell-Dulay, I.: Szerszámgépek automatizálása, Nemzeti Tankönyvkiadó, Miskolc, *1993*

[*79*] Backé, W.: Umdruck zur Vorlesung Grundlagen der Ölhydraulik, RWTH-Aachen, 8. Auflage, *1992*

[*80*] Heisel, U., W. Fiebig, N. Mittwollen, M. Oehler: Luftblaseneinfluss auf Schallgeschwindigkeit und Druckschwingungen in einem hydraulischen System, O+P Ölhydraulik und Pneumatik *38*, Nr. *7*, pp. *420-423*, *1994*

[*81*] Smereka, P.: A Vlasov equation for pressure wave propagation in bubbly liquids, Journal of Fluid Mechanics, Vol. *454*, pp. *287-325*, *2002*

[*82*] Wilson, P. S.: Sound Propagation and Scattering in Bubbly Liquids, Dissertation, Boston University, USA, *2002*

[*83*] Brennen C. E.: Cavitation and Bubble Dynamics, Oxford University Press, *1995*

[*84*] Gössele, R.: Messung von Volumenstromschwankungen bei hydrostatischen Pumpen, O+P Ölhydraulik und Pneumatik *21*, Nr.*2*, pp. *92-94*, *1977*

[*85*] Theissen, H.: Volumenstrompulsation von Kolbenpumpen, O+P Ölhydraulik und Pneumatik *24*, Nr. *8*, pp. *588-591*, *1980*

[*86*] Larsson, P., Palmberg, J-O., Weddfelt, K.: Analysis and Measurement of Pressure Ripple of Fluid Power Pumps, *8th* IASTED International Symposium MECO' *86*, Taormina, Italy, *1986*

[*87*] Schellinger, S., Goenechea, E.: Automatisiertes Selbstregelsystem für einen Reflexionsarmen Leitungsabschluss (RALA), O+P Ölhydraulik und Pneumatik *47*, Nr. *4*, pp. *271-275*, *2003*

[*88*] Kurr, K.-J., Menshen K.: Einfluss von Rohrschellen auf das Resonanzverhalten von Rohrsystemen, O+P Ölhydraulik und Pneumatik *35*, Nr.*12*, pp. *914-916*, *1991*

[*89*] Weisstein, E. W: Mathworld Interactive Mathematics Encyclopedia, www.mathworld.wolfram.com

[*90*] Griese, K.: Zahnradpumpen und Motoren, O+P Ölhydraulik und Pneumatik *42*, Nr. *9*, pp. *564-571*, *1998*

[*91*] Amann, R.: Zahnradpumpen mit Evolventenverzahnung, Mitteilungen des Hydraulischen Instituts München, Nr. *1*, *1926*

[*92*] Gössele, R.: Volumenstromschwankungen hydrostatischer Pumpen - Vergleich von Theorie und praktischem Verhalten, O+P Ölhydraulik und Pneumatik *23*, Nr. *5*, pp. *371-376*, *1979*

[*93*] Schwuchow, D.: Pulsationssenkung bei Zahnradpumpen, O+P Ölhydraulik und Pneumatik *43*, Nr. *1*, pp. *42-45*, *1999*

[*94*] Schwuchow, D.: Auslegungswerkzeuge für moderne Aussenzahnradpumpen, O+P Ölhydraulik und Pneumatik *46*, Nr. *7*, pp. *420-423*, *2002*

[*95*] Zarotti, M., Guidetti, M.: Reduzierung von Strömungspulstationen durch ein neues Konzept von Zahnradpumpen, O+P Ölhydraulik und Pneumatik *44*, Nr. *1*, pp. *33-36*, *2000*

[*96*] Brendenfeld, G., Schwuchow, D., Egger, N.: Spielfreie Aussenzahnradpumpen – Wirkungsweise und Langzeitverhalten, O+P Ölhydraulik und Pneumatik *43*, Nr. *7*, pp. *522-525*, *1999*

[*97*] Ickiewicz, J. S.: Einfluss der Betriebsparameter auf Pulsationen und Geräusch von Zahnradpumpen, O+P Ölhydraulik und Pneumatik *23*, Nr. *5*, pp. *381-382*, *1979*

[*98*] Fiebig, W., Lang, C. M.: Berechnung der Druckpulsation von Aussenzahnradpumpen, O+P Ölhydraulik und Pneumatik *34*, Nr. *4*, pp. *262-267*, *1990*

[*99*] Grbovic, V.: Förderstromschwankungen einer Zahnradpumpe, Dissertation, Technischen Hochschule Zürich, *1983*

[*100*] Ivantysyn J., Ivantysyn, M.: Hydrostatische Pumpen und Motoren, Vogel Fachbuch, *1993*

Statement of originality

This thesis does not contain any material, which has been accepted for the award of any degree and diploma in this university or other institution. Unless where stated or referenced, this work contains no material, which has been previously published or written by another researcher.

Permission is given by the author to the relevant bodies within the University, for the purpose of photocopying and reproduction.

Róbert Nagy